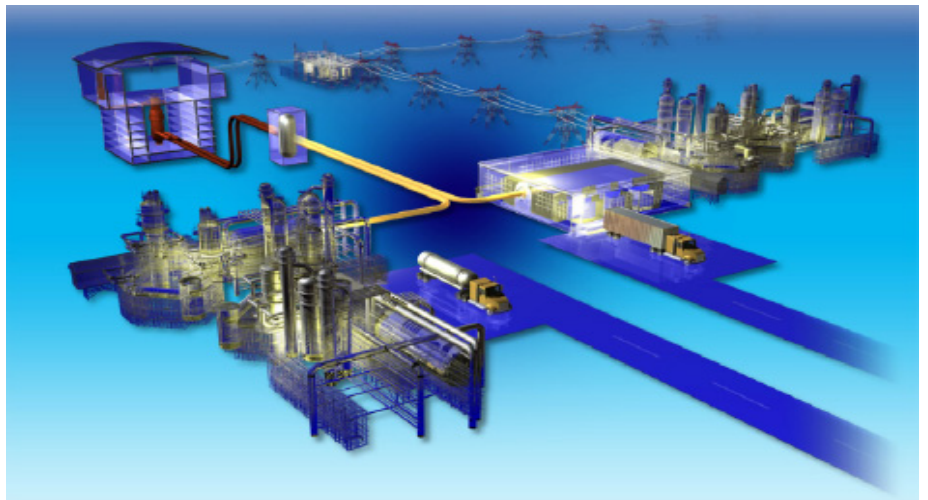# Conceptual Design of Forced Convection Molten Salt Heat Transfer Testing Loop

Manohar S. Sohal
Piyush Sabharwall
Pattrick Calderoni
Alan K. Wertsching
Brandon S. Grover
Phil Sharpe

September 2010

The INL is a U.S. Department of Energy National Laboratory operated by Battelle Energy Alliance

INL
Idaho National Laboratory

Conceptual Design of Forced Convection Molten Salt Heat Transfer Testing Loop

Manohar S. Sohal
Piyush Sabharwall
Pattrick Calderoni
Alan K. Wertsching
Brandon S. Grover
Phil Sharpe

September 2010

**Idaho National Laboratory
Idaho Falls, Idaho 83415**

Conceptual Design of Forced Convection Molten Salt Heat Transfer Testing Loop

INL/EXT-10-19908

September 2010

Approved by:
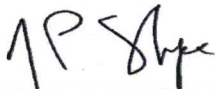
_____   9-28-2010
Piyush Sabharwall   Date
Author

_____   9-29-2010
Manohar S. Sohal   Date
Reviewer
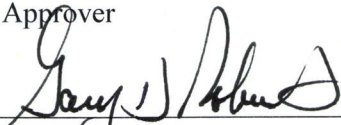
_____   9/29/2010
Phil Sharpe   Date
Approver

_____   9/30/2010
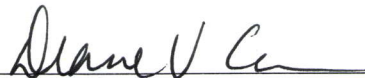Gary D. Roberts   Date
VHTR TDO Quality Assurance

_____   9/30/10
Diane V. Croson   Date
VHTR TDO Deputy Director

ABSTRACT

This report develops a proposal to design and construct a forced convection test loop. A detailed test plan will then be conducted to obtain data on heat transfer, thermodynamic, and corrosion characteristics of the molten salts and fluid-solid interaction. In particular, this report outlines an experimental research and development test plan. The most important initial requirement for heat transfer test of molten salt systems is the establishment of reference coolant materials to use in the experiments. An earlier report produced within the same project highlighted how thermophysical properties of the materials that directly impact the heat transfer behavior are strongly correlated to the composition and impurities concentration of the melt. It is therefore essential to establish laboratory techniques that can measure the melt composition, and to develop purification methods that would allow the production of large quantities of coolant with the desired purity. A companion report describes the options available to reach such objectives. In particular, that report outlines an experimental research and development test plan that would include following steps:

- Molten salts: The candidate molten salts for investigation will be selected.

- Materials of construction: Materials of construction for the test loop, heat exchangers, and fluid-solid corrosion tests in the test loop will also be selected.

- Scaling analysis: Scaling analysis to design the test loop will be performed.

- Test plan: A comprehensive test plan to include all the tests that are being planned in the short and long term time frame will be developed.

- Design the test loop: The forced convection test loop will be designed including extensive mechanical design, instrument selection, data acquisition system, safety requirements, and related precautionary measures.

- Fabricate the test loop.

- Perform the tests.

- Uncertainty analysis: As a part of the data collection, uncertainty analysis will be performed to develop probability of confidence in what is measured in the test loop.

Overall, the testing loop will allow development of needed heat-transfer-related thermophysical parameters for all the salts, validate existing correlations, validate measuring instruments under harsh environment, and have extensive corrosion testing of materials of construction.

CONTENTS

FIGURES

TABLES

NOMENCLATURE

a	flow area
C_l	constant
C_p	specific heat capacity, J/kg·K
d	diameter of a tube, m
d_h	hydraulic diameter
e	specific internal energy
f	friction factor
g	gravity constant
h	enthalpy
j	flux term
k	thermal conductivity, W/m·K
K	loss Coefficient
l	conduit length, m
L_{th}	distance between heat source and heat sink thermal centers
M	sodium, potassium, or lithium
Nu	Nusselt number
Pr	Prandtl number, $C_p·\mu/k$
$\dot{q}$	power or heat transport rate
Q	volumetric flow rate
Re	Reynolds number, $\rho·d·v/\mu$
S	source term
T	temperature, K
U	velocity
v	velocity, m/s
V	volume
Π	characteristic time ratio (dimensionless parameter)
τ	residence time constant
ψ_k	ρ, ρu or $\rho\varepsilon$ (mass, momentum or energy per unit volume)

ρ   density, kg/m^3

μ   dynamic viscosity, Pa·**s**

γ   surface tension, N/m

Subscripts

b   bulk fluid

w   wall

ACRONYMS

AHTR	Advanced High Temperature Reactor
ARE	Aircraft Reactor Experiment
ASME	American Society of Mechanical Engineers
DF	distortion factor
FCL	forced convection test loop
FHR	fluoride salt-cooled high temperature reactor
FLiNaK	lithium fluoride-sodium fluoride-potassium fluoride
FLiBe	lithium fluoride - beryllium fluoride
HTGR	high temperature gas-cooled reactor
ICP-AES	inductively coupled plasma atomic emission spectroscopy
ICP-MS	inductively coupled plasma mass spectroscopy
IHX	intermediate heat exchanger
INL	Idaho National Laboratory
LWR	light water reactor
MSBR	Molten Salt Breeder Reactor
MSR	Molten Salt Reactor
MSRE	Molten Salt Reactor Experiment
NGNP	Next Generation Nuclear Plant
ORNL	Oak Ridge National Laboratory
PDF	probability density function
PIRT	Phenomena Identification and Ranking Table
R&D	research and development
RTD	resistance temperature device
VHTR	very high temperature reactor

Conceptual Design of Forced Convection Molten Salt Heat Transfer Testing Loop

1.   INTRODUCTION

The U.S. Department of Energy is working with industry to develop a Very High Temperature Reactor (VHTR) as a part of the effort to supply the United States with abundant, clean, and secure energy as initiated by the *Energy Policy Act of 2005* (Public Law 109–58, 2005). Other thermal reactor concept is theMolten Salt Reactors officially started by the Generation IV International Forum (GIF) to improve nuclear safety, proliferation resistance and to minimize waste.Figure 1-1 presents a schematic of a molten salt reactor concept, which uses a liquid core made up of a molten alkaline fluoride salt and may also use molten salt in the heat exchanger.
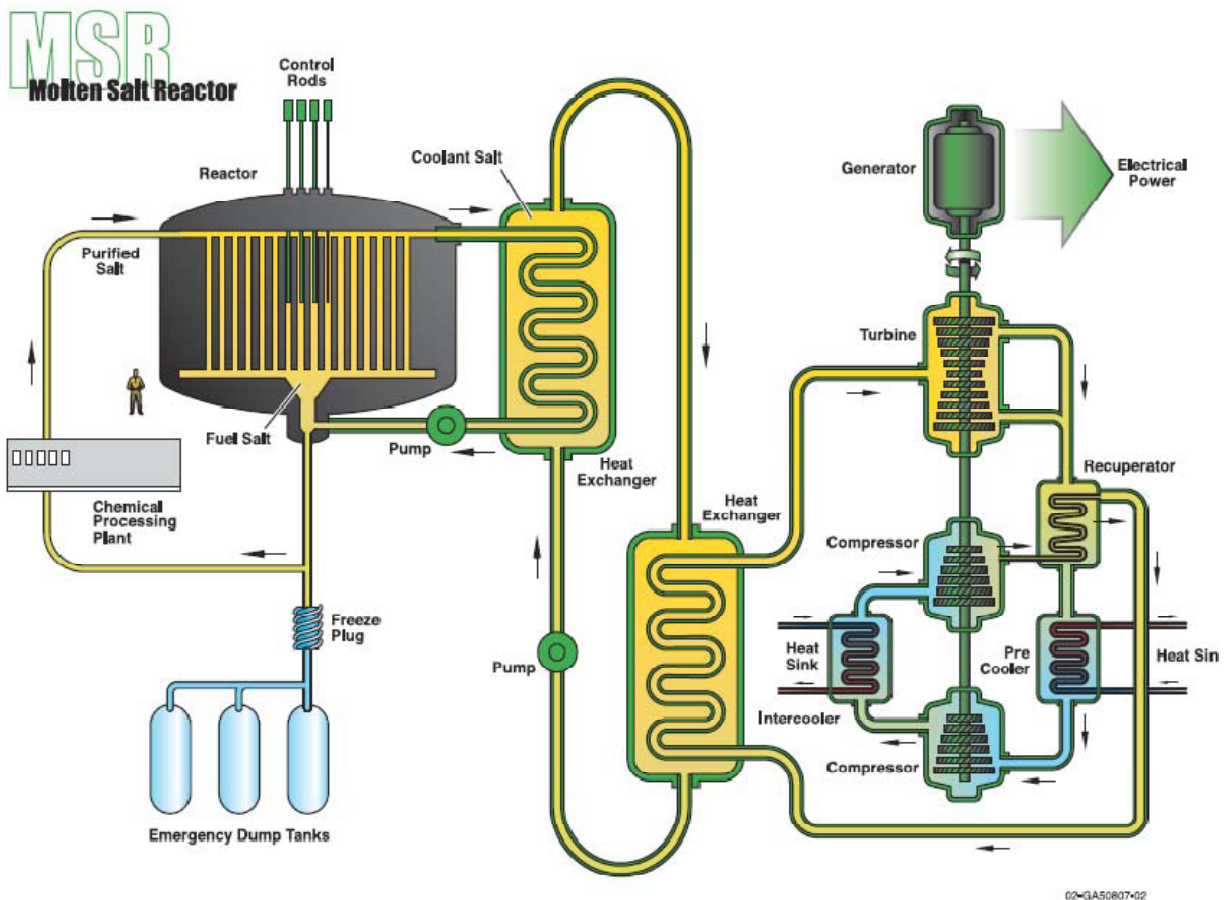
Figure 1-1. Schematic of a molten salt reactor concept.

1.1   Historical Background

Investigation started in the late 1940s as part of the U.S. program to develop a nuclear-powered airplane. Molten salt was initially used as the heat transfer/transport fluid for the jet engine. Several different ideas of compact reactors for generating heat in a jet engine were being considered in 1943. One idea at Oak Ridge National Laboratory (ORNL) involved using a high-temperature liquid fuel that could be circulated and be drained for refueling. In 1947, after experiments were started to explore molten-salt

fuels, molten fluorides were selected for the main effort of the Aircraft Nuclear Propulsion program at ORNL. Fluoride salt was selected because of its low vapor pressure at jet-engine temperatures, reasonably good heat transfer properties, immunity to radiation damage, and nonviolent reaction with air or water. In 1954, a 2.5-MWth molten salt reactor, also called Aircraft Reactor Experiment (ARE), was built and fueled with UF_4 dissolved in a mixture of zirconium and sodium fluorides, moderated with beryllium oxide; it operated successfully for nine days at steady-state outlet salt temperatures approaching 900°C. No mechanical or chemical problems were encountered, and the reactor was found to be stable and self-regulating as indicated by Holcomb et al. (2009).

The ARE, which was built of Inconnel 600, corroded too rapidly at the design temperature for long-term use and was not strong enough. The existing alloys were screened for corrosion resistance at this temperature and only two were found to be satisfactory: Hastelloy-B (Ni-28% Mo-5% Fe) and Hastelloy-W (Ni-25% Mo-5% Cr-5.5% Fe). However, both aged at the service temperature and became quite brittle because of the formation of Ni-Mo intermetallic compounds. These observations led to development of an alloy program in which INOR-8, or Hastelloy-N, was developed, which has the chemical composition shown in Table 1-1.

Table 1-1. Chemical composition of Hastelloy-N (Rosenthal et al. 1972).

Element	Content (% by weight)[a]	
	Standard Alloy	Favored Modified Alloy
Nickel	Base	Base
Molybdenum	15-18	11-13
Chromium	6-8	6-8
Iron	5	0.1[b]
Manganese	1	0.15-0.25[b]
Silicon	1	0.1
Phosphorus	0.015	0.01
Sulfur	0.02	0.01
Boron	0.01	0.001
Titanium and hafnium		2
Niobium		0-2

a. Single values are maximum amounts allowed. The actual concentrations of these elements in an alloy can be much lower.

b. These elements are not felt to be very important. Alloys are not being purchased with the small concentration specified, but the specification may be changed in the future to allow a higher concentration.

Before construction of the Molten Salt Reactor Experiment (MSRE), the physical and mechanical properties of Hastelloy-N were comprehensively evaluated. The property changes with time are found to be minute because the alloy does not form intermetallic compounds, only small amounts of fine carbides. The strength of this alloy is also very good because it is 16% molybdenum.

Familiarity with ARE was the foundation for and carried over into the development studies conducted in support of the design, construction, and successful operation of the MSRE, and subsequently in support of the conceptual design studies of the Molten Salt Breeder Reactor (MSBR). Operation of the MSRE for

more than 13,000 equivalent full-power hours provided the most experience related to nuclear operation (Rosenthal et al. 1972).

The use of nuclear power to drive an airplane would require a large power density to be available in the core. Since sodium coolant was unable to remove the heat and keep the fuel rods at a reasonable operating temperature, the ARE used a fuel-bearing salt (NaF-ZrF_4-UF_3 salt) in the reactor core, which allowed power densities to reach higher levels than those of the sodium-cooled reactors. After the ARE, the technology was applied to power reactors under the MSRE, which was an 8-MW reactor containing a fuel salt of $LiBeF_2$-UF_3-ThF_4. This led to much research on fluoride salts, which have the highest volumetric heat capacity—an important criterion in determining the amount of energy that can be contained in a unit volume of salt.

The MSBR has some favorable features and a few negative features when compared with other power plant concepts. Its favorable features are (Rosenthal et al. 1972):

- Nuclear characteristics.

- Positive moderator coefficient, which contributes to making the isothermal temperature coefficient of reactivity fairly small, resulting in very modest control reactivity requirements for maneuvering that permits very small loaded excess reactivity.

- Large heat capacity of the molten salt, which serves as a buffer to absorb the effects of reactivity transients and lessens their influence on the plant; melting of fuel is not a limitation since it is already molten.

- Gaseous fission products are continuously stripped from the salt, greatly reducing their usual reactivity effects, and the entire reactor fuel system operates from a low base pressure.

- Long prompt-neutron lifetimes and a large prompt negative temperature coefficient of reactivity, which yields very desirable control characteristics; the capacity for fast transients results in fairly small conceivable reactivity.

However, its negative features are high freezing temperatures of the salts that complicate both control and protection to some extent in that special provisions must be made to avoid freezing of salt during power or load changes (Rosenthal et al. 1972).

The Molten Salt Reactor (MSR) program was initiated in 1957 at ORNL. By 1960, enough constructive results were obtained to support authorization and construction of a 7.4-MW$_{th}$ MSRE. For simplicity, it was designed with a simple single fluid, without thorium, and just a simple tank of graphite with flow channels. It operated at a temperature of 650°C to allow for a long life of the nickel alloy used as piping and heat exchangers, and had a highly successful run for almost 5 years between 1965 and 1969. The MSRE provided facilities for testing fuel salt, graphite, and Hastelloy-N under reactor operating conditions, as shown in Figure 1-2. The basic reactor performance was outstanding, indicating that the desirable features of the molten salt concept could be embodied in a practical reactor that can be constructed, operated, and maintained safely and reliably. The most important result that came out of the MSRE program was the conclusion that MSR is a practical concept.
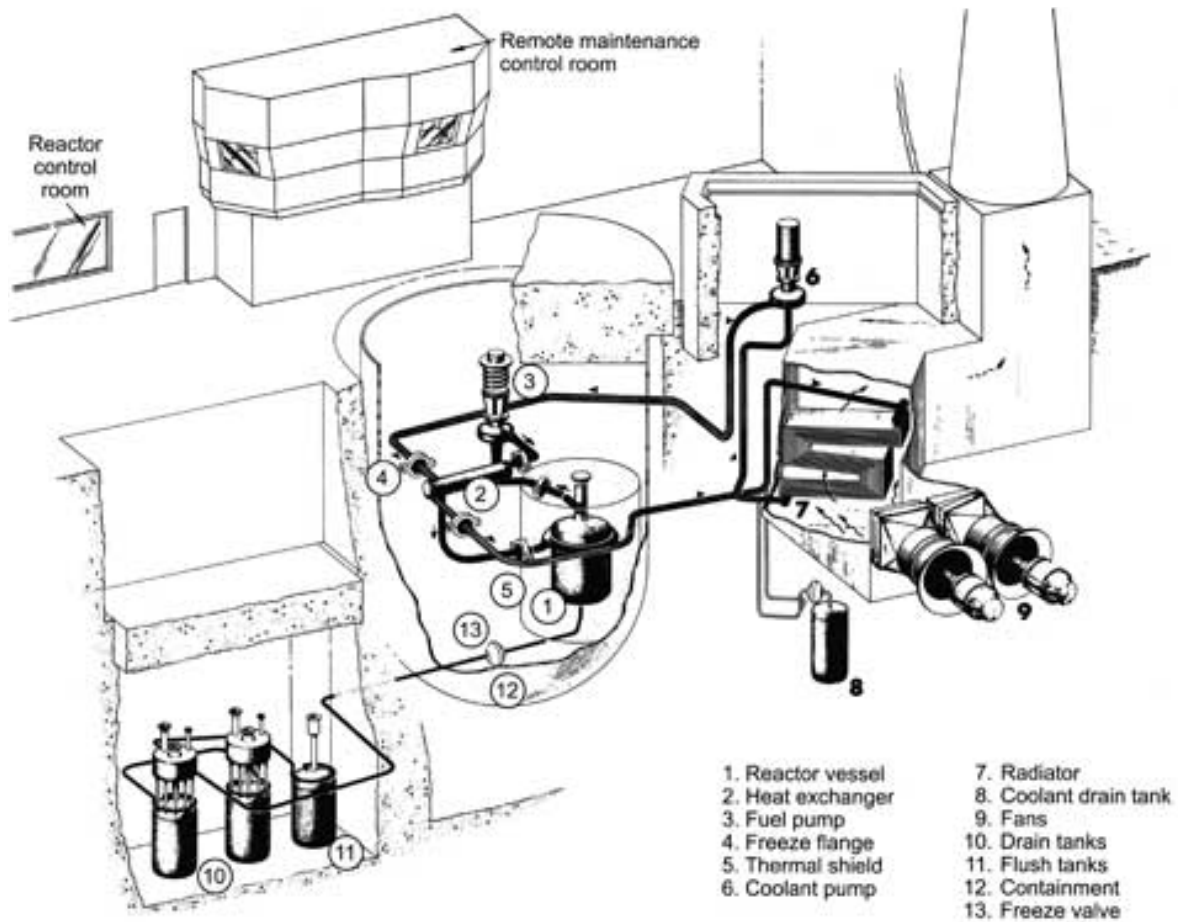
Figure 1-2. Molten salt reactor experiment at ORNL (Rosenthal et al. 1972).

MSRs have a number of advantages over conventional reactor designs. They run at low pressures and so do not need the large pressure vessels required in light water reactors (LWRs). The MSR containment vessel for the same power duty is wider but much shorter than those of LWRs. And, as shown in Figure 1-3, it does not need the huge volume and ability to deal with steam pressure buildup as is the case for LWRs. It can run on a variety of fuels and can even burn transuranic waste produced at other reactors (LeBlanc 2010a). These designs have very strong negative temperature and void coefficients, which have a short response time (act instantly), aiding safety and allowing automatic load following operation. The fuel is in molten state (hence the name "molten salt"), so meltdown of the core is irrelevant. Also, the fluid nature of the fuel means meltdown is an irrelevant term. In the event of an emergency, the fuel salt is automatically drained to passively cooled, critically safe, drain tanks. The other major issue with nuclear power plants is the generation of minor actinides; most fission products in MSRs are from stable fluorides that will stay within the salt during any leak or accident. MSRs also produce plutonium and other transuranic elements at much lower rates and recycle them; thus, the long-lived radio-toxicity of MSR waste is 1/10,000th that of a LWR. Others are volatile or insoluble and can be passively and continuously removed. Xenon gas, which represents almost half of all neutron absorptions to fission products in most solid-fuel reactors, will just bubble out of the fuel salt and can be stored outside the reactor loop with ease.
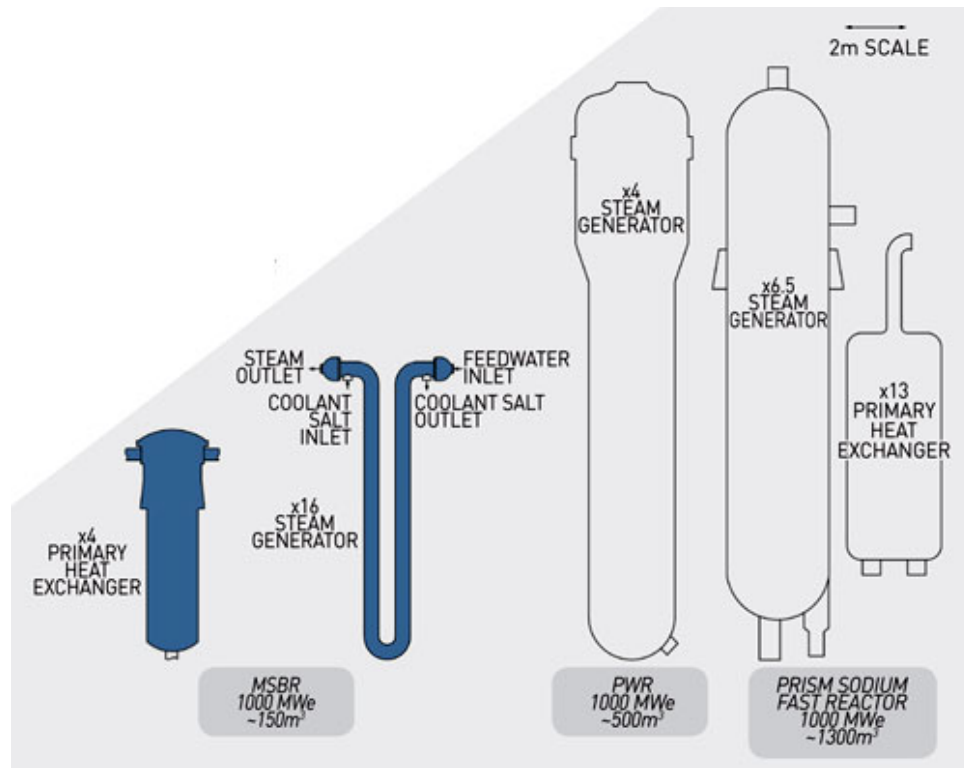
Figure 1-3. Comparison of heat transfer components for different types of reactors (LeBlanc 2010a).

Although there are many design variations for MSRs, they can be grouped into two main categories: breeders and converters. Breeder reactors tend to produce their own fissile fuel after start up. Fertile thorium for example, decays to U-233 after neutron capture. No other reactor is as well suited for breeding U-233 with fuel that is mechanically robust, chemically refractive, and radiologically self-guarding (Holcomb et al. 2009). This cycle could be achieved in a softer neutron spectrum, but the conversion of uranium to plutonium requires a harder spectrum. Without fuel processing, MSRs can run as simple converters with excellent uranium utilization, even on a once-through cycle. They can also run off low-enriched uranium (LeBlanc 2010a).

Unlike other reactors, MSRs have no water or sodium in the primary fluid, so there is no possibility of steam exploding or hydrogen being produced within the containment. MSR (sometimes referred to as liquid fluoride reactors) contains no fuel pellets. Instead, the fissile and fertile materials are dissolved in a fluid medium. The fluid can be one of various fluorides of uranium, thorium, or plutonium, which form low-melting-point eutectics when combined with certain carrier salts such as $27LiF-BeF_2$ (FLiBe). Further, the heat from the radioactive primary salt is transferred to intermediate salt, which then transfers the thermal energy for power production or for a process heat application plant. Previous studies (mainly with MSBR and MSRE) have shown that fluoride salts are the most promising fluids because of their lower melting points and material compatibility with nickel or carbon-based conduit materials, although their compatibility at intermediate loop temperatures (650–950°C) is yet to be proven. The ARE program, which had a different fuel system ($NaF-ZrF_4-UF_4$) and a different metal (Inconel rather than Hastelloy-N), provided little information directly related to the MSBR, but it produced a lot of background experience and information. The mechanism by which corrosion occurs was recognized, and the importance of extraneous impurities in the corrosion process was demonstrated. The corrosion of metals by fluorides, such as the nickel-based alloys, was shown to be acceptable (Ambrosek 2010).

Molten salts have been used as nuclear reactor fuel and coolants, heat-treating media, and thermal storage material. These processes take advantage of the large volumetric heat capacity of these salts along with their high-temperature stability. Since the 1980s, salts have also been used as thermal storage material, capturing energy and storing it in receptacles for use at a later date.

An extensive study of many characteristics of molten salts, such as fluoroborate chemistry, has been conducted, but additional work is needed in several areas. It seems unlikely that the findings of further research will affect the feasibility of using molten salt as a process heat transfer fluid.

The NGNP is intended to increase energy efficiency in the production of electricity and/or provide high temperature heat for industrial processes. The coolant salts must satisfy a number of requirements for use as a primary coolant fluid in the reactor system, including:

- Chemical stability at temperatures of 800°C or greater (for primary coolant)

- Radiolytic stability in a high radiation environment (for primary coolant)

- Low melting point and high boiling point

- Large specific heat and thermal conductivity

- Low vapor pressures, substantially less than one atmosphere at operating temperatures

- Compatibility with high-temperature alloys.

The process plant will be separated from the nuclear plant because of safety, contamination, and licensing requirements (Sabharwall and Gunnerson 2009). Therefore, the heat transfer fluid will have to travel significant distances without much, if any, temperature drop, as all of the process heat applications are temperature driven. Several fluids could be used to transfer the thermal energy between the VHTR, such as the NGNP, and the downstream processes, including molten salts, alkali metals, and helium.

1.2 Molten Salt as Heat Transfer Carrier

The behavior and material compatibility of various molten salts as a heat transfer agent for nuclear reactors was studied extensively by ORNL from the 1950s through the 1970s in support of the ARE, the MSRE, and the MSBR programs, but uncertainty in data and correlations still exist. Liquid salt technology has been used for many decades in industrial process heat transfer, thermal storage, and materials processing applications. Applicability of molten salts as a heat transfer medium has been assessed by Williams (2006) and Williams et al. (2006), who concluded that molten salts appear to be excellent candidates that meet most of the essential requirements. However, no single-component salt meets all the requirement of low melting temperature. Therefore, multicomponent eutectic mixtures are needed to meet the melting temperature requirement.

The most widely considered salt in nuclear applications is the lithium fluoride (LiF) and beryllium di-fluoride (BeF_2) eutectic. The binary mixture phase diagram is shown in Figure 1-4 (Baes 1974). A liquid-phase eutectic composition exists in equilibrium with the solid with melting point as low as 363.5°C. However, since the eutectic viscosity rapidly increases with the BeF_2 content (and consequently the pumping power for forced convection loops), the reference composition adopted is the 67 mol% LiF and 33 mol% BeF_2, also known as FLiBe. In the MSRE and related experiments, FLiBe was the solvent matrix carrying the homogenously distributed fuel as well as the heat transfer media in the intermediate heat exchanger (IHX).
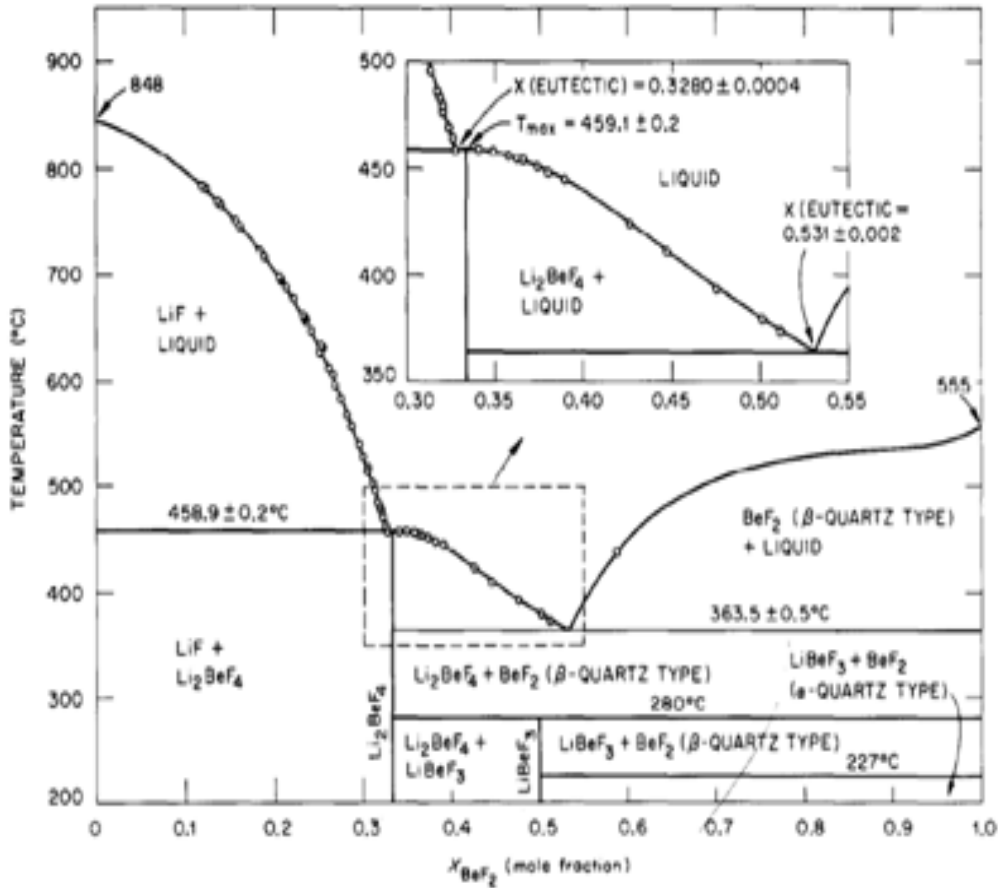
Figure 1-4. Lithium fluoride (LiF) and beryllium di-fluoride (BeF_2) eutectic phase diagram (Baes 1974).

The work reported herein is a significant intermediate step in reaching the final goal of commercial-scale deployment and usage of molten salt as the primary heat transport medium for process heat applications. The information presented in this report is based upon design and operational experience of a MSR, development program of MSBR, advanced high temperature reactor design (AHTR), and technological status and operating principles of fluoride salt-cooled high temperature reactor components. Various loops will be needed to overcome the present issues in the molten salt technology, but in this report a forced convection loop (FCL) is proposed to demonstrate confidence in the physical properties and heat transfer correlations through benchmarking, which would support large-scale deployment.

AHTR is a reactor concept that most closely relates to the objectives of the report because it has adopted molten salt cooling for both the primary and secondary loop, and it envisions operating conditions up to 1000ºC outlet temperatures. The AHTR is a new reactor concept that has three technical characteristics: high temperature, passive safety, and a large power output. The high temperature is required to produce hydrogen and efficiently produce electricity. The passive safety features are required to reduce operating costs and improve public acceptance. The large power output, passive safety features, and high efficiency of electricity production (a consequence of high temperatures) are the enabling technologies to improve economics. The development is a joint effort between ORNL, Sandia National Laboratories, and the University of California at Berkeley (Forsberg et al. 2003).

7

The AHTR uses coated-particle graphite-matrix fuels and a molten-fluoride-salt coolant. The fuel is the same type used in modular high temperature gas-cooled reactors (HTGRs), with fuel failure temperatures in excess of 1600ºC. The optically transparent molten salt coolant is a mixture of fluoride salts with freezing points near 400ºC and atmospheric boiling points of ~1400ºC. As mentioned elsewhere, several different salts are being evaluated as the primary coolant with FLiBe as the main candidate. The reactor operates at near-atmospheric pressure. At operating conditions, the molten-salt heat-transfer properties are similar to those of water. Heat is transferred from the reactor core by the primary molten-salt coolant to an intermediate heat-transfer loop. The intermediate heat-transfer loop uses a secondary molten-salt coolant to move the heat to the turbine. In the turbine, the heat is transferred to a multi-reheat nitrogen or helium Brayton cycle power conversion system. For hydrogen production, the heat is transferred to the thermochemical hydrogen production facility, which converts water and high-temperature heat to hydrogen and oxygen. A schematic of the AHTR system is shown in Figure 1-5, while the main operating parameters are listed in Table 1-2.
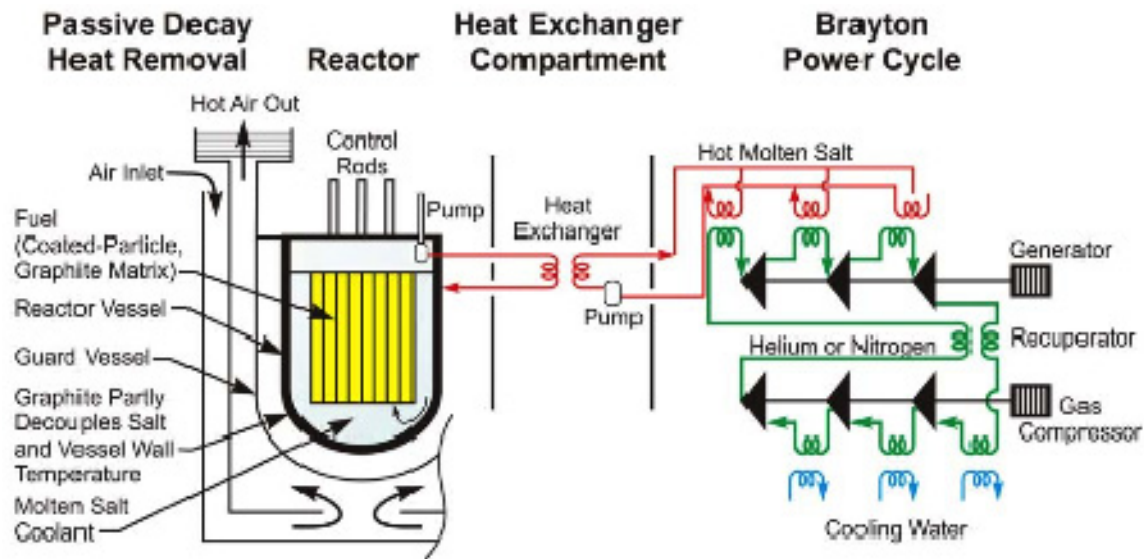
Figure 1-5. AHTR system schematic (Forsberg et al. 2003).

Table 1-2. AHTR main operating parameters (Forsberg et al. 2003).

Power level	2400 MW(t)	Power cycle	3-stage multi-reheat Brayton
Core inlet/outlet temperature	900°C / 1000°C	Electricity	1357 MW(e) at 1000°C
	700°C / 800°C 670°C / 705°C		1235 MWe at 800°C 1151 MWe at 705°C
Coolant	2 LiF - BeF$_2$	Power cycle working fluid	Nitrogen (Helium longer-term option)
	NaF – ZrF$_4$	Power cycle working fluid	Nitrogen (Helium longer-term option)
Fuel		Vessel	
Kernel	Uranium carbide / oxide	Diameter	9.2 m
Enrichment	10.36 wt% ^{235}U	Height	19.5 m
Form	Prismatic	Reactor core	
Block diam.	0.36 m (across flats)	Shape	Annular
Block height	0.79 m	Diameter	7.8 m
Columns	324	Height	7.9 m

Decay heat system	Air cooled	Fuel annulus	2.3
Volumetric flow rate	5.54 m^3/s	Power density	8.3 W/cm^3
Coolant velocity	2.32 m/s	Reflector (outer)	138 fuel columns
		Reflector (inner)	55 fuel columns

Recent studies have evaluated alternative salt compositions to FLiBe for various nuclear applications (Baes 1974, Williams et al. 2005, Williams 2006, Williams et al. 2006). No credible alternative was identified as coolant material for the core, primary circuit, or even heterogeneous fuel concepts in which the molten salt is only used as a heat transfer media. The main shortcomings of FLiBe are the increased sensibility of regulatory agencies to the toxicity of beryllium (and related licensing issues and handling costs), high Li content (resulting in the generation of large amounts of tritium), and high cost of fluoride raw materials. However, the neutronic properties of FLiBe are favorable when compared to other mixtures or chloride-based salts that FLiBe remains the main candidate material for reactor core cooling. On the other hand, several alternatives have been identified as heat transfer fluids in the secondary loop, which offer selected advantages with respect to some of the FLiBe shortcomings. Of those, the ternary fluoride eutectic LiF-NaF-KF (46.5, 11.5, 42 mol%, respectively), also known as FLiNaK, emerged as main alternative because of its low toxicity, excellent heat transfer properties, and chemical properties similar to those of FLiBe. This work therefore focuses on those two salt compositions, although many of the general considerations would apply to other materials. Fluoride salts (such as FLiBe and FLiNaK) have been considered as leading candidates to transfer heat from the NGNP to the hydrogen production plant because of its higher heat transfer capabilities. Four heat transfer molten salts have been identified as possible candidates for use in the secondary side for process heat applications. Several types of molten salt, including LiF-NaF-KF (46.5, 11.5, and 52 mol%, respectively; also known as FLiNaK), LiF-BeF$_2$ (67 and 33 mol%, respectively; also known as FLiBe), and KCl-MgCl$_2$ (67 and 33 mol%, respectively), have been investigated recently by several Japanese and U.S. groups, as well as the University of Wisconsin (KCl-MgCl$_2$ and FLiNaK) in support of fusion reactor and AHTR concepts, respectively.

The use of a liquid salt provides the potential for improved heat transfer and reduced pumping powers, but also introduces materials compatibility issues. Task et al. (2005) compared helium and liquid salt for the same given duty in a heat exchanger. If the log mean temperature difference is the same for both helium and liquid salt (50%LiF-50%BeF)2, the power required to pump the fluid through the heat exchanger is over 3½ times greater for helium than that for liquid salt. Also, the required volume of the heat exchanger is much higher for helium than that for liquid salt because liquid salt have much higher volumetric heat capacity. Since liquid salts are not as pressurized as helium, a leak in the system would not cause an extreme pressure difference in the plant. Molten salts have a 25% higher volumetric heat capacity than pressurized water, and nearly five-times that of liquid sodium as indicated by LeBlanc (2010a).

However, chloride salts, because of their high thermal neutron absorption cross section, have never been considered as a fuel salt or primary coolant. Chlorides could be used for primary coolants only if the salt is purified isotopically to 37Cl to avoid nuclear transmutation issues. However, because of the similarity of molecular structure and free energy of formation to fluoride salts, radiolytic and thermal stability is expected for the chlorides (Grimes et al. 1972). Molten chloride salts have long been used by industry for heat transfer, heat treatments, high-temperature electrochemical coatings, and other processes. The corrosion characteristics have been studied for some common structural alloys in a variety of salts, but few data have been generated for eutectic KCl-MgCl$_2$. Limited data have been published for some high-nickel alloys (Ambrosek 2010, Olson 2009, Sridharan et al. 2008). It is also very chemically stable across a wide range of temperatures, with boiling temperatures around 1400°C. Also, no gross chemical exothermal reactions take place between the reactor, intermediate loop, and power cycle coolants as explained by Renault et al. (2009).

Significant R&D efforts are needed to obtain much-needed technical information and resolve some of the issues in the molten salt technology. The current challenge is to achieve a significant advancement in nuclear technology while setting the stage for an economically viable deployment of new technology in the commercial sector. For that to happen, verification and validation has to be carried out at a forced convection test loop. The work reported herein is a significant intermediate step in reaching the final goal of commercial-scale deployment and usage of molten salt as the primary heat transport medium for process heat applications. Therefore, to support large-scale deployment, a forced convection test loop (FCL) is proposed to experimentally investigate thermophysical properties, thermal-hydraulics correlations, and chemistry control phenomena of the molten salt. The test loop could then be designed to resolve specific issues, such as: material issues, salt purification and chemistry, thermophysical properties (mainly heat capacity and conductivity values at higher temperature), uncertainty and validation existing in current theoretical models and correlations, and heat transport components behavior in liquid salt environments.

Therefore, construction of a forced convection engineering-scaled loop like the FCL is being proposed at INL in collaboration with ORNL to study the problems and issues. The operation of such a loop is expected to resolve many of the remaining uncertainties in coolant salt technology. The main purpose of this report is to discuss a proposed loop, point out the importance of these remaining uncertainties, identify the further work needed, and assess the probability of success in obtaining reliable components and systems.

1.3 Thermodynamic and Thermophysical Properties of Molten Salts

In the liquid state, molten salts' viscosity and appearance are similar to water. A mixture of sodium and potassium nitrate, with a melting temperature of ~222°C, is commonly used in solar applications. A primary advantage of molten salt technology is that the molten salt can be heated to ~560°C, which allows high-energy steam to be generated at utility-standard temperatures (11.4 MPa, 550°C), achieving high thermodynamic cycle efficiencies of approximately 40% in modern steam turbine systems. Table 1-3 lists the thermophysical properties of several types of molten salts.

Table 1-3. Some thermophysical properties of molten salts of interest and a few others for reference.

Molten salt coolant	Mol % (Wt%)	Formula Weight (g/mol)	Freezing/ Melting Point (K)	Boiling Point (K)	Density (kg/m³)	Specific Heat Capacity (J/kg K)	Viscosity (Pa·s)	Thermal Conductivity (W/m K)	Prandtl No.
LiF-NaF-KF (FLiNaK)	46.5-11.5-42 (29-12-59)	41.3	727	1843	2020	1882.8	0.0029	0.92	5.938
LiF-BeF$_2$	67-33 (53-47)	33.0	733	—	1940	2414.17	0.0056	1.0	13.525
KCl-MgCl$_2$	68-32 (62-38)	81.44	708	—	1664	1158.97	0.0014	0.40	4.0
NaNO$_3$-NaNO$_2$-KNO$_3$ @ 400°C	7- 49 - 44 (7- 40 -53)	1.77-1.98	415	—	1790	1560	0.0013-0.0016	0.51-0.605	—
NaNO$_3$- KNO$_3$ @ 400°C	48-52	93.37	495	—	1840	2660.19	0.0017	0.55	8.222
LiF-NaF-BeF$_2$	—	38.9	588	—	2000	2045.98	0.005	0.97	10.551
LiF-NaF-RbF	—	67.7	708	—	2690	987.42	0.0026	0.62	4.14
NaF-BeF$_2$	—	44.1	613	—	2010	2175.68	0.007	0.87	17.513
H$_2$O @ 20°C	—	18	273	—	1000	4184	0.001	0.6	7
He (P = 7.5 MPa)	—	4	—	—	3.8	5505.31	0.000042	0.29	0.8
Na @ 550°C	—	23	370.8	—	820	—	0.00023	62	0.004

Heat transfer characteristics of molten salts depend on their thermophysical properties. The fundamental properties for heat transfer applications are those considered in the nondimensional analysis leading to engineering correlations for heat transfer based on the Nusselt, Reynolds, and Prandtl numbers. Those are:

- Density, ρ (kg/m^3)

- Specific heat capacity, Cp (J/kg·K)

- Viscosity, μ (Pa·s)

- Surface tension, γ (N/m)

- Thermal conductivity, k (W/m·K).

In ideal conditions for each eutectic composition, those properties are a function of the temperature only. However, for molten salt, their experimental determination presents unique challenges when compared to traditional heat transfer fluids (Lovering and Gale 1983). The major challenges include:

- High temperature range, often incompatible with commercial instruments

- Limited material compatibility to contact salt's liquid or vapor phase

- Difficulty of controlling composition, both in terms of eutectic mixture and of impurities concentrations, particularly for small batches.

Those handling challenges and the necessity of developing ad hoc instruments result in limited accuracy and repeatability of the measurements. The already-cited report developed as part of this project provides a complete assessment of the available database of measured properties and citations to available references for several salt compositions (Sohal et al. 2010). Summary plots for FLiBe and FLiNaK are reported here in Figures 1-6 through 1-11. The main reason is to identify the limitation of the existing database, particularly in the higher temperature range of interest for VHTR applications. Based on this assessment, an experimental test aimed at developing molten salt heat transfer components would have to include the capability of measuring the salt thermophysical properties to the upper temperature range of interest. In particular, experimental needs include:

- Extend properties database to high temperature range.

- Investigate temperature dependence and establish correlation for design studies across a wider operating range: some properties, in particular thermal conductivity, were assumed constant across the small temperature range of MSRE operations, and the assumption is commonly extrapolated to higher temperatures. However, experimental verification is required since conductivity is the single most important physical property for heat transfer analysis.

- Improve accuracy and repeatability of measurements by diagnostic system development: a renewed effort must be made to test the accuracy of properties data with improved and more accurate measuring instrumentation that can take advantage of technological improvements since MSRE operation.

- Consider the effect of salt mixture composition variation on thermophysical properties: heat transfer components are part of a complex system with interfaces to process fluids, pumping equipment, etc. Because of material compatibility issues or impurities contamination, the salt composition in such systems is dynamically changing, with average composition maintained by chemistry control. However, local or transient variations in composition are expected. It is therefore necessary to evaluate heat transfer properties not only for the reference salt composition, but also within the composition variations expected in a real system.
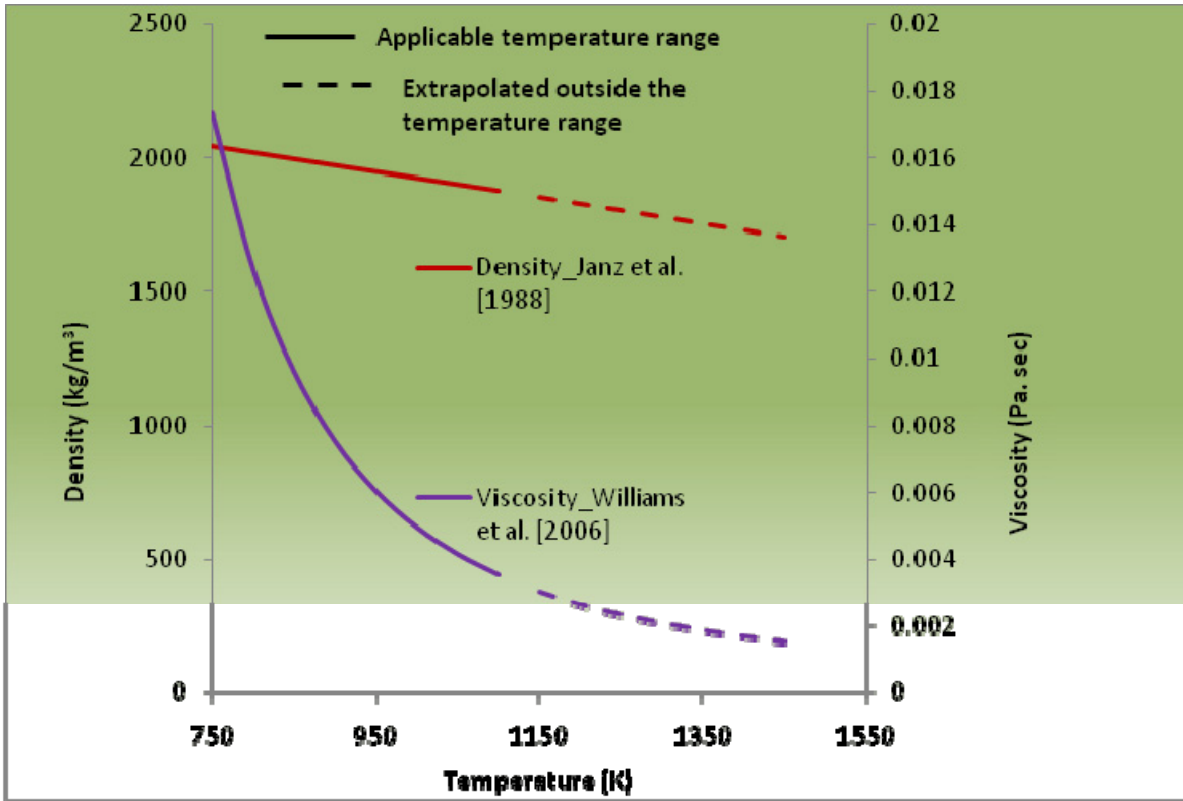
Figure 1-6. FLiBe density and viscosity.
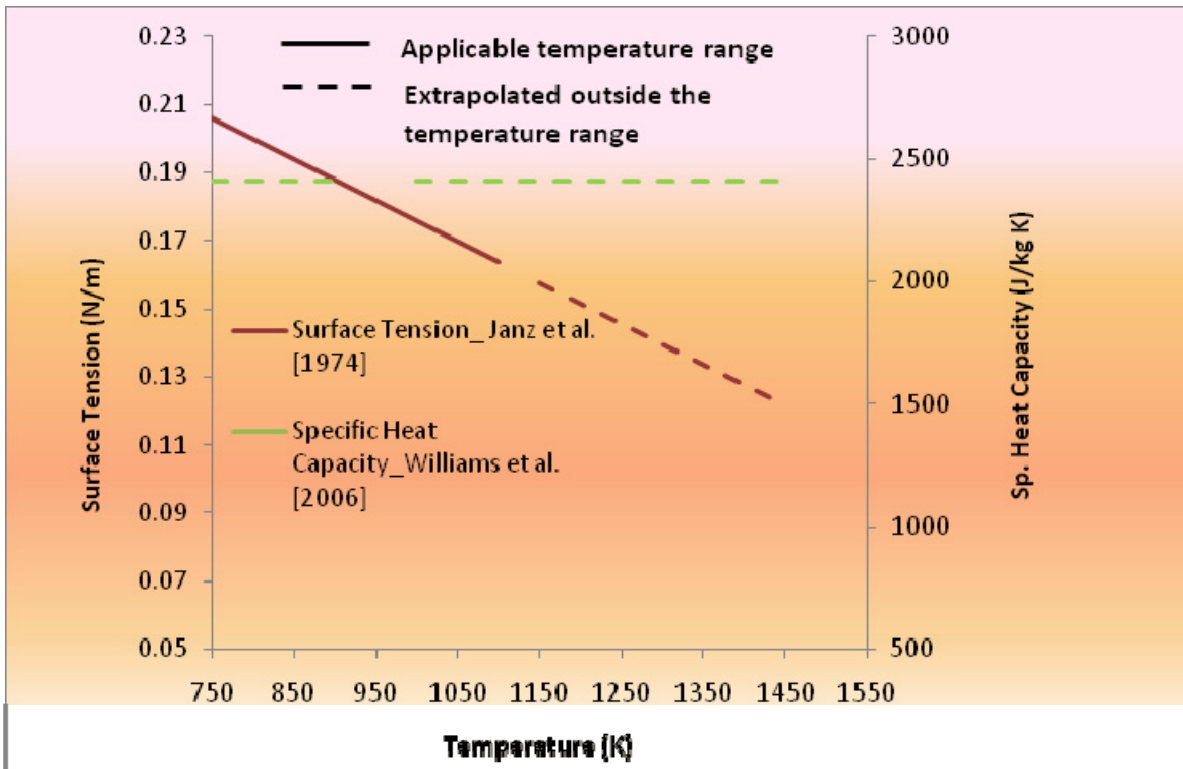
Figure 1-7. FLiBe surface tension and specific heat capacity.
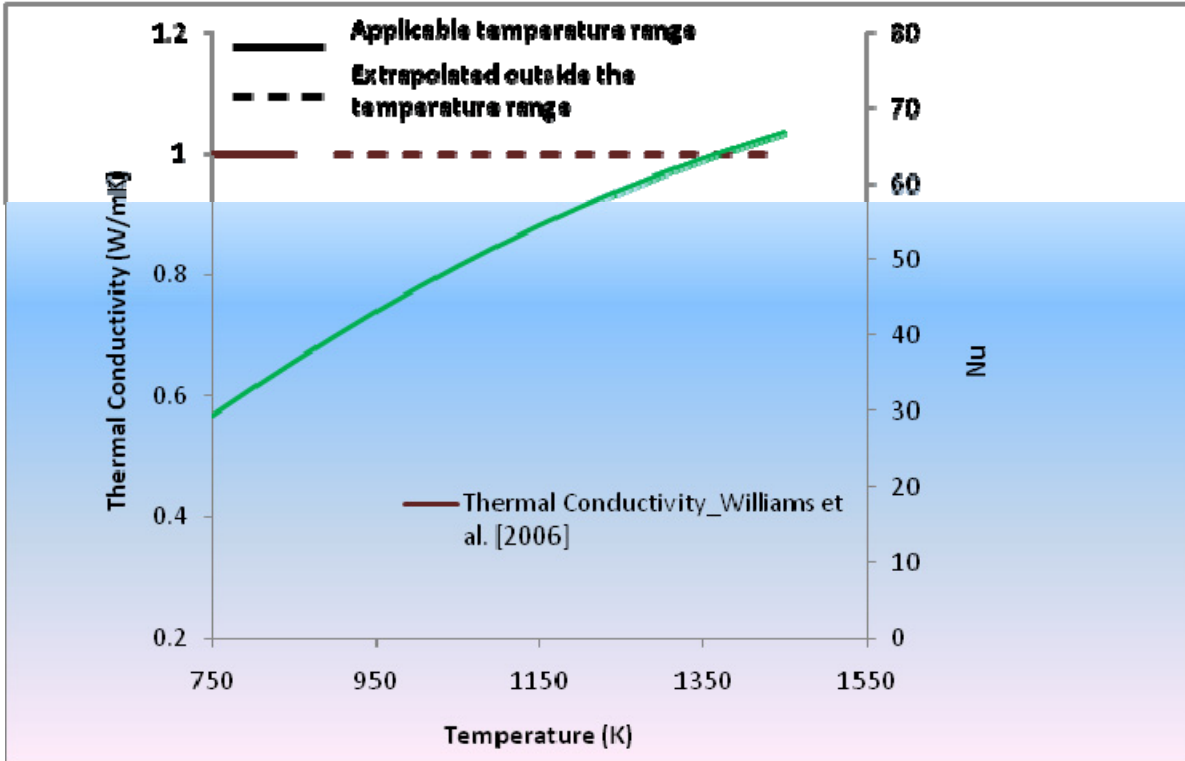
Figure 1-8. FLiBe thermal conductivity and Nusselt number according to Dittus-Boelter correlation.
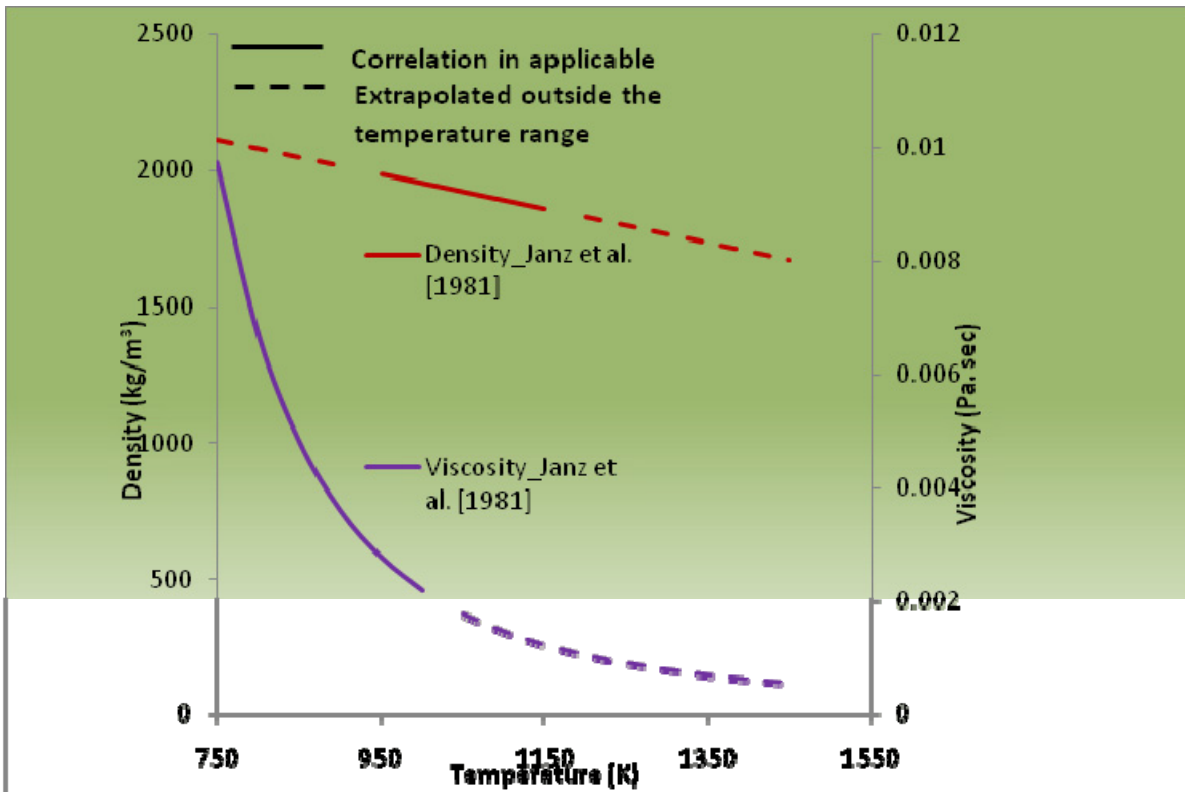
Figure 1-9. FLiNaK density and viscosity.
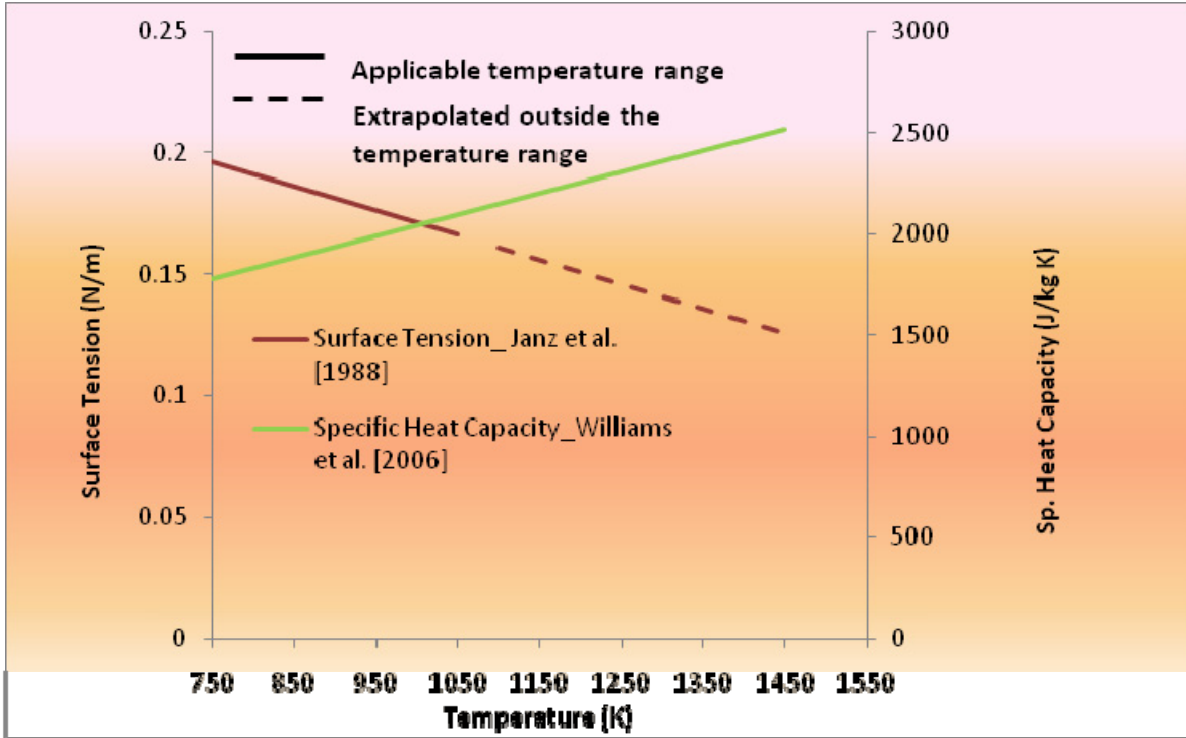
Figure 1-10. FLiNaK surface tension and specific heat capacity.
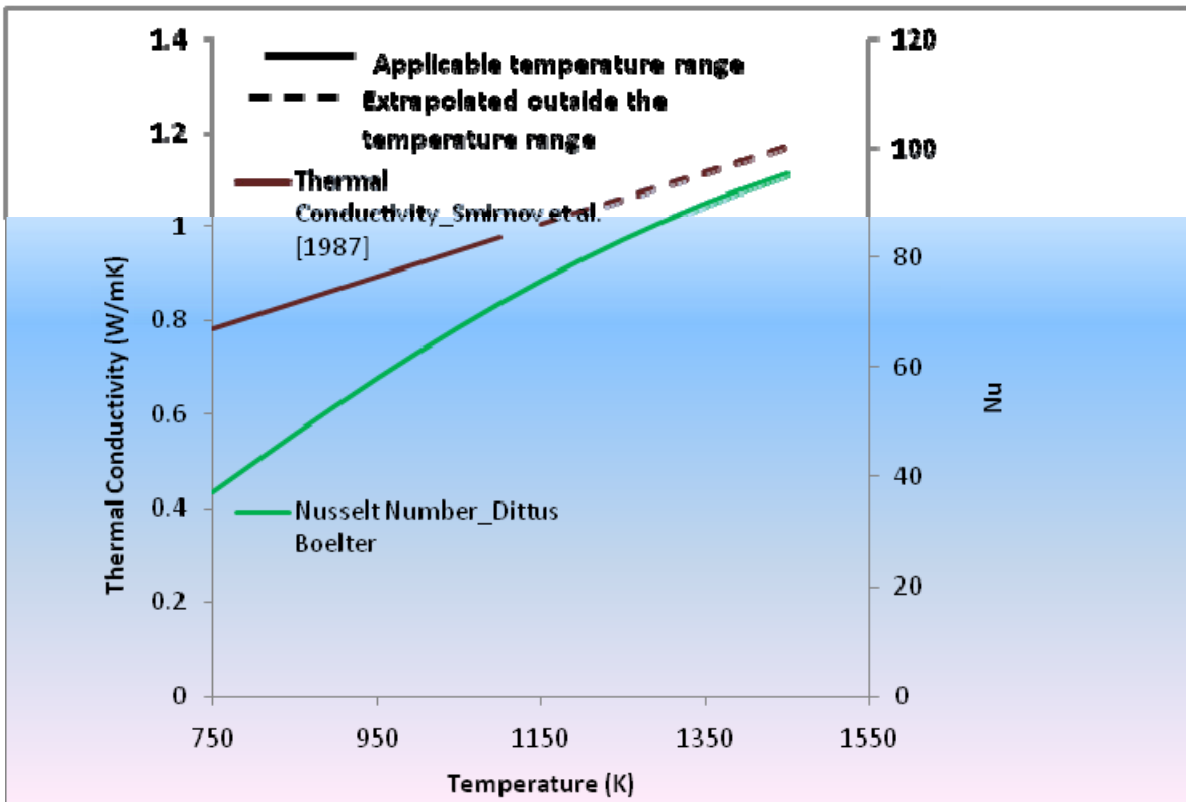
Figure 1-11. FLiNaK thermal conductivity and Nusselt number according to Dittus-Boelter correlation.

14

1.4 Correlations for Convective Heat Transfer in Molten Salts

The heat transfer coefficient is an important concept for heat exchanger design, as it quantitatively represents the convective heat flux per unit of temperature difference as explained in detail by Sabharwall et al. (2008).The heat transfer coefficient is often derived from dimensionless groups, such as Nusselt Number (Nu) and Prandtl Number (Pr). Heat transfer characteristics of molten salts depend on thermophysical properties. Therefore, in this section, simple convective heat transfer data and corresponding correlations applicable for molten salts are briefly reviewed. The objective is to establish the effect of the thermophysical properties that significantly impact the Nusselt number calculations.

Ambrosek et al. (2009) showed that for FLiNaK salt, the Dittus-Boelter correlation (Equation 1-1) predicts convective heat transfer by ~15% higher than the experimental data. The analysis of the experimental data using either Smirnov et al.'s (1987) correlation for thermal conductivity, or the value of 1.0 W/m·K, which shows that the experimental convective heat transfer data over-predict the Dittus-Boelter correlation by ~15% for the Reynolds numbers range of ~10,000 to 100,000.

Liu et al. (2009) performed experiments with molten salt ($LiNO^3$) in the Reynolds number range of 19,800 to 46,000. The Pr of $LiNO_3$ is in the range of 12.7 to 14.7. They used the well-known convective heat transfer correlations by Dittus-Boelter, Sieder-Tate, Hausen, and Gnielinski. These correlations are shown in *Equations (3-1)* through *(3-4)*:

Dittus-Boelter: $Nu = 0.023\ Re^{0.8}\ Pr^{n}$, where $0.3 < n < 0.4$ (1-1)

Sieder-Tate: $Nu = 0.0242\ Re^{0.81}\ Pr^{0.333}\ (\mu_b/\mu_w)^{0.14}$ (1-2)

Hausen: $Nu = 0.037\ (Re^{0.75} - 180)\ Pr^{0.42}\ (1 + d/l)^{2/3})\ (\mu_b/\mu_w)^{0.14}$ (1-3)

Gnielinski: $Nu = 0.012\ (Re^{0.87} - 280)\ Pr^{0.4}\ (1 + d/l)^{2/3})\ (Pr_b/Pr_w)^{0.11}$ (1-4)

Liu et al. (2009) determined that Dittus-Bolter (*Equation [1-1]*) and Colburn (*Equation [1-2]* without the viscosity ratio) correlations under-predict their molten salt data by about 25% and 18%, respectively. They correlated their Nu data with the Dittus-Boelter type equation given in *Equation (1-5)*, which correlation predicts their data within ±10%:

$Nu = 0.024\ Re^{0.807}\ Pr^{0.301}$.   (1-5)

Liu et al. (2009) data can also be predicted within ±10% with Sieder-Tate *Equation (1-2)*. The Pr of molten salt changes from 12.7 to 14.7. To take into account these variations, Liu et al. (2009) correlated their data with a Sieder-Tate-type convective heat transfer equation shown in *Equation (1-2)*. To account for molten salt Pr variation (changing from 12.7 to 14.7), Liu et al. (2009) concluded that a Dittus-Boelte-type correlation with $Pr^{0.4}$ correlates data satisfactorily. Based on the Gnielinski correlation, Wu et al. (2009) developed a slightly modified correlation as:

$Nu = 0.012\ (Re^{0.87} - 280)\ Pr^{0.4}\ (1 + d/l)^{2/3})\ (Pr_b/Pr_w)^{0.11}$.   (1-6)

Liu et al. (2009) data correlates satisfactorily, within ±15%, with the correlations by Wu et al. (2009) (*Equation 1.6*), Gnielinski (*Equation 1-4*), and Hausen (*Equation 1-3*). Two correlations, *Equation (1-6)* and Gnielinski (*Equation 1-4*), were used to correlate the data, and these show that an exponential of 0.4 on Pr can correlate the molten salt data satisfactorily. Figures 1-12 through 1-15 compare these correlations with data and emphasize the need for more accurate data.

These correlations show that some thermophysical properties need to be adequately acounted for, which has been accomplished by Wu et al. (2009) with a Pr exponential of 0.4 and bulk and wall viscosities ratio.
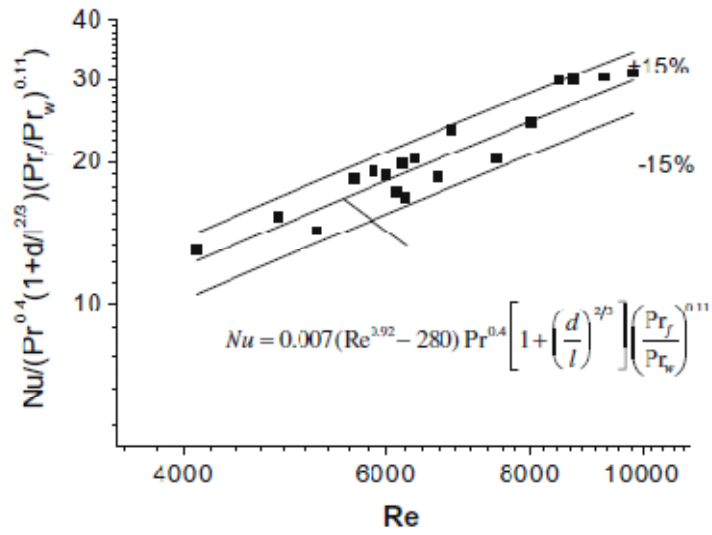
Figure 1-12. Correlation of Liu et al. (2009) molten salt data with *Equation (1-6)* (Wu et al. 2009).
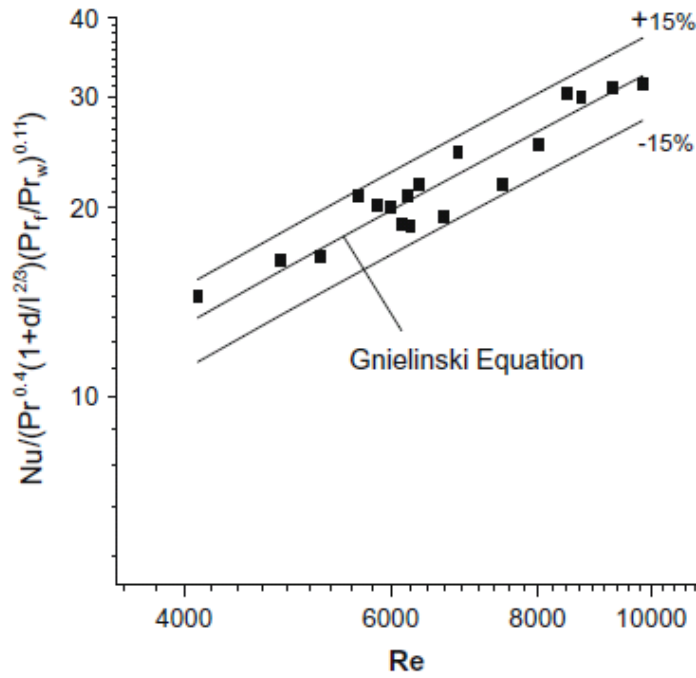
Figure 1-13. Correlation of Lu et al. (2009) molten salt data with Gnielinski (*Equation [1-4]*) (Wu et al. 2009).
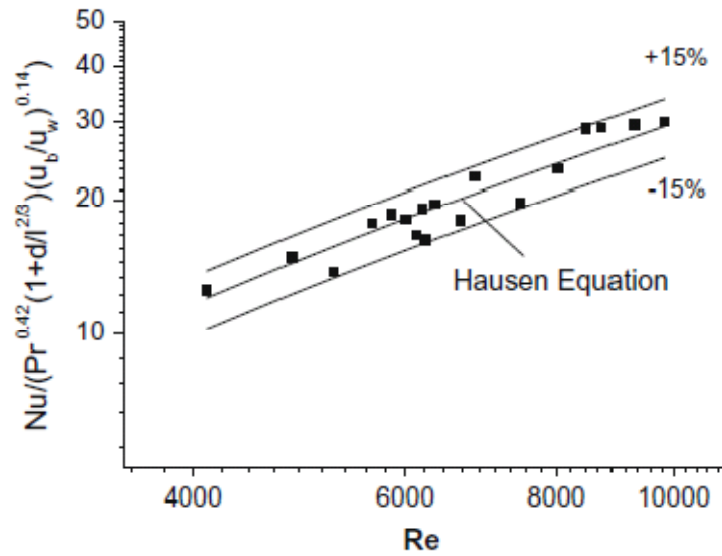
Figure 1-14. Correlation of Lu et al. (2009) molten salt data with Hausen, *Equation (1-3)* (Wu et al. 2009).
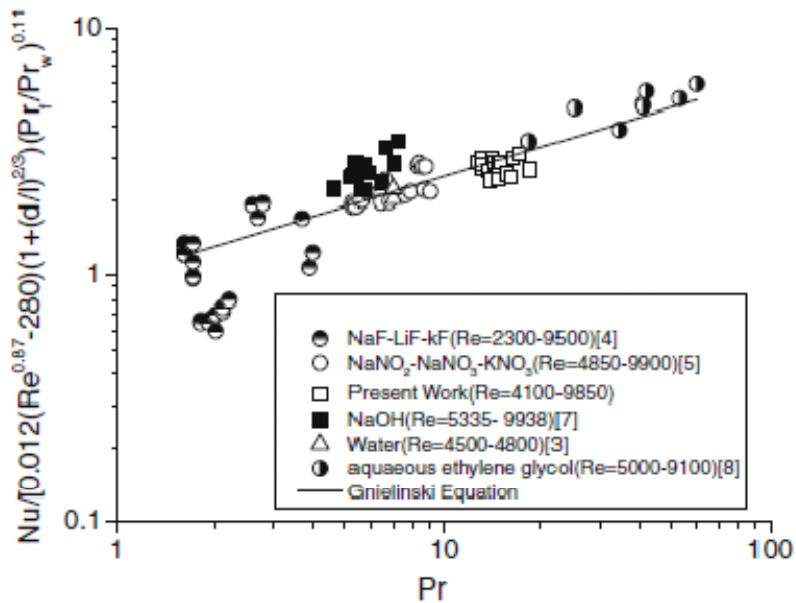
Figure 1-15. Thermophysical properties dependency in terms of Pr exponential derived from convective heat transfer data for molten salts and some other fluids (Wu et al. 2009).

2. SCALING ANALYSIS TO DESIGN A TEST LOOP

The subject of scaling is very complex, and in principle, a scale-down experimental facility can be designed at a linear scale, but it is more important to ensure that the relevant thermal-hydraulic phenomena are preserved in the model. To design the convection loop, one has to answer a question relating to the suitability and accuracy of the proposed design. When the data from the loop are obtained, one has to evaluate its scalability for application in a full-size plant. The overall objective of a scaling analysis is to obtain the physical design and operating conditions of a smaller scale test facility capable of simulating heat transfer and fluid flow phenomena of the full-scale nuclear reactor system under investigation. All the scaling requirements for all the processes cannot be simultaneously met in a model. This section discusses these issues and introduces basic methodology to resolve some of these questions.

2.1 Scaling Analysis for Scale-down Systems

The scaling studies related to nuclear plant certification has been a topic of great importance. During 1980s and 1990s, many U.S. researchers established scaling parameters to build integral test systems to test and predict thermal hydraulic phenomena in nuclear reactors. They also established the methodology to achieve desired objectives. The bulk of the material included in this section is provided by Kocamustafaogullari and Ishii (1983); Ishii and Kataoka (1984); Ishii et al. (1998); Ransom, Wang, and Ishii (1998); Vijayan and Austregesilo (1994); Yadigaroglu and Zeller (1994); Wulff (1996); Reyes and Hochreiter (1998); Reyes (2007); and Zuber (2001).

Traditional scaling analyses consist of first normalizing the conservation equations on the subsystem or component level for the test section, then repeating this subsystem level scaling for all the components in the system and collecting all the local scaling criteria into a set of system scaling criteria. The claim is then made that the dynamic component interaction and the global system response should be scaled successfully with the set of criteria for local component scaling, because the system is the sum of its components. This principle applies only if all the local criteria are met and complete similitude exists. Complete similarity, however, is physically impossible, because all scaling requirements cannot be met simultaneously for a system in which areas and volumes and, therefore, area-dependent transfer rates and volume-dependent capacities, scale with different powers of the length parameter, thereby producing conflicting scaling requirements.

According to Reyes (2001, 2007), the following specific objectives must be met to develop a scaled test facility:

- Identify the thermal hydraulic phenomena that should be modeled

- Obtain the similarity criteria that should be preserved between the full-scale prototype and test facility

- Establish priorities for preserving the similarity criteria

- Design the scale-down test facility

- Quantify biases due to scaling distortions

- Identify the critical attributes of the test facility that must be preserved to meet Quality Assurance requirements.

2.2   Scaling Procedure

Yadigaroglu and Zeller (1994) described four main categories of scaling approaches:

1. *Linear Scaling*: In linear scaling, all length ratios are preserved and the mass, momentum, and energy equations of a system are nondimensionalized. The resulting parameters derived from these conditions will lead to distortion in time scale of the scale-down system.

2. *Time (or Flow Length) Preserving Scaling*: This technique also is based on scaling parameters coming from the nondimensionalized conservation equations. Models scaled by this technique preserve the flow lengths, while areas, volumes, flow rates, and power are reduced proportionally in the scaled-down model.

3. *Time-Distorted Scaling*: Ishii and Kataoka (1984) developed these criteria for natural circulation loop where the designer has the flexibility to choose the height of the model. This scaling method becomes quite complex because the driving forces for natural convection and heat transfer processes are coupled.

4. *Hierarchical Two-Tiered Scaling (H2TS)*: A "structured" scaling methodology, also termed as hierarchical two-tiered scaling (H2TS), was proposed by Zuber (1991). In this approach, shown in Figure 2-1, the scaling issues are addressed in two tiers: a top-down system approach, followed by a bottom-up, process and phenomena approach, because component-level scaling and traditional local level scaling alone cannot produce the scaling criteria for component interaction.

The H2TS analysis method presents the four basic steps. The first step consists of subdividing the plant into a hierarchy of systems. Each system is subdivided into interacting subsystems, which are subdivided into interacting modules, which are subdivided into interacting materials, which are subdivided into interacting matter (liquid or solid). Each matter can be characterized by one or more geometrical configurations and each geometrical configuration can be described by three field equations (mass, energy, and momentum conservation equations). Each field equation can incorporate several processes.

The top-down scaling analysis describes how the fluid velocity and mass flow rate would be expected to scale with the model size. The governing control volume balance equations are written and expressed in dimensionless form by specifying dimensionless groups in terms of the constant initial and boundary conditions. The simplifying assumptions are as follows:

*   Steady-state flow

*   One-dimensional flow along the loop axis

*   Uniform fluid properties at a given cross section

*   Chemical equilibrium

*   No phase change

*   Viscous effects included in form losses.

The assumptions listed above are used to write the conservation equations such as mass, momentum, and energy equations. These equations are integrated to obtain loop balance equations. The purpose is to use the conservation equations at a given scaling level to obtain characteristic time ratios and similarity criteria. It also identified the important processes to be addressed in the bottom-up scaling analysis.
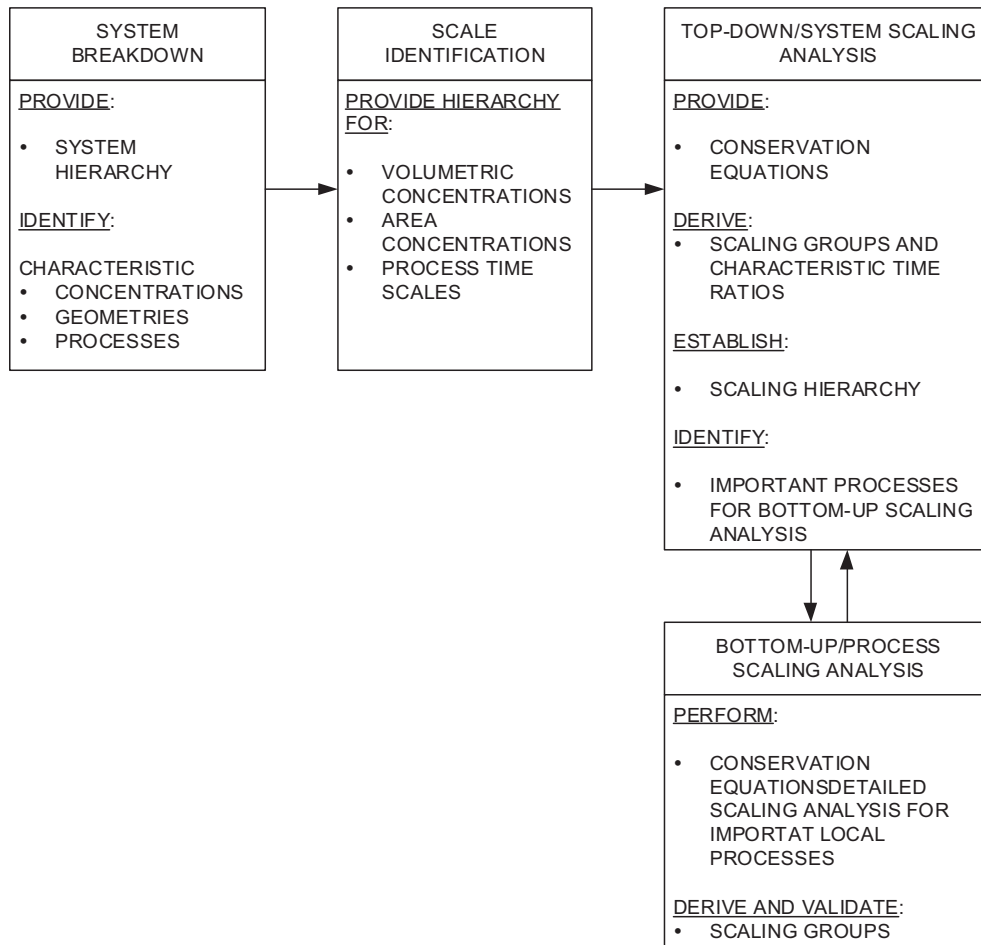
Figure 2-1. Flow diagram for the hierarchical, two-tiered scaling analysis (Zuber 1991).

Bottom-up scaling analysis is used to provide closure relations for the characteristic time ratios. The closure relations consist of models or correlations for specific processes. The focus of the closure relations are used to develop the final form of the scaling criteria for purposes of scaling the individual processes of importance to system behavior as identified by the Phenomena Identification and Ranking Table (PIRT). This analysis provides similarity criteria for specific processes such as flow dependent heat transfer.

The H2TS approach is further explained by Wulff (1996) and Reyes and Hochreiter (1998). The following is a summary of this approach.

4.a Thermal Hydraulic Phenomena: Identify the dominating thermal hydraulic phenomena, processes, and characteristics that should be reproduced in the test loop. Based on the phenomena to be studied, specific design tests can be defined. For example, if heat transport is the main phenomenon to be studied, then Reynolds number and Nu become important criteria.

4.b Phenomena Identification and Ranking Table (PIRT): Establish priority (ranking) of preserving the similarity criteria, i.e., develop PIRTs as shown in Figure 2-2. In the PIRT analysis, the phenomenon significantly affecting the process is ranked "High" (H) while other phenomena can be ranked "Medium" (M) or "Low" (L). Alternately, one could even rank the phenomena on a scale of 1 to 5 (low to highest). A "Not Applicable" (or 0) ranking means that the phenomenon has no impact on the system under study.

```
          ┌─────────────────────────┐
          │  Define Evaluation Criteria
          │  and Ranking Method
          │
          │  • Impact on PCT?
          │  • Impact on Core Liquid
          │    Level?
          │  • Rank H, M, L
          └─────────────────────────┘
```

┌──────────────────────┐   ┌─────────────────────────┐   ┌─────────────────────────┐
│ Existing Related PIRTs│   │ Establish PIRT Framework│   │ Full-Scale Plant Data
│   │   │   │   │ (Prototype)
│   │   │ • Partition Scenario into
│   │   │   Time Phases
│   │   │ • Partition Plant into
│   │   │   Components
│   │   │ • Identify Phenomena
└──────────────────────┘   └─────────────────────────┘   └─────────────────────────┘

          ┌─────────────────────────┐
          │   Expert Ranking
          │
          │ • Rank Components and
          │   Phenomena
          │ • Document Rationale
          └─────────────────────────┘
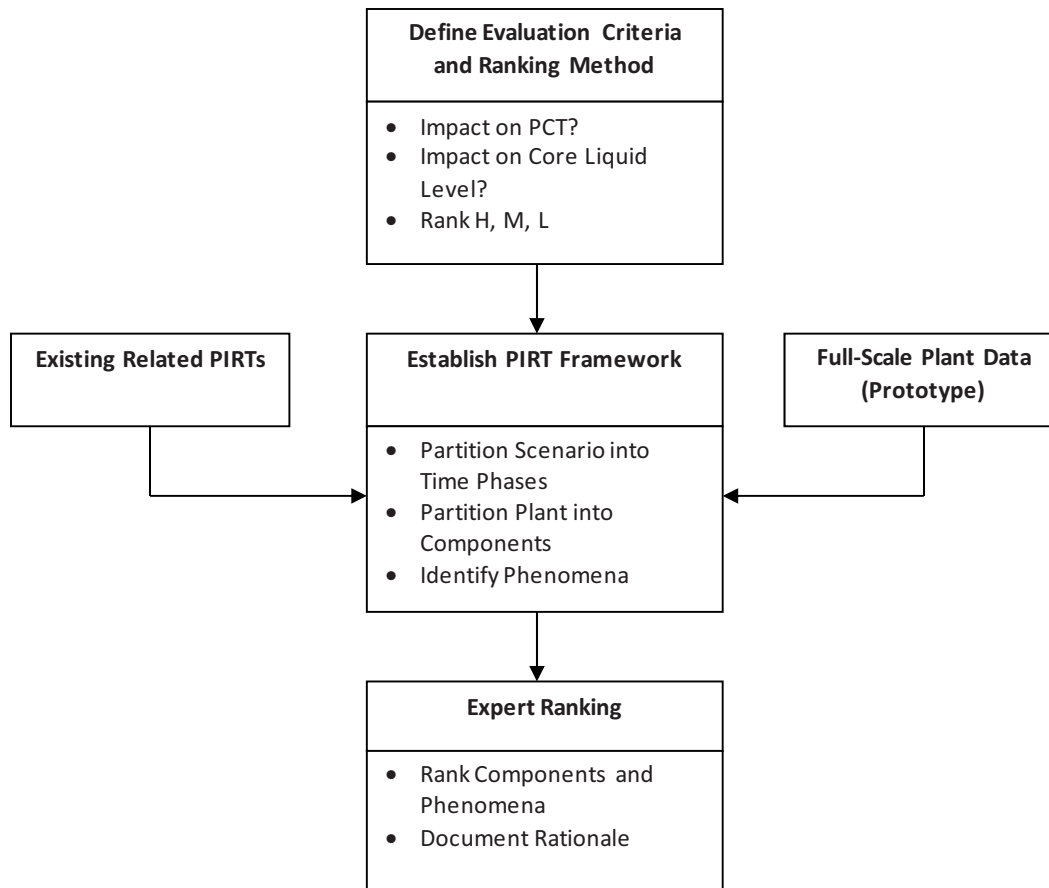
Figure 2-2. Process used to develop PIRTs (Reyes 2001).

4.c Similarity Criteria: Establish the similarity criteria that need to be preserved between the full-scale plant and the test facility. After obtaining the pertinent set of similarity criteria, a set of scale ratios can be determined to specify the physical dimensions of the test facility, initial conditions, and boundary conditions.

Similarity groups can be derived using several methods, but two fundamental principles of scaling must be met (Wulff 1996).

The governing equations are normalized such that the normalized variables and their derivatives with respect to normalized time and space coordinates are of order unity, and the magnitude of the normalized conservation equation is measured by its normalizing, constant coefficient.

The governing equations are then scaled by division through the coefficient of the driving term; this renders the driving term of order unity and yields fewer nondimensional scaling groups, which measure the magnitudes of their respective terms, and therewith the importance of the associated transfer processes relative to the driving term.

It is nearly impossible to simultaneously satisfy all the similarity criteria, so a set of similarity criteria that must be satisfied (as identified in the PIRT table) are developed, which results in a set of characteristic dimensionless Π group. These dimensionless ratios in a prototype must match those in the model at each level. That is,

$$\Pi_m = \Pi_p \text{ or } \Pi_m/\Pi_p = 1. \tag{2-1}$$

The similarity criteria for a single-phase system can be obtained by considering the one-dimensional, area-averaged conservation equations for continuity, momentum, and energy for the loop. By nondimensionalizing the equations and applying the boundary conditions, nondimensional groups—characterizing geometric, kinematic, dynamic, and energy-exchange parameters—can be derived. Each similarity criterion can be satisfied by adjusting the physical geometry, fluid properties, and operating conditions of the model, which will provide guidelines for the model design. Ishii and Kataoka (1984) have derived the similarity groups given in Table 2-1.

Table 2-1. Dimensionless groups for the segment I of a single-phase loop, Ishii and Kataoka (1984). Subscripts 0 denote the reference scale of a variable, while s refers to the solid wall.

Nondimensional Number	Parametric Definition	Physical Representation
Richardson, R_i	$\dfrac{g\beta\,\Delta T_0 l_0}{u_0^2}$	$\dfrac{Buoyancy}{Inertia\ Force}$
Friction, F_i	$\left(\dfrac{4fl}{d_h}+K\right)_i \left(\dfrac{a_0}{a_i}\right)^2$	$\dfrac{Friction}{Inertia\ Force}$
Modified Stanton, St_i	$\left(\dfrac{4h\,l_0}{\rho\,C_p\,u_0 d_h}\right)_i$	$\dfrac{Wall\ convection}{Axial\ convection}$
Wall time ratio, T_i^*	$\left(\dfrac{a_s\,l_0}{\delta^2\,u_0}\right)_i$	$\dfrac{Axial\ transport\ time}{Wall\ conduction\ time}$
Biot, Bi_i	$\left(\dfrac{h\delta}{k_s}\right)_i$	$\dfrac{Convection}{Wall\ conduction}$
Heat source, Q_{si}	$\left(\dfrac{q_s'''l_0}{\rho_s C_{ps}u_0\Delta T_0}\right)_i$	$\dfrac{Heat\ Source}{Wall\ heat\ capacity}$
Length ratio, L_i	$\dfrac{l_i}{l_0}$	
Area ratio, A_i	$\dfrac{a_i}{a_0}$	

4.d Allowable Distortion: Ensure optimal similarity and smallest scale distortions. If the operating condition of the scale-model introduces significant distortions, another iteration of scaling may be required by changing perhaps the length scale, or volume scale, or working fluid. The distortion introduced by the scale model is evaluated by calculating the distortion factor (DF) as follows:

$$DF = \frac{[\Pi_i]_p - [\Pi_i]_m}{[\Pi_i]_p} \tag{2-2}$$

The DF represents the fractional difference in the amount of conserved physical property transferred through a specific process occurring in the prototype to the amount of conserved physical property transferred through the same process in the model during the respective residence times. It means that a DF of zero implies that the model simulates the physical process perfectly.

4.e Design: The parametric design of the reduced-size test facility should be completed. The outcome of the scaling analysis is, therefore, a set of characteristic time ratios (dimensionless Π groups) and similarity criteria for each mode of operation. These scaling criteria are expressed in terms of ratios of model to prototype fluid properties, material properties, and geometrical properties. Next, working fluid, component materials, operating pressure, and the length, diameter, and time scales can be selected.

4.f Test Matrix: The conditions for operating experiments (test matrix) should to be developed, such that at least the dominant phenomena taking place in the full-size plant are reproduced in the experimental test facility over the range of plant conditions.

The above methodology is summarized by Reyes (2001), as shown in Figure 2-3.
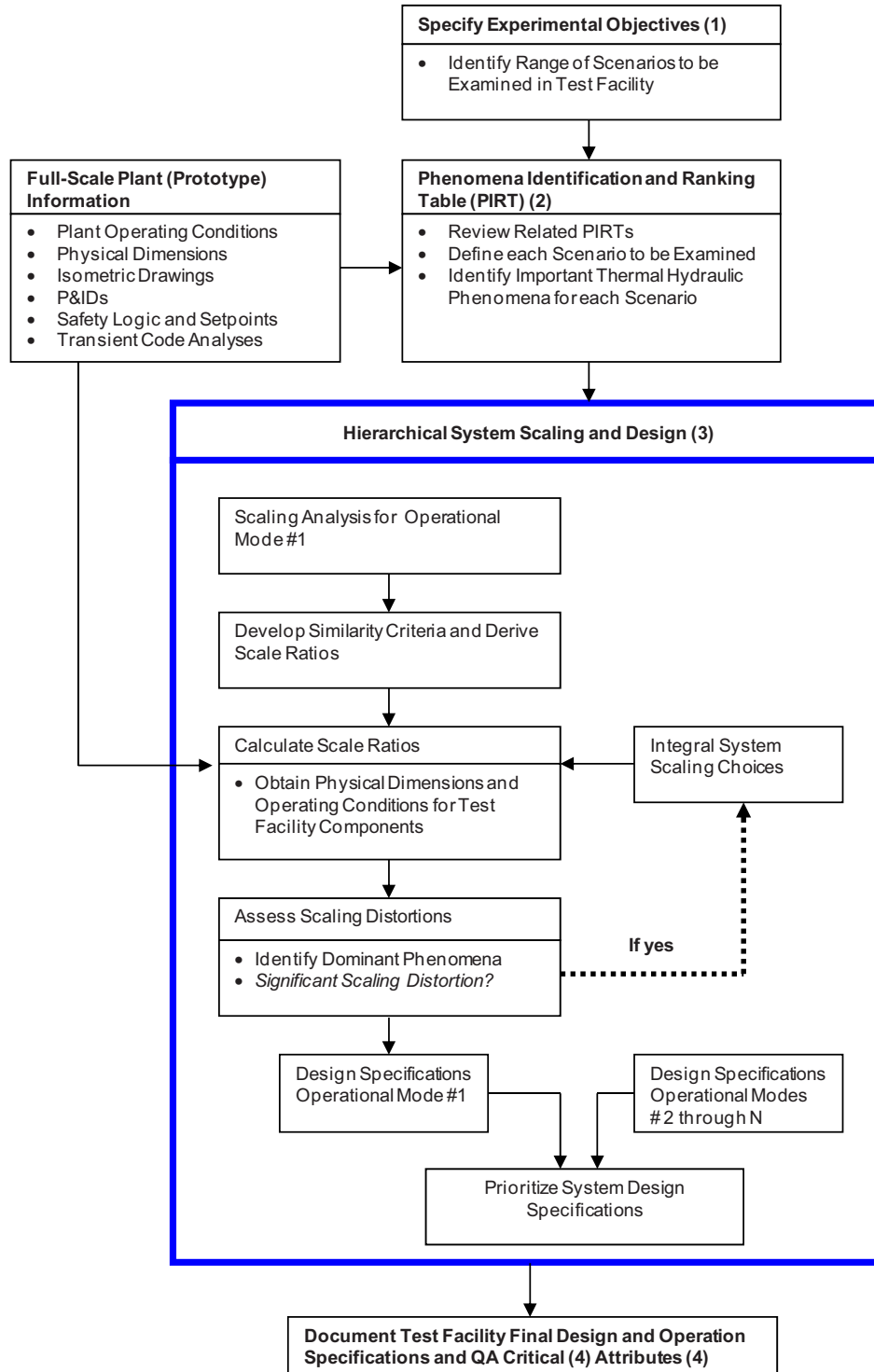
Figure 2-3. Summary of scaling procedure (Reyes 2001).

The similarity criteria for a single-phase fluid circulation loop are obtained by setting the model-to-prototype ratios of each dimensionless group (some shown in Table 2-1) to unity. Expressions for the time, length, and velocity scale ratios are obtained using the ratio of the characteristic time constant and the steady-state solution for the fluid velocity at the core inlet. The flow area scale ratio is set to unity to preserve the kinematic behavior within the loop components. To obtain a closed set of design parameters, the designer must select values for the time, length, flow area, and the loop resistance scale ratios. In the present context, the working fluid is expected to be the same for the test loop. Reyes (2001, 2007) has given the details of the governing equations for natural convection, dimensionless balance equations, initial and boundary conditions, dimensionless groups, and many length and time ratios. These equations can provide guidelines for a case when the test loop needs to be scaled and designed. However, these equations cannot be used as is for the specific case of molten salt loop design. Just for the sake of completeness, an example of these equations from Reyes (2001, 2007) is given here in Section 2.3.

2.3   An Example of Governing Equations for Scaling

For single-phase "natural circulation," Reyes (2001, 2007) proposed following governing equations and normalizing ratios. However, appropriate modifications need to be made for molten salt forced convection loop design. The objective of this report is to establish the procedure that needs to be taken to develop correct governing equations in the future, if warranted. Therefore, *Equations (2-3)–(2-29)* should be used only to provide guidelines for the scaling of a molten salt loop and must not be taken as the governing equations for the proposed loop design.

Loop momentum balance equation:

$$\sum_{i=1}^{N}\left(\frac{l_i}{a_i}\right)\cdot\frac{d\dot{m}}{dt} = \beta g \rho (T_H - T_C)L_{th} - \frac{\dot{m}^2}{\rho_l a_c^2}\sum_{i=1}^{N}\left[\frac{1}{2}\left(\frac{fl}{d_h}+K\right)_i\left(\frac{a_c}{a_i}\right)^2\right]$$

(2-3)

Loop energy balance equation:

$$C_{vl}M_{sys}\frac{d(T_M - T_C)}{dt} = \dot{m}C_{pl}(T_H - T_C) - \dot{q}_{SG} - \dot{q}_{loss}$$

(2-4)

Dimensionless initial and boundary conditions

$$t^+ = \frac{t}{\tau_{loop}}$$

(2-5)

$$\dot{m}^+ = \frac{\dot{m}}{\dot{m}_o}$$

(2-6)

$$\dot{q}_{SG}^+ = \frac{\dot{q}_{SG}}{\dot{q}_{SG_o}}$$

(2-7)

$$\dot{q}_{loss}^+ = \frac{\dot{q}_{loss}}{\dot{q}_{loss_o}}$$

(2-8)

$$(T_M - T_C)^+ = \frac{(T_M - T_C)}{(T_M - T_C)_o} \tag{2-9}$$

$$(T_H - T_C)^+ = \frac{(T_H - T_C)}{(T_H - T_C)_o} \tag{2-10}$$

$$\left\{ \sum_{i=1}^{N} \left[\frac{1}{2} \left(\frac{fl}{d_h} + K \right) \left(\frac{a_c}{a_i} \right)^2 \right]_i \right\}^+ = \frac{\sum_{i=1}^{N} \left[\frac{1}{2} \left(\frac{fl}{d_h} + K \right) \left(\frac{a_c}{a_i} \right)^2 \right]_i}{\sum_{i=1}^{N} \left[\frac{1}{2} \left(\frac{fl}{d_h} + K \right) \left(\frac{a_c}{a_i} \right)^2 \right]_{i,o}} \tag{2-11}$$

Dimensionless loop momentum balance equation:

$$\Pi_L \frac{d\dot{m}^+}{dt^+} = \Pi_{Ri}(T_H - T_C)^+ - \Pi_{Fl}(\dot{m}^+)^2 \left\{ \sum_{i=1}^{N} \left[\frac{1}{2} \left(\frac{fl}{d_h} + K \right) \left(\frac{a_c}{a_i} \right)^2 \right]_i \right\}^+ \tag{2-12}$$

Dimensionless loop energy balance equation:

$$\frac{1}{\gamma} \frac{d(T_M - T_C)^+}{dt^+} = \Pi_T \dot{m}^+ (T_H - T_C)^+ - \Pi_{SG} \dot{q}_{SG}^+ - \Pi_{loss} \dot{q}_{loss}^+ \tag{2-13}$$

Characteristic time constant:

$$\tau_{loop} = \sum_{i=1}^{N} \frac{l_i}{u_i} = \sum_{i=1}^{N} \tau_i = \frac{M_{sys}}{\dot{m}_o} = \frac{M_{sys}}{\rho_l u_{co} a_c} \tag{2-14}$$

Loop reference length number:

$$\Pi_L = \sum_{i=1}^{N} \frac{l_i}{l_{ref}} \frac{a_c}{a_i}, \quad \text{where} \quad l_{ref} = \frac{M_{sys}}{\rho_l a_c} \tag{2-15}$$

Loop Richardson number:

$$\Pi_{Ri} = \frac{\beta g (T_H - T_C)_o L_{th}}{u_{co}^2} \tag{2-16}$$

$$\text{Or} \quad \Pi_{Ri} = \frac{\beta g \dot{q}_{co} L_{th}}{\rho_l a_c C_{pl} u_{co}^3} \tag{2-17}$$

Loop resistance number:

$$\Pi_{Fl} = \sum_{i=1}^{N} \left\{ \frac{1}{2} \left(\frac{fl}{d_h} + K \right)_i \left(\frac{a_c}{a_i} \right)^2 \right\}$$

(2-18)

Ratio of specific heats:

$$\gamma = \frac{C_{pl}}{C_{vl}}$$

(2-19)

Loop energy ratio:

$$\Pi_T = \frac{(T_H - T_C)_o}{(T_M - T_C)_o}$$

(2-20)

Steam generator heat transport number:

$$\Pi_{SG} = \frac{\dot{q}_{SGo}}{\rho_l u_{co} a_c C_{pl} (T_M - T_C)_o}$$

(2-21)

Loop heat loss number:

$$\Pi_{Loss} = \frac{\dot{q}_{loss,o}}{\rho_l u_{co} a_c C_{pl} (T_M - T_C)_o}$$

(2-22)

Time scale ratio:

$$\tau_{loop,R} = \left(\frac{\rho_l C_{pl}}{\beta} \right)_R^{1/3} \left(\frac{a_c \Pi_{Fl} l^2}{\dot{q}_{co}} \right)_R^{1/3}$$

(2-23)

Fluid velocity scale ratio:

$$u_R = \left(\frac{\beta}{\rho_l C_{pl}} \right)_R^{1/3} \left(\frac{\dot{q}_{co} l}{a_c \Pi_{Fl}} \right)_R^{1/3}$$

(2-24)

Loop length scale ratio:

$$l_R = (L_{th})_R$$

(2-25)

Loop energy scale ratio:

$$\left(\frac{a_i}{a_c} \right)_R = 1$$

(2-26)

Steam generator power scale ratio:

$$\left[\frac{(T_H - T_C)_o}{(T_M - T_C)_o}\right]_R = 1 \tag{2-27}$$

Heat loss scale ratio:

$$\left(\frac{\dot{q}_{SGo}}{\dot{q}_{co}}\right)_R = 1 \tag{2-28}$$

Flow area scale ratio (kinematic similarity):

$$\left(\frac{a_i}{a_c}\right)_R = 1 \tag{2-29}$$

3. FORCED CONVECTION TEST LOOP DESCRIPTION

INL studied several past and current flow test loops built with the same or similar objectives. Some examples of these are at ORNL, University of Wisconsin, and the lead-bismuth test loop built at Los Alamos National Laboratory. The proposed loop is the outcome of considering the past experiences of several other researchers around the nation. The proposed molten salt forced convection loop will be designed, built, and operated with the goal of obtaining much-needed technical information on convective heat transfer, thermophysical and thermochemical properties, corrosion properties, and any other thermal-hydraulic characteristics that are essential in developing larger-scale nuclear power plants. The convection loop is expected to simulate all essential thermodynamic and transport phenomena, except nuclear radiation.

3.1 Conceptual Loop System Design

The functional requirement of the forced convection test loop, illustrated in Figure 3-1, is to provide and maintain an adequate flow rate at the temperature and pressure that the liquid salt will be subjected to in the full-scale prototype system, such that the thermophysical properties and heat transfer correlations could be obtained with reduced uncertainty spread and higher probability. The scaling analysis approach discussed in Section 2 should be used to scale down the components from the prototype so the physical phenomena can be preserved.
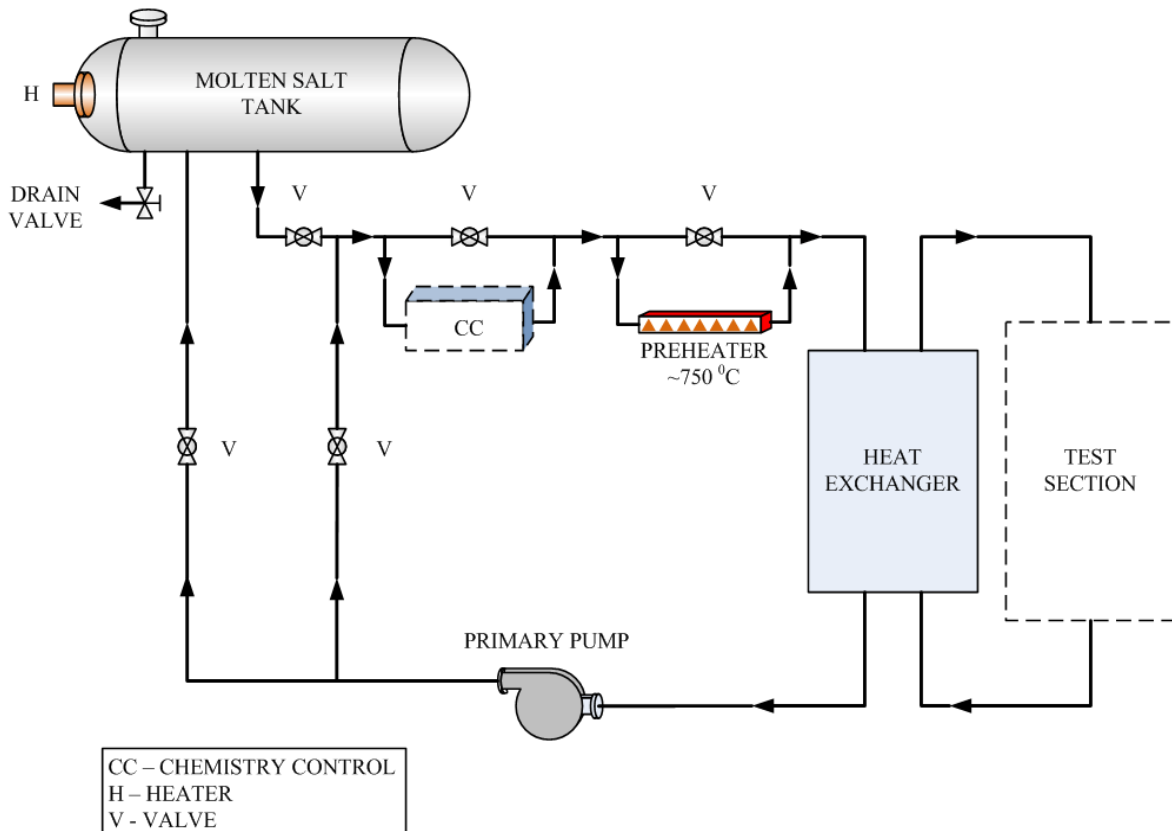
Figure 3-1. Schamatic of an FCL designed to deliver molten salt at controlled temperature and flow through the test section.

The main purpose of an FCL is to study the behavior of molten/liquid salt as VHTR primary coolant and as NGNP process heat transport fluid. It is envisioned that the loop will have the capability to reach

temperatures up to ~750°C. The loop will primarily use Alloy 800H or some other high-temperature nickel alloy for higher temperatures. The molten salt reservoir tank could be made from stainless steel 316 because of its lower temperature requirement. Currently, most of the high-temperature alloys are not readily available in pipe form. As a substitute, Inconel Alloy 600 could be used, but the construction material should not solely be selected based on design temperature alone but also allowable design stress at high temperatures should be considered (Sabharwall 2009).

The small-scale forced convection test loop will be required to test specific components and gain experience that will apply directly to a full-scale reactor. Specific objectives of loop testing, apart from validation of physical properties and correlation, are to verify the performance of the components and evaluate their service life and maintenance requirements.

The liquid salt will be heated by an electric heater to simulate the thermal conditions of the reactor coolant. A vacuum will be drawn on the test facility to allow the salt to naturally drain into the corresponding subsystems when the respective valves are open and to prevent voids in the salts. Electric trace heaters will be used on the pipes to compensate for the heat loss through the pipe system and prevent the liquid salt from freezing.

The measuring instruments for the test loop have to be installed such that the instruments do not come in direct contact with the salt. Thermowells with K-type thermocouples with Hastelloy-N as the thermowell sheath material (will have to be customized) are being considered for temperature measurements, even though fiber optic sensors could be another choice. Clamp-on ultrasonic flow meters are being planned to measure the flow rates of the primary and secondary salts. A Venturi flow meter will be an alternate instrument to measure the flow rate. Potential of pressure and differential pressure transducers with remote seals will be examined for measuring the pressure and differential pressure.

After detailed design of the engineering test facility is complete, the facility will be constructed at INL in collaboration with ORNL. The lead organization has fairly extensive experience with VHTRs and molten salt reactor technology as well as with design and construction of a high-temperature test facility. Past experience with small- to large-scale test equipment, advanced high-temperature instrumentation, high-temperature materials, and fabrication methodology will be critical in constructing this test facility.

The main issue with molten salt will be compatibility with the heat exchanger and pipe material, whereas the main concern on the (helium) primary side will be the material strength at elevated temperature and pressure. If a reduced environment is maintained for the molten salt and suitable pipe material is chosen, corrosion from fluoride-based molten salts should not be a problem (Task et al. 2005).

Most of the high-temperature materials will have a high nickel and medium chromium content. Chromium is one of the more soluble elements in most alloys when fluoride salts are used. Therefore, an alloy with high nickel concentration and low chromium concentration will be preferred for the test loop material. The tendency for corrosion of the conduit material in contact with fluoride salts is reduced when the conduit material composition is on the order of Ni<Co<Fe<Cr<Al (Task et al. 2005). Another alternative to a nickel-based alloy is carbon-carbon composite material, which has a low coefficient of thermal expansion and is resistant to oxidation. Its tensile strength remains constant with increase in temperature, unlike ceramics and superalloys, where the tensile strength decreases. In order for the loop to maintain full mechanical strength, vapor-infiltrated carbon coating could be applied on the inside surface of the test loop as proposed by Task et al. (2005), but this concept is yet to be proven.

Holcomb et al. (2009) lists the following requirements for loop testing:

- Identify the loop component safety, reliability, and performance requirements
- Determine the information necessary to provide reasonable assurance that the components will satisfy the requirements

- Develop a methodology to efficiently acquire the required information for each component and for the integrated operation of components as a system

- Establish component test facility requirements necessary to acquire the component performance data.

The proposed forced convection loop could potentially serve the following purposes:

- Verify physical properties (mainly conductivity, heat capacity) and validate heat transfer correlations for molten salts

- Use the data provided to benchmark thermal-hydraulic and computational fluid dynamics codes

- Establish the compatibility of material under a prototypical environment

- Measure test parameters and demonstrate new instrumentation and control equipment in relevant environments

- Use current available instrumentation and specific materials at high temperature and moderate pressures for the FCL to provide information about availability and technical maturity that would be significant for the further development of molten salt heat transport technology.

The construction material of the test loop should have the following characteristics:

- Low thermal expansion coefficient

- Low creep

- High strength helium pressure and temperatures.

Thermal hydraulic characteristics of the test loop can be summarized as follows:

- The temperature of the molten salt at the inlet and outlet of the test section could be varied between melting temperature of the salt and 900°C by heaters and preheaters

- To prevent an overpressure accident (in a gas-to-molten salt heat exchanger), the pressure of the primary coolant (gas) must be used as one of the trigger signals for system safety

- The temperature of the test section must be below the threshold temperature of the material

- The temperature and pressure of the molten salt should be monitored to ensure safe operation of the test loop and to scale-up the design parameters for the prototypical system.

3.2 Heat Exchanger

The next-generation reactors are intended to produce electricity and/or provide high-temperature heat for industrial processes. The efficient transfer of energy for industrial applications depends on the efficient and cost-effective heat exchangers between the source heat from a nuclear reactor and the industrial process heat sink system and for several potential industrial applications. However, the need to meet efficiency, compactness, and safety requirements will challenge the boundaries of existing heat exchanger technology. Heat exchangers will be expected to maintain their structural integrity during their design lifetime, including thermal transients caused by normal operations, various plant abnormalities, and emergency operating conditions. Potential types of heat exchangers that could be used for transferring thermal energy are shell-and-tube (conventional design), printed circuit, spiral or helical coil, ceramic, plate and fin, and plate. However, experience in designing, constructing, and operating these systems

using high-temperature molten salts is limited to shell-and-tube heat exchangers, so it is expected that significant development of these designs will be needed before they can be incorporated into the VHTR applicable design or used for process heat transfer applications.

The heat exchanger is an equivalent Class 1/Class 2 high-temperature component and will therefore need to be designed in accordance with American Society of Mechanical Engineers (ASME) Boiler and Pressure Vessel Code, Section III. The heat exchangers must be constructed to maintain system integrity under normal, off-normal, and accident conditions. Optimizing heat exchanger designs will involve iterations that improve performance for one criterion with acceptable compromises for other criteria.

The heat exchanger is the interface component between primary fluid (such as helium) and secondary fluid (molten salt), which makes it a significant component in the effective transfer of heat used for power production or process applications. Its effectiveness, therefore, determines the temperature and pressure drop along with high to moderate values for convective heat transfer coefficient. Some thought will be given to tritium migration, which would most likely occur through the IHX, the coldest part in the primary circuit, where the probability of tritium migration is the greatest compared to any other heat transfer component. There are many variables to be evaluated in the selection of a particular type of heat exchanger for a given application. Since the evaluation metrics will be developed at a later stage, those are not included in this report.

The MSRE primary heat exchanger (the shell-and-tube design) is the most widely used heat exchanger and therefore has a substantial operating history. In the MSRE design, the secondary coolant has a slightly higher pressure than the primary coolant so that the radioactivity will be contained in the primary loop should a leak develop. According to Holcomb et al. (2009), the shell-and-tube design has two major advantages: it can be easily inspected while in-service (provided the heat exchanger design allows access to its interior), and it can be designed to minimize steady-state and transient thermal expansion stresses. Hastelloy-N, Alloy 617, or Alloy 800H are the potential candidates for the construction material of the heat exchanger.

Both shell-and-tube and printed circuit heat exchangers could be made of Hastelloy-N or a high-nickel alloy like Alloy 617. The heat exchanger selected should be able to keep up its structural integrity during its design life, which will encompass thermal transients caused by normal operations, various plant upsets, and emergencies (Rosenthal et al. 1972). The printed circuit heat exchanger design could be modified so that the fouling and blockage issues can be minimized.

3.2.1 Heat Exchanger Design Considerations and Parameters

Heat exchanger design requires consideration of fluid heat transfer rates and the mechanical power expended to overcome the fluid friction. High-density fluids such as molten salts have small friction power expenditures relative to their heat transfer rate. The actual heat exchanger system design entails two steps: rating/duty and sizing. The sizing problem relates to determining the physical size (dimensions such as length, width, height, and surface areas) on each side of the heat exchanger. Rating/duty refers to the heat transfer rate and pressure drop in the heat exchanger. The heat exchanger design poses a sizing, rating, and selection criteria problem because of the need to establish temperatures and flow rates that will achieve a desired effectiveness and a moderate or acceptable pressure drop as well as geometric dimensions. The selection criteria for the heat exchanger will look at thermal hydraulic criteria and other issues, such as fabrication, fouling, etc.

3.2.2   Issues with IHXs (Process Temperature Applications)

The following issues should be considered for IHXs:

- Heat transfer from helium gas to molten salt: the gas side would require high velocities or high heat transfer surface area along with high pressure, which would impose stringent requirements on the heat exchanger design

- Material compatibility at these high temperatures and differences in pressure on the primary and secondary side

- Tritium permeation resistance to restrict the contamination of molten salt in the secondary loop

- Designs, other than the shell-and-tube, are lacking substantial experience

- Joining processes such as diffusion bonding, brazing, and bi-metallic welding will be one of the biggest challenges

- The integrity of the metal or bi-metal; the interface and the resistance of the nickel to intergranular separation. If it is positive, then joining techniques must be assessed

- Fabrication of the heat exchangers

- Maintenance and inspection of the heat exchangers

- Ability of the IHX design to withstand thermal cycling caused by heat-up/cool-down cycles during start-up and shut-down.

3.3   Insulation

Reducing heat loss from the loop is very significant for an effective process heat system. Therefore, optimum insulation with the ability to withstand high temperatures is a must for the loop. To date, few high-temperature insulations have been presented (Tasks et al. 2005).

3.4   Materials

The material chosen for the construction of the loop should have a low coefficient of thermal expansion because the massive temperature increase during startup and decrease during shut down will cause the pipe to expand and contract significantly. This may lead to high mechanical and thermal stresses in the material (Task et al. 2005).

The selective leaching of chromium would be the main mechanism for corrosion of iron-and nickel-based alloys by molten fluorides. Therefore, the concentration of chromium is an important factor when selecting an alloy to be used in liquid-salt loop. Since iron is more easily oxidized by salts than nickel, a nickel-based alloy is selected over an iron-based alloy (Rosenthal et al. 1972). Good resistance to oxidation in N_2-O_2 environments is favored by high chromium concentrations.

The material must be able to bear the stresses during service to satisfying the requirement for compatibility with the coolant salt. An FCL will function at relatively low temperatures; thus, a high-strength material is considered unnecessary. Thermal stresses will possibly control the design, so a material with moderate strength will be used.

The structural material should be such that it could be fabricated into the components required to construct an engineering system. The basic shapes needed are plate, piping, tubing, and forgings. There are many nickel- and iron-based alloys that meet the requirements, but the technology is more advanced for some than others. The most important factor here would be the ability to work with the material.

The metal to be used for the fabrication of the forced convection test loop should meet the following requirements:

- Compatibility with working fluids (salts and steam)

- Since all parts of the system do not have the same requirements, a single material that satisfies all the requirements is not needed, but will be considered for FCL design.

Hastelloy-N is the highest temperature rated, currently available alloy for liquid salt reactor pressure vessel service. Using Hastelloy-N as the coolant pressure boundary limits the reactor temperature to 704°C because Hastelloy-N softens significantly at higher temperatures. Notably, Alloys 800H and 617 have significant residual strength to over 850°C. While neither of these alloys is chemically compatible with fluoride salts at high temperatures, nickel is highly compatible with the salt, and if a system clad with a nickel-based high temperature material can be proven, the fluoride salt-cooled high-temperature reactor (FHR) test-scale loop outlet temperature would increase to the limits of the new alloy. Because the lower pressure of an FHR compared to an HTGR results in lower stress on the primary pressure boundary materials, the FHR test-scale loop (TSL) may be able to use HTGR-developed alloys at significantly higher temperatures than would be useful in a gas-cooled reactor with the same core outlet temperature.

Hastelloy-N is preferred, but its usage depends on its success to alter the composition to stop intergranular cracking. The highest temperature with the materials used would likely be 704°C. Type 304 or 316 stainless steel would be the second choice for use in the primary circuit because of its excellent resistance to damage by tellurium (Rosenthal et al. 1972). Stainless steel will not likely have adequate corrosion resistance to the coolant salt, and a transition to Hastelloy-N would be made in the IHX or the testing loop. A change would be necessary only if it becomes evident that Hastelloy-N cannot be further changed to improve its resistance to intergranular cracking. If a change is required, nickel-based alloys appear preferable to iron-based alloys because the salt can be more oxidized with nickel. However, research indicates that iron-based alloys offer more resistance to intergranular cracking. These two factors should be considered in choosing a material that may be possible only when more data are available on the resistance of different alloys to cracking and their corrosion resistance in salt. The third choice would be Alloy 617, which will be used to fabricate a system having a high composition of nickel with a moderate-to-low composition of chromium alloy. The fourth choice would be Alloy 800H.

The key factor is whether it has adequate corrosion resistance at a reasonable operating temperature. Simultaneous programs should be carried out on all four types of materials discussed above. Based on the findings, some materials will be dropped and others added. If a duplex system is needed, more work will be required because methods must be developed for making dissimilar joints, duplex tubing, and weld overlays.

A process heat transfer loop will run at high temperatures, so creep rate, thermal expansion, corrosion, and oxidation are significant for any heat transfer fluid.

3.5   Liquid Salt Pumps

The liquid salt pump provides pressure to establish an adequate level of forced circulation of the salt in the loop. The type of pump employed in the loop is strongly a function of salt density and viscosity; salt density mainly affects the torque requirement for the pump impeller: the shaft must have sufficient torsional strength to handle the salt density. The salt's viscosity and material compatibility strongly affect the life characteristics of the hydrodynamic bearings, which would be needed for long shaft pumps (Holcomb et al. 2009). Actual service in pumping molten salt is probably the only way to ensure that the subtle design has been considered with the changes that will be necessary for pumping molten salt. Until now, many experiments have been done by using a prototypical fluid (e.g., oil, water) rather than the salt

itself, in which case, the up-thrust on the motor that occurs when pumping salt could be easily missed because it might not occur with the prototypical fluid (Smith et al. 1992).

Considerable operating experience exists with liquid salt pumps from the MSRE and MSBR test. Electromagnetic and centrifugal pumps have thus been considered for salt system applications. The low electrical conductivity of molten fluoride salts deters the application of electromagnetic pumps, so they are not used in fluoride salt systems. In comparison, centrifugal pumps do much better and have been applied satisfactorily to fluoride salt systems.

The main requirements for developing a salt pump include proof and endurance testing of the shaft seal and endurance testing of a prototype pump with molten salt. A long-shaft salt pump will also require proof of the potential to fabricate long pump shafts to precise concentricity, straightness, and dynamic balancing requirements. A series of tests with molten salt on the prototype will be performed to authenticate its performance and to provide assurance of its durability. Figures 3.2 and 3.3 show photographs of a cantilever and long-shaft pump, which have successfully worked in liquid salt environments (Barth 2009).
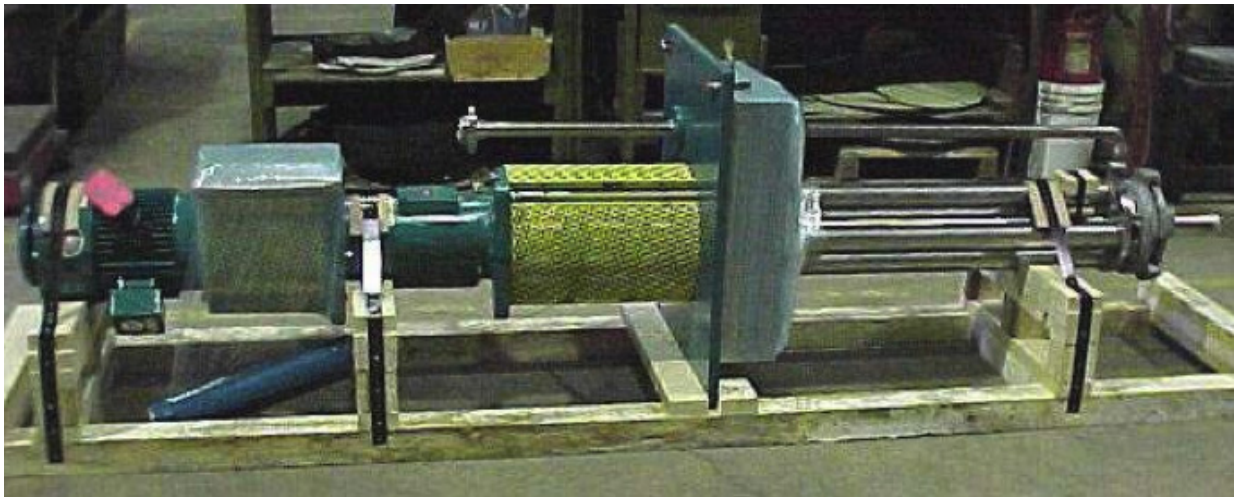
Figure 3-2. High-temperature cantilever pump (Barth 2009).

Figure 3-3. Long-shafted pump (Barth 2009).

Each test in FCL would be designed to exercise the high-temperature components such as valves and pumps in a manner similar to operation in a commercial plant. While cycling through the various flow rates (by adjusting the pump), the valves are cycling to control flow and pressures. The flanged connections for FCL will be minimized because of the potential for leaks but will be used for chemistry control and a test section as can be seen from the schematic of the loop, but would have higher than required pressure ratings to minimize leaks.

The loss of circulator/pump power in the FCL could cause freezing, which would make it impossible to melt all the salt in the pipes or, for that matter, the test section or heat exchanger. If such heating was possible, the thermal expansion of the salt could cause pipes to rupture. To avoid the freezing issue, the FCL circulator should have an alternate power source and the loop should either have heat tracing wire around the pipe or a mechanism to input warm/hot gas into the loop in order to melt the salt. A complete economic analysis should be carried out to decide if it is more beneficial to install and run a gas heating system or to run the heat tracing when initially warming the loop. It might be a good idea for the loop to have both of these possibilities in order to compare the net cost and effectiveness of each, which will be directly applicable to the prototype.

Task et al. (2005) gave an example of optimal diameter for helium and molten salt transport at varying intermediate loop inlet temperatures and found that for a given pressure drop of 112 kPa and pipe roughness of 0.15 mm, the helium loop diameter was five times that of molten salt. Total energy loss (heat loss through the pipe walls and thermal pump power required) was minimized by varying the pipe diameter, which is plotted in Figure 3-4 for the molten salt (50%LiF-50%BeF$_2$) at a number of inlet temperatures.
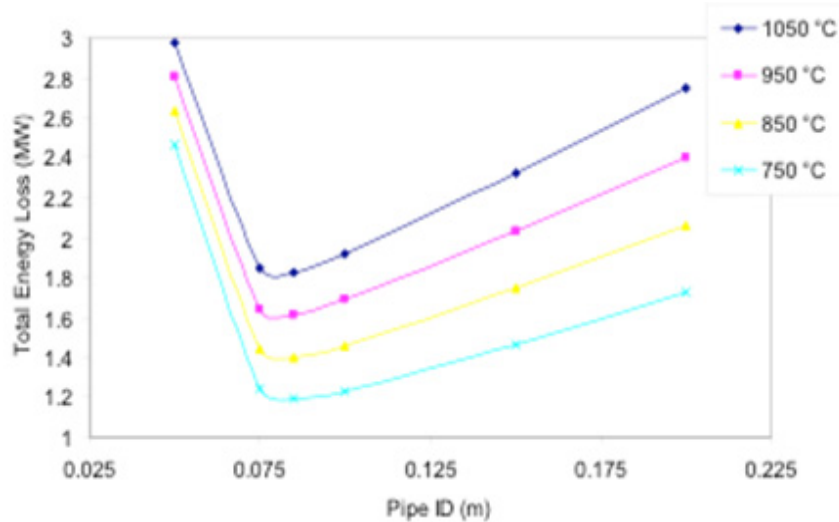
Figure 3-4. Optimal diameter for liquid salt transport at varying intermediate loop inlet temperatures (Task et al. 2005).

Test objectives proposed by Smith et al. (1992) for pumps over the range of loop operating conditions are to:

- Verify pump performance
- Check for vibration and wear
- Check pump seals and bearings
- Evaluate pump maintainability
- Identify operating procedures that yield the best performance.

Figure 3-5 shows the general trend of a pump, which is called a pump curve, where pump efficiency and pump head are plotted against flow rate generated by the pump. A similar plot will be obtained for the pump being used in the FCL, and the motor pump design will be analyzed to ensure that the motor bearings are adequate for the loads imposed by the pump.
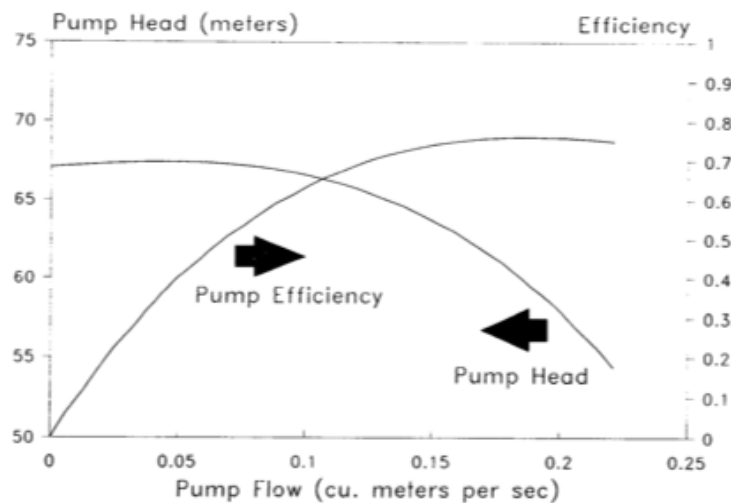
Figure 3-5. Plot of efficiency and pump curve for the pump (Smith et al. 1992).

3.6 Heater

The main purpose of the heater, which could be an induction or resistance type, is to ensure that the salt remains in the molten state. The MSRE primary heat exchanger employed 30 kW of electrical resistance heaters installed outside the shell to avoid freezing. The heaters used in the FCL will be divided into multiple control zones, actively controlled by a simple on/off control system, and insulated with high-temperature insulation such as ceramic fiber.

A preheater will be added in the loop to raise the temperature of the flowing molten salt, if needed for testing purposes. The loop will also be designed with overcooling transients in mind to prevent freeze-up of the liquid salt.

3.7 Chemistry Control Loop

The main purpose of the chemistry control loop is to maintain required purity levels and the fluorine potential level of the liquid fluoride salt. A special monitoring system will be employed to detect the level of water vapor and oxygen in order to keep corrosion in check. In order to observe the long-term behavior of the loop, a chemistry control loop will be installed to contaminate the pure salt with some parts per million (ppm) levels of impurities in order to see the long-term (aging) effect. The instrumentation to measure chemistry in the loop must accommodate the range of potential contaminant levels for individual contaminants and combinations of various contaminant levels. The type and amount (concentration) of the impurities have not been decided.

3.8 Valves

Valves are primarily used in a loop to control flow during normal and off-normal operation, apart from isolating the flow during startup and shutdown. The valves included in the loop will be tested in the molten salt environment. Fluoride salts are excellent fluxing agents, so self-welding and galling become important design issues for valve seats and actuator seals (Holcomb et al. 2009). Three types of valves will be required: shutoff, throttling, and pressure relieve valves. Shutoff service should be accomplished using a conventional mechanical design: freeze valves and a combination of valves that close to restrict most of the flow mechanically, with final close-off by a freeze seal within the valve. Freeze valves are better for applications where tight shutoff is required for a long time because of its high reliability and zero salt leakage (Rosenthal et al. 1972).

Most loops with fluoride salt circulating systems use freeze valves instead of mechanical valves, which have performed well during freeze-thaw operations. The valve used in the FCL will have a variable speed pump motor to control flow and avoid the need for mechanical throttling valves (Holcomb et al. 2009).

In the MSRE experiment, one of the 1½-inch valves leaked a few grams of salt during the final shutdown of the reactor because of thermal stresses caused by a field modification of a shroud in the valve to aid attachment of a larger cooling line. Design modifications should be made to eliminate this problem. Valves should be tested expansively in conditions similar to a reactor system to verify performance as explained by Rosenthal et al. (1972).

Testing objectives for valves have previously been proposed by Smith et al. (1992) for the following control and isolation applications:

- Evaluate/compare valve seats at FCL operating conditions

- Test valves for long-term cycling

- Verify valve seat/trim design and materials at conditions for control and shutoff

- Check for evidence of valve erosion, corrosion, and wear.

The valves could be purchased according to specifications for a given intended service for the FCL.

3.9   Flow Loop Instrumentation and Controls

The choice of measurement techniques for the instruments typically depends on many factors, including the required accuracy, drift, repeatability, cost, and serviceability. Additional literature searches may be undertaken to better refine the adaptation of the standard flow measurement techniques and their associated uncertainties specific to the molten salt. The importance of uncertainty will be explained in the later section of the report.

The instrumentation requirement for this loop differs from others, mainly because of the high temperatures and the molten salt environment. The main instrumentation required for the loop will be to control/monitor temperature, pressure, flow rate, and corrosion. Liquid salt flow measurement will most likely either be performed using external, ultrasonic flow meters or Venturi-type flow meters that use differential pressure gauges as their active element (Holcomb et al. 2009). All instruments produce electrical signals that could further be connected as inputs to the control system.

Specific operating features and mechanical components have not been short listed in this report, but the issues have been presented. The operational performance of the instrumentation can be directly taken from the loop to provide confidence for the prototype system.

High-temperature instrumentation applicable to molten salts is a developing field driven by user requirements. It is therefore fair to state that the high-temperature instrumentation is not yet commercially available with long term reliability and drift performance data. A sufficient market has not existed for commercial vendors to establish and maintain sources of supply for the specialized instrumentation.

3.9.1   Precautions in Selecting Pressure Transmitters

Some types of pressure and differential pressure instruments can be damaged by a significant vacuum, so care must be taken to specify instruments that can withstand a vacuum or provide reliable ways to isolate the instruments when a vacuum is applied to the loop (Phoenix 2010). The INL high-temperature test loop uses vacuum pumps to quickly remove moisture before heating test sections, and undoubtedly, a vacuum will be applied to other test sections and the FCL to remove moisture prior to operating at high temperatures.

3.9.2   Precautions in Flow Measurements

ASME and the National Institute for Science and Technology have standards for required lengths of pipe to produce accurate flow measurements. Adverse flow profiles found with short lengths of pipe can be ameliorated by placing a flow straightener, a flat plate with holes, ahead of the differential producer. The effect of piping lengths in flow loops on flow measurement accuracy is very significant and will be considered in the FCL design. For example, the aspect ratio is typically described in terms of the ratio of the length (L) of pipe to its inside diameter (D), or L/D. For example, 20 L/D downstream of a single elbow may be sufficient for accurate measurements with cold water, whereas 100 L/D may be required for very hot but still subcooled water.

Flow meters are commercially available that can operate at high temperatures, but they require flow rates that are significantly greater than those used in the laminar flow loop (Phoenix 2010). Currently, General Electric produces ultrasonic flow meters that can operate at temperatures of up to 600°C, and Foxboro Model 83 F-T01 series vortex flow meters are capable of temperatures up to 430°C in liquid salts (Sabharwall et al. 2010a).

3.9.3   Temperature Measurements

3.9.3.1   *Thermocouples*

Thermocouples are the most used temperature measuring sensors today. High-temperature environments pose several challenges, including melting of leads and oxidation (Phoenix 2010). Longevity is an issue because thermocouples must physically withstand high-temperature helium environments for the time measurements required. The main problem with thermocouples is drift—the time-dependent change of reading in a constant temperature environment. Thermocouples drift, and the amount of drift depends on the type of thermocouple. Drift might become a significant consideration in test chambers, loops, and reactors that will operate for many months to years without an opportunity to replace the thermocouples. The high-temperature environments in test chambers and loops offer opportunities to assess thermocouple drift. A thermocouple is a simple instrument. The sensitive portion is the junction where wires of two dissimilar metals meet. The junction produces a small voltage (several millivolts) proportional to the temperature. Thermocouples are identified by the material of their wires, noted by letters K, N, R, etc. Two types, K and N, are commonly cited in the literature for high-temperature loops and HTGRs.

Two junctions are required to make a thermocouple temperature measurement. The other junction is made from the same sensing junction and is called the reference junction. The voltage difference between the two junctions is proportional to the difference in temperature. It is therefore very important for the temperature of the reference junction to be accurately measured. A typical reference junction temperature is 0°C, or ice temperature, and is often measured by a highly accurate resistance temperature device (RTD). The voltage difference between the reference and sensing junctions is measured by a voltmeter. The relationship between voltage and temperature can be programmed into the reader, or the voltage can be manually converted to temperature by using a chart of temperature versus voltage.

Thermocouples are subject to several well-known failure and degradation mechanisms. The junction can oxidize such that the dissimilar metals are no longer in contact, and the voltage being produced by the junction falls to zero—a certain indication of failure. Leads can touch and form virtual junctions so the measurement is the temperature at the virtual junction, a situation that is more likely under vibration and high temperature.

Numerous refractory metal permutations of tungsten, rhenium, tantalum, niobium, molybdenum, iridium, ruthenium, and osmium (all of them have melting points above 2000°C) and their alloys have been studied (Wilkins and Evans 2005) in the search for useful thermocouple properties.

3.9.3.2   *Resistance Temperature Devices*

Temperatures below approximately 650°C can be accurately measured by a RTD. The high accuracy of RTDs requires high-purity platinum. When temperatures reach ~650°C, metals in the RTD's sheath migrate into the platinum and contaminate it. The RTD has traditionally been a more expensive device, but under low vibration, relatively low thermal shock conditions, and <650°C, it can have excellent accuracy, much lower drift rates than thermocouples, and be extremely reliable and long-lasting. Theoretically, any metal can be used for this purpose, but very few metals meet the criteria for suitable variation of electrical resistance. Commercially, most of the RTDs use platinum sensors to supply good temperature resolution. The main reason for using platinum sensors is because they have a large temperature coefficient of resistance (known as the α value). Application of these RTDs is restricted to about 660°C (Wilkins and Evans 2005).

Experience with LWRs shows that the temperature signal from the RTD remains accurate until shortly before the wire breaks. Thermal shock, such as changes of approximately 150°C or more in one or

two seconds, has also been shown to decalibrate RTDs. The RTD is widely used in commercial LWRs. The reactor protection systems of pressurized LWRs rely on highly accurate RTDs to measure the temperature of primary coolant entering and exiting the reactor core. Many large motors, including primary coolant pump and circulating water motors, use RTDs. Development of migration-resistant sheath materials could extend the useful temperature range of the RTDs and potentially reduce uncertainty in design and operating margins.

Since tungsten is brittle and difficult to work with, it is not a preferred material for RTDs. Still, it has also been utilized infrequently as an RTD sensor element for higher temperatures. The optimum temperature for a tungsten RTD is about -100 to 1,200°C (Wilkins and Evans 2005).

Thermocouples being used inside a reactor can transmute (change from one element to another), but this is not an issue for the FCL. The level of transmutation depends on neutron flux density, exposure time, and the half-lives of the isotopes, velocity, and absorption cross section of the wire. The precise calculations of the transmutation products for the various elements found in thermocouples become involved because of the various multiple transmutations and half-lives of the isotopes involved.

3.9.3.3   *Thermistors*

Thermistors are a type of resistor whose resistance varies with temperature. They can be used as small fast-responding temperature sensors, but can also drift more and are somewhat less accurate than RTDs. Thermistors are made of heat-treated metallic oxides, and most thermistors differ from ordinary resistors by having a negative coefficient of resistance with temperature. Their small size and fast response make them potentially attractive as temperature rakes for low-temperature applications (<300°C).

3.9.3.4   *Methods for Temperature Measurement in High Temperature Loops*

Table 3-2 compares currently applied methods for measuring temperatures in high-temperature loops.

Table 3-2. Comparison of methods for measuring temperature in high temperature loops (Phoenix 2010).

Item	Thermocouple	RTD	Optical Fiber	Infra-Red	Ultrasonic
Sensor	Junction of dissimilar metals.	Pure platinum wound around small bobbin.	Tip to entire length of one optical fiber.	Surface sensitive to infrared radiation.	Ultrasonic sensors.
Construction	Two dissimilar metal wires are joined at one spot. The metal leads can be coated with insulation and/or located within insulation and enclosed in a tube several mm in diameter called a "sheath."	Pure platinum wound around small bobbin. The platinum is attached to wires and enclosed in a tube of several mm in diameter, a "sheath," which can contain a set of wires called "compensating leads."	One strand of optical fiber in a protective sheath.	Sensing device sensitive to infrared radiation enclosed in a housing.	Several types such as pairs of nonintrusive sensors and a metal rod with step changes in diameter attached to an ultrasonic transducer and protruding into a fluid stream.
Size of device including leads	Bare thermocouple junction and wire leads, to thermocouple in thin (typically 3 to 6 mm in diameter) metal and as long as many cm sheath, to metal sheath in a thick thermal well.	Thin (typically 3 to 6 mm in diameter) metal sheath, to metal sheath in a thick thermal well.	Long and very thin. No thermal well possible.	Fairly large. Requires optical path at infrared frequencies.	Diameter of the pipe plus probes about the size of a thermal well (perhaps 25 to 30 mm in diameter) and as long as required to reject sufficient heat to protect the transducer.
Sensitive location	Local region around the junction of two dissimilar metals.	Local region around the platinum sensor at the tip of the RTD.	Tip and along length.	Heat-sensitive sensor inside probe.	Transducers.

Item	Thermocouple	RTD	Optical Fiber	Infra-Red	Ultrasonic
Response time	<<1 second with bare junction, <1 second with bare sheath, <2 to 3 seconds in thermal well.	<1 second with bare sheath, <2 to 3 seconds in thermal well.	<<1 second.	Varies with design, typically ~1 second.	Varies with design, typically ~1 second.
Accuracy	Varies with thermocouple. Generic values are often listed in tables. Pairs of calibrated cold and hot junction thermocouples can be <±0.1°C.	Specially calibrated RTDs can be as accurate as ±0.01%22.	Under development.	Model OS35-20 with 0 to 1000°C range is ±1.5°C or ±2.0% with repeatability of ±1°C.	Time of flight typically <±1/2°C.
Drift	Varies with type of thermocouple and temperature.	Essentially zero unless severely thermally shocked and < ≈ 650°C. Further evaluation required.	In development.	Probably low.	Probably low.
Cost	Low.	Moderate to High.	In development.	Probably low.	Probably low.
Ease of use	Easy, well-developed, must avoid multiple grounds, requires cold junction.	Easy, well-developed, must avoid multiple grounds, requires cold junction.	In development.	Easy.	Probably easy.
Lifetime in low radiation fields.	Many years, depending on temperature.	Decades < ≈ 500°C to 650°C.	Currently ≈800 hours at 800°C; research is aimed at increasing lifetime.	Sensor is years, optical window not known.	Probably limited by sensor lifetime, believed to be years.
Penetration into reactor coolant system, test vessel, or test loop	Well-developed, sheathed thermocouple through a penetration or enclosed in a thermal well.	Well-developed, thermal well or penetration of bare sheath into the pipe with the RTD being secured with a Swagelok or similar fitting.	Well-developed for low and moderate temperature; can probably be adapted to high temperature.	Window optically transparent to infrared required for the sensor. Might be a significant barrier.	Threaded fitting on the pipe vessel.
Vulnerabilities and failure modes	Virtual junctions; open circuits due to oxidation of the junction and interconnecting wires.	1. Open circuits due to excessive vibration. 2. Drift from internal contamination >about 500°C. 3. Drift due to rapid extreme thermal cycling.	Optical window clouding due to thermal and radiation aging.	Optical window clouding unknown; sensor probably several years.	Transducers can be damaged by heat.
Sensitivity to vibration	Low.	RTD must be well supported in low to moderate vibration. Poor in high vibration.	Probably low; in development	Optical window likely to be low.	Probably low if properly supported.
Sensitivity to thermal shock	Low.	Moderate. Extreme shock will decalibrate. (Example: rapidly inserting cold sensor into very hot area.)	Relatively insensitive.	Sensor is low. Optical window is probably most vulnerable component.	Probably very low because the vulnerable component, the sensor, will be in a reasonably cool area.
Potential uses	Gas, fluid, metal, electrical conductor temperature.	Gas, fluid, metal, electrical conductor temperature.	Pressure, temperature, strain along length. Fiber optics might also provide paths for laser-based applications such as flow and particle tracking.	Temperature of surfaces.	Gas and fluid temperature.

Item	Thermocouple	RTD	Optical Fiber	Infra-Red	Ultrasonic
Compatibility of materials with coolant and contaminants	Varies with temperature and gas composition.	Some types are incompatible with graphite.	Unknown effect of contaminants including graphite dust.	Unknown effect of contaminants including graphite dust.	Contaminants and coolant probably have little effect on the probes.

3.9.4   Control System

A typical control system or control loop as explained by Phoenix (2010), includes:

- Sensors to measure physical processes such as flow, pressure, temperature, vibration, and component position within a chamber or loop that are continuously converting the process values such as electrical or optical signals.

- Surveillance and diagnostics to monitor sensor signals, computers, and other devices for abnormalities.

- Communication and transfer of data and information via analog or digital signals through fiber optics, wire, or radio (wireless).

- Control, regulation, and safety computers or instruments and data storage and management devices that use the variables from sensors combined with algorithms to manage and optimize plant operation, store data, and maintain operation within a predefined envelope.

- Human-machine interfaces to provide human operators with information and allow human control of process control components.

- Process control components such as valve actuators, motor controllers, or other devices whose action changes the process being controlled.

- Displays of the status of process control components such as valve actuators showing open/closed or intermediate travel, or actual position. Control systems involve unambiguous and predictable actions, and are highly repeatable and testable.

Process sensors and instrumentation have to be highly reliable and accurate within the test section and loop for long durations.

3.9.5   Protection System

Protection systems are the systems totally dedicated to protecting the loop or an individual; they place the test chamber and the loop in a safe condition when conditions warrant. A separate system such as the protection system will be put in place for the FCL.

4.   UNCERTAINTY IN EXPERIMENTAL SYSTEMS

4.1   Introduction

All experimental data or computational results have some uncertainties. The quantification of the uncertainties in the experimental data is essential to be able to use the data appropriately. Uncertainty or error analysis of measurement results is not an exact science; rather, it is probabilistic in nature. When a measurement is made, it is generally assumed that some exact or "true value" exists based on the definition of what is being measured. Guidelines prepared by National Institute of Standards and Technology present a uniform approach to describe the uncertainty in an experimental measurement (Taylor and Kuyatt 1994). Moffat (1988) defines uncertainty to be the difference between the true value and the measured value (uncertainty = true value – measured value) with a certain probability. However, there is no way that the true value of the parameter being measured can be known with 100% certainty. Within the time and resources available, an attempt is made to measure or determine the true value. Different measuring methods or several measurements using the same method may lead to different measured values. Therefore, the measured data must be reported with an uncertainty range (measured data ± uncertainty). The ambiguity about what is being measured and what contributes to measurement errors and uncertainty results in significant confusion about the uncertainty analysis. For example, Moffat (1988) gives four possible interpretations of a measured value of temperature by a thermocouple in a flowing gas stream. The measured value could be indicative of any of the following possible values:

- Temperature of the thermocouple junction itself

- Temperature of the gas at the thermocouple junction location

- Temperature of the gas at the thermocouple junction location, had the thermocouple not disturbed the gas flow

- Mass-flow weighted average temperature of the gas in the conduit at the axial location of the thermocouple junction.

Kline and McClintock (1953) clarify the difference between error and uncertainty. For a single observation, the error is the difference between the true value and measured value and is a definite number. The uncertainty is what one thinks the error might be and depends upon the particular conditions of the measurement. Accuracy is the degree of agreement between a measured value and the true value of the parameter. Precision is quantifying the accuracy of the measured data, i.e., how well a result can be determined (without reference to a theoretical or true value). The terms "uncertainty" and "error" are often used interchangeably to describe both inaccuracy and imprecision. It should be clarified whether the term means accuracy or precision, or both.

Therefore, the objective of uncertainty analysis is to methodically estimate the range of possible deviation/error from the reported measured value corresponding to a specified probability. Conversely, a probability of the measured data being within a specified uncertainty is estimated as the two situations are uniquely related to each other. It is impossible to measure a true value, and it is also impossible to determine the measured value's uncertainty with a 100% probability. Therefore, a measured value is only reliable if its uncertainty is quantified. Even then, the measured value is not absolutely certain, but only probable.

Moffat (1985, 1988) defined the uncertainty in mathematical terms. Consider a variable X_i, which has a measured value of X_i^m and a known uncertainty of δX_i. The measured value, X_i^m represents the measured value in a single-sample experiment or the mean of a set of N measured values in a multiple-sample experiment. The uncertainty is expressed in the following manner.

$$X_i = X_i^m \pm \delta X_i \ \ (N:1) \tag{4-1}$$

where the best measured value of X_i is X_i^m, the uncertainty in X_i^m is $\pm \delta X_i$, and (N-1) out of N measured values will be within $(X_i^m \pm \delta X_i)$.

If the experimental reading/result, R, is calculated from a set of N measurements $\{X_1, X_2, \ldots X_i, \ldots X_N\}$, then R can be expressed as

R = function of $\{X_1, X_2, \ldots X_i, \ldots X_N\}$ $\hspace{3cm}$ (4-2)

Experiments can be single-sample or multiple-sample. In each, the uncertainty is calculated using different correlations. Kline and McClintock (1953) showed that uncertainty can be reasonably estimated using a root-sum square combination of the effects of each individual measurement. The effect of the uncertainty in a single measurement on the resulting value R can be calculated corresponding to either one and all measurements being in error.

So if only one parameter measurement X_i is in error, the deviation/uncertainty would be given by:

$$\delta R_{x_i} = \frac{\partial R}{\partial X_i} \delta X_i \hspace{3cm} (4\text{-}3)$$

When several independent parameters are used to calculate the function R, then the deviation or uncertainty would be given by the root-sum-square method

$$\delta R = \left\{ \sum_{i=1}^{N} \left(\frac{\partial R}{\partial X_i} \delta X_i \right)^2 \right\}^{\frac{1}{2}} \hspace{3cm} (4\text{-}4)$$

Equation (4-4) is a basic equation for calculating uncertainty. Each term represents the uncertainty corresponding to a deviation/uncertainty δX_i corresponding to a parameter X_i.

If the uncertainty is desired as a fraction/percentage of the measurement reading, then *Equation (4-4)* can be put in that form. However, if the result can be put in an equation form—for example, as shown in *Equation (4-5)*—then the fractional uncertainty can also be determined as shown in *Equation (4-6)*.

$$R = X_1^{a_1} X_2^{a_2} X_3^{a_3} \ldots X_i^{a_i} \ldots X_N^{a_N} \hspace{3cm} (4\text{-}5)$$

$$\frac{\delta R}{R} = \left\{ \sum_{i=1}^{N} \left(a_i \frac{\delta X_i}{X_i} \right)^2 \right\}^{\frac{1}{2}} \hspace{3cm} (4\text{-}6)$$

Uncertainty analysis for a single measured value was given by Kline and McClintock (1953), whereas the multiple-sample analysis was summarized by Abernethy et al. (1985). Both types of observations must take Moffat (1988) into account. Common experimental strategy is to reduce as many sources of error as possible and then to keep track of those errors that cannot be eliminated. It is useful to study the types of errors that may occur, so they can be recognized when they arise.

4.2   Types and Common Sources of Uncertainties

Uncertainties or measurement errors may be classified as either random/statistical or systematic/bias, depending on how the measurement was obtained. A measuring instrument could cause a random error in one situation and a systematic error in another.

4.2.1   Random (Precision) Uncertainties

Random errors are statistical fluctuations in either direction (high or low) of some mean value of the measured data. These errors may be caused by the precision limitations of the measuring instruments or the observer. This type of uncertainty is a probable range of measurement errors; it is intrinsically random

in nature (since measurements cannot be perfectly controlled and executed), and it could be well approximated with some kind of statistical distribution. Random errors can be reduced by averaging the measured data over a large number of observations. Random variations are not predictable but they do tend to follow some mathematical pattern called a probability density function (PDF). Random errors are scatters of the measured data and are the result of following system errors:

- Resolution of the measuring instrument, which can be reduced or eliminated by using a null or balance method. It involves using instrumentation to measure the difference between two similar quantities, one of which is known exactly and is adjustable. The adjustable reference quantity is varied until the difference is reduced to zero. The two quantities are then balanced and the magnitude of the quantity to be measured can be found by comparing it with:
    - The reference sample
    - Random variations in properties with respect to time and spatial coordinates
    - Variations in process/system-related conditions
    - Physical variations over the entire range being investigated.
- Errors in repeatability.
- Errors in measuring procedure and technique.

Unless there is a special reason, most of the random errors can be approximated by Gaussian distribution for a large number of measurements, or with a Student's t-distribution for a small number of measurements. The PDF is described by its mean and variance values. The mean is the location of the PDF and the variance is the scatter of the PDF. The positive square root of the variance is defined to be the standard deviation, and it is a measure of the width of the PDF. Mathematical equations and analysis to calculate random uncertainties are given in many standard text books—for example, Coleman and Steele (2009).

4.2.2   Systematic (Bias) Uncertainties

Systematic errors are reproducible and consistent inaccuracies that are always in the same direction (higher or lower). Unlike random errors, systematic errors cannot be detected, analyzed statistically, or reduced by increasing the number of observations. Bias errors are the result of the following situations:

- Failure to calibrate accurately and calibration errors, or check zero of measuring instrument
- Using different methods to measure the same data
- Different experimental/laboratory set-up
- Personal/operator errors
- Drift in electronic instruments readings that gets introduced over time
- Lag time in measuring devices required to reach equilibrium and taking a measurement before the instrument is stable
- Failure to account for all possible factors except the one independent variable that is being analyzed; sometimes a correction can be applied to a result after taking data to account for an error that was not detected
- Errors introduced by immediate working environment such as vibrations, noise, drafts, changes in temperature.

Systematic errors relate to instrument accuracy and may result from incorrect calibration of the measuring instrument. If the systematic error of calibration is identified against a standard, the bias can be

reduced by applying a correction to compensate for the error. However, some researchers have argued that even the bias or nonstatistical uncertainties are actually random and statistical. It is so because one can never be sure whether the error is positive or negative, and the magnitude is only estimated with a specified confidence based on many previous observations of similar instruments and measuring methods. Once a bias error is systematically verified and specific correction is determined, it is no longer uncertain. It is then reduced to random uncertainty of an instrument and measuring method. Thus, a bias, nonstatistical uncertainty of a measuring instrument represents a possible error with a specified confidence level for a group of similar instruments to be used within a certain specification.

Some errors can be considered in either or both (random or systematic) categories. The experimenter may measure incorrectly, use poor technique in taking a measurement, or introduce a bias into measurements by unreasonably expecting the results to follow a certain trend. Visual errors can occur if, in the absence of an electronic reading, the experimenter is required to visually read the data. Personal errors are generally excluded from the error analysis discussion because it is generally assumed that the experimental data were obtained by following the correct procedures.

4.3   Uncertainty Analysis in Experimental Design

Moffat (1985), Harrison (2000), and Coleman and Steel (2009) have given guidelines for planning and conducting experiments by taking into account the experimental uncertainties. All possible experimental errors should be considered before conducting an experiment to assess the goodness/accuracy of the measured data. Uncertainties in the measured data result from uncertainties in the independent thermophysical parameters (temperature, velocity, pressure, etc.). Because uncertainties propagate proportional to the square of the uncertainties in the independent parameters, the large uncertainty values dominate the measured result. Thus, in designing an experiment, very little is gained by reducing the smaller uncertainties. Therefore, to improve the overall experimental results, the large uncertainties must be reduced (Moffat 1985, 1988).

4.3.1   Single-Sample Experiments

The uncertainty of a single measurement is limited by the precision and accuracy of the measuring instrument, along with any other factors that might affect the ability of the experimenter to make the measurement. To conduct single-sample uncertainty analysis, three levels of total uncertainty corresponding to three kinds of experimental replication need to be evaluated. It quantifies the scatter (uncertainty) in the data if the experiment were repeated according to a particular set of constraints. These types of uncertainties are explained as follows:

- *Zeroth order uncertainty* estimates the uncertainty in the instrument system with zero variability in the process. It is used to assess the suitability of a proposed instrumentation for the planned experiment.

- *First order uncertainty* estimates uncertainty with all the errors/uncertainties of zero order case plus uncertainties resulting from variabilities of the process. However, it does not include any fixed errors. It is performed during the debugging phase of an experiment to assess the scatter in the experimental data. However, first order uncertainty should not be used to assess the difference between data from two different experimental setups.

- *Nth order uncertainty* estimates the overall uncertainty in the experiment while it is being run, including all possible uncertainties. It includes all possible errors, including the fixed and variable errors in the measuring system. This is the uncertainty that must be reported in publication of the experimental results.

4.3.2 Multiple-Sample Experiments

In a multiple-sample test, enough data are taken to statistically interpret the random errors. In multiple-sample experiments, the reported value is a mean of a set of experimental observations and the uncertainty is around this mean value. Multiple sample analysis implies that the mean of a set of measured observations is likely to reduce the effects of random errors caused by both the instrumentation system and process variability, because these uncertainties should average out.

Whenever possible, a measurement should be repeated several times and an average of the results should be taken. This average is the best estimate of the true value. The more repetitions of a measurement that can be made, the better the estimate will be. However, the average is the best available estimate of the measurement, but it is certainly not exact. An average of an infinite number of measurements has to be obtained to approach the true mean value, and even then, the mean value is not guaranteed accurate because there is still some systematic fixed error in the measuring instrument that can never be eliminated, even by calibrating the instrument perfectly.

4.3.3 Uncertainties in Planning and Conducting an Experiment

The general uncertainty analysis as explained by Coleman and Steel (1999) is used to plan the experimental test facility. A summary of the procedure that needs to be followed is given in Table 4-1.

Table 4-1. Uncertainty analysis of an experimental investigation (Coleman and Steele 2009).

Various Stages of an Experiment	Level of Uncertainty Analysis	Purpose of Uncertainty Analysis
1. Planning	General	To choose an experiment and preliminary design.
2. Design	Detailed	To choose instrumentation (zeroth-order estimates) and develop detailed design (Nth-order estimates).
3. Construction/setup	Detailed	To decide on the experiment fabrication and setup.
4. Shakedown/debugging	Detailed	To verify and qualify experimental operation; first-order and Nth-order comparisons.
5. Execution	Detailed	To balance checks of instrument readings and monitor experimental operation; choice of test runs.
6. Data analysis	Detailed	To decide on the choice of uncertainty analysis techniques.
7. Reporting	Detailed	To report uncertainties (random, systematic, and overall)

4.3.4 Uncertainty Analysis Example

Moffat (1985) gave an example of a simple heat transfer experiment and its uncertainty analysis. A cylindrical rod of diameter D and length L is heated by electrical energy input W. Air at T_∞ flows on the surface of the rod and with energy balance, convective heat transfer coefficient h from the rod is calculated. Assuming a steady-state and neglecting radiation heat transfer from the rod (and applying a few other assumptions to make the example simplified), the convective heat transfer will be given by

$$h = \frac{W}{A(T - T_\infty)} .$$

(4-7)

Applying *Equation (4-7)* to calculate uncertainty in steady-state case, following relation in terms of uncertainties, δ, can be obtained as

$$\frac{\delta h}{h} = \left\{ \left(\frac{\delta W}{W} \right)^2 + \left(\frac{\delta D}{D} \right)^2 + \left(\frac{\delta L}{L} \right)^2 + \left(\frac{\delta \Delta T}{\Delta T} \right)^2 \right\}^{\frac{1}{2}}$$

(4-8)

For each instrument (used the measure the data), the following uncertainties are assumed:

$\delta W = 0.5$ W

$\delta D = 0.025$ mm

$\delta L = 0.127$ mm

$\delta \Delta T = 0.2$ºC.

Throughout the conduct of the experiment, the dimensions of the rod, D = 0.0254 m and L = 0.254 m do not change. It is assumed that the surface temperature of the rod is arbitrarily kept constant throughout the duration of the experiment. If $\Delta T = 20$ºC, the relative uncertainty in ΔT ($\delta \Delta T$) will be 1%. The overall uncertainty of the measurement of h will depend on the power input W, which will change as the velocity of flowing air changes. This simple analysis shows that at power inputs of 20, 100, and 1000 W, corresponding approximate uncertainties will be 12, 2, and 1%, respectively. These numbers are not exact but illustrate the basic thought behind calculating uncertainty. It also shows that the uncertainty in power input W dominates the uncertainty. At higher h, uncertainty decreases.

4.4 Uncertainty Analysis of Heat Exchanger Thermal Hydraulic Design

The loop is being proposed to test thermal hydraulics characteristics (heat transfer correlations, thermophysical properties, etc.) of molten salt, which are needed to design a heat exchanger. A heat exchanger design based on nominal performance characteristics is likely to result in an undersized heat exchanger. Cho (1987) points out that the probability that a heat exchanger designed in this manner will meet its demand is only 50%. A crude, but more common practical method to account for uncertainties in thermal hydraulic properties is to design the heat exchanger with an ad hoc safety factor. Practical engineers assign this under performance of the heat exchangers to a fouling resistance and maintenance problem. However, that method is being replaced by a more scientific method of analyzing uncertainties in individual properties.

To perform an experiment for measuring the thermal performance of a heat exchanger, correct information on several parameters is needed. One needs data on heat transfer coefficient, pressure drop parameters, tube dimensions, thermophysical properties of the fluids, and the tube material. However, convective heat transfer coefficients have data scattered around the mean value, tube dimensions are never as specified by the manufacturer and thermophysical properties can never be known exactly. Cho (1987), Badar et al. (1993), and James et al. (1995) have discussed uncertainty analysis relating to designing and testing of a heat exchanger. Cho (1987) presented a statistically based method for sizing a heat exchanger based on probability or confidence level of meeting the desired duty. The main purpose of doing uncertainty analysis for planning an experiment is to determine how the uncertainties in each of the parameters propagate through the governing equations and identify the dominating parameter contributing to the uncertainty.

Most of the governing equations for the design of a heat exchanger can be found in heat exchanger textbooks. Cho (1987) also gave some of these equations which are being reproduced here for the sake of completeness. If Q is the rate of heat transfer, U the overall heat transfer coefficient, A the heat transfer surface area, A_f and A_t the fin and total surface area, η_f and η_t are fin and total efficiency, R_f and R_w are fouling and wall resistances, ΔT_m the mean temperature difference, and F is the mean temperature difference correction factor, then heat transfer process can be written as

$Q = U A \Delta T_m$ (4-9)

$\Delta T_m = F ((\Delta T_a - \Delta T_b)/\ln(\Delta Ta/\Delta T_b))$ (4-10)

$1/U = (A/(\eta_t hA)_i + AR_{f,i}/A_i + R_w + AR_{f,o}/A_o + A//(\eta_t hA)_o)$ (4-11)

$\eta_t = 1 - (1 - \eta_f)A_f/A_t$ (4-12)

where $R_w = A \ln(D_o/D_i)/(2\pi k_w L)$ for a cylindrical tube wall and $R_w = t/k_w$ for a plane wall,

$\Delta T_a = (T_{h,in} - T_{c,out})$ (4-13)

$\Delta T_b = (T_{h,out} - T_{c,in})$ (4-14)

The MTD correction factor F is a function of flow configuration and the following two temperature relations, P and R. Usually plots to estimate F are available for different heat exchanger flow passes.

$P = (T_{t,out} - T_{t,in})/ (T_{s,in} - T_{t,in})$ (4-15)

$R = (T_{s,in} - T_{s,out})/ (T_{t,out} - T_{t,in})$ (4-16)

where subscripts s and t refer to shell-side and tube-side fluids, respectively.

If a dependent variable $Y = f(X_i)$, $i = 1$ to N, then the standard deviation, σ_Y, of the dependent variable Y in terms of standard deviation σ_{Xi}, of the independent variable X_i can be calculated as

$$\sigma_Y = \left[\Sigma_i^N \left(\frac{\partial Y}{\partial X_i} \right)^2 \sigma_{X_i}^2 \right]^{½}.$$ (4-17)

Cho (1987) assumed a Gaussian form of data distribution for all uncertain parameters. It leads to a root-sum-square method of establishing the probability or confidence level that the heat exchanger design will meet its stated duty. For a Gaussian distribution, probability of normally distributed data being within standard deviation $\pm\sigma$ of the mean value $\bar{X}$ is given by $P(\bar{X}-\sigma, \bar{X}+\sigma) = 0.6826$. It means that 68.26% of the total data points will lie within $(\bar{X}-\sigma)$ and $(\bar{X}+\sigma)$. If one expands the data band to $(\bar{X}-3\sigma)$ and $(\bar{X}+3\sigma)$, then the probability of normally distributed data to be within $\pm3\sigma$ becomes 99.72%. Cho (1987) calculated the effect of uncertainties of tube inside convective heat transfer coefficient, tube outside heat transfer coefficient, and tube wall thickness (outside tube diameter), which lead to an excess of 6.3% of surface area for an 80% design confidence level.

Instead of using Gaussian normal distribution, Badar et al. (1993) used log-normal and Weibull distributions. They used Monte Carlo method to show that additional heat transfer surface area required for a confidence level of 80% is ~6.6 to 6.8%. For a confidence level of 99%, additional surface area required is ~29.4 to 30.3%.

James et al. (1995) applied general experimental uncertainty analysis coupled with a traditional cross-flow heat exchanger design analysis to obtain insight into the important physical parameters and provide a reliable alternative to the ad-hoc method of over-specifying fouling factor and other safety factors.

Some of their results are interesting. Partial derivative of an experimental result (heat transfer duty, surface area, etc.) with respect to a measured parameter is termed *sensitive coefficient*. They specified the uncertainties to all the input parameters, which gave relative contribution of that parameter on the performance. They determined that even by absurdly over-specifying fouling factor (as a safety factor), its relative contribution to the heat transfer rating is small (~11%). They also determined that the heat transfer rating of a heat exchanger is more sensitive to the fluid stream characteristics than to the geometry of the heat exchanger.

Clarke et al. (2001) used the Monte Carlo method to study the sensitivity and uncertainty of heat exchanger designs to physical properties estimation, especially at high temperatures. They specified appropriate probability functions for the random and systematic errors based on different data sources, historic data, expert opinion, and other reliable sources. Systematic and bias errors (~5%) were introduced in thermal conductivity, density, heat capacity, and viscosity. Their work showed that information about reliability of the property values must be available for reliable design and performance calculations. For a systematic error of 10% in the physical properties of a cross-flow heat exchanger, the outlet gas temperature can vary as much as 40 K and the overall heat transfer coefficient can vary by as much as 80 W/m²K.

Coblentz (2002) reviewed several methods and performed calculations to obtain uncertainty in heat exchangers. Her calculations showed a range of 1 to 82% in heat transfer, Nu, Reynolds number, and heat transfer coefficient.

5. DETECTION AND CONTROL OF MELT CHEMICAL COMPOSITION IN A TEST LOOP FACILITY

5.1   Purification

The level of impurities present in the molten salt can directly affect heat transfer and thermophysical properties, and therefore must be considered in the analysis of fundamental properties measurements. But more importantly, impurities strongly affect the design and operation of any test facility because they dominate physical and chemical processes related to the control of molten salt composition and material compatibility, such as corrosion of structural materials, deposition in cold leg and flow restrictions, and response to electrochemical analytical instruments. The design and operation of any molten salt test facility must include an R&D test plan aimed at the characterization and control of impurities present in the system.

5.1.1   Purification by Chemical Processing

Initial impurities in a molten salt largely stem from the purity of the starting powders (oxide and sulfates levels) and the amount of hydration that occurs in the salts, particularly LiF because of its hygroscopic nature. Typically, powders of mixed salts are baked under vacuum or reduced pressure to remove the moisture. In the case of FLiBe, because of the toxicity and complications stemming from handling the BeF_2 salt, it is often preferred to heat the individual salts to around 450°C while being purged with a He/H_2 gas mixture at a flow rate of 100 to 200 sccm. This will drive off hydrated and absorbed moisture, allowing more accurately weighed amounts of the LiF and BeF_2 salts for use in obtaining targeted compositions.

The reduction of the oxides (Be, Ni, Fe, and Cr) and also fluorides of these metals from corrosion processes has been accomplished by purging the molten salt bath with H_2/HF gas mixtures. This process has been well described by Shaffer (1964, 1971). By controlling the ratio of H_2 to HF in the gas mixture to ~10, a balance may be achieved between the rates of the reduction of impurities and corrosion to the containment materials. Oxide ions from metal oxides are reduced, providing water and fluoride ions by the reaction

$$O^{2-} + 2HF \leftrightarrow 2F^- + H_2O \ . \tag{5-1}$$

When HF reacts with the container material, it produces fluorides from the alloy constituents during the corrosion process according to the reaction given in (5-2), where M represents Ni, Fe, and Cr. The nickel and iron fluorides can be effectively reduced during a final H_2 purge. Metallic chromium can also replace the Ni and Fe from the fluorides from reaction (5-2). The CrF_2 formed by these mechanisms is not so easily reduced by a H_2 purge. It requires reduction by a more reactive metal addition such as Be or Zr. In addition to oxides inherently introduced from the salts, oxides existing on the container material will be converted into fluorides. Additional Cr can thus be displaced from the structural alloy. In fact, reaction (5-1) demonstrates the ineffectiveness of oxide layers toward achieving corrosion resistance

$$2HF + M \leftrightarrow MF_2 + H_2 \ . \tag{5-2}$$

Sulfur impurity can exist as a sulfate in BeF_2 and can be a problem. The sulfate can be reduced to sulfide using metallic Be turnings or powder. The sulfide in turn can be reduced with a H_2/HF sparging treatment. This treatment produces H_2S that can enhance corrosion to the container material and downstream components. However, Shaffer (1964, 1971) points out that the reductions can be accomplished successfully if sufficiently high H_2 to H_2S ratios are maintained.

5.1.2   Purification by Electrochemical Methods

The chemical purification process removes most anion impurities from the melt. The metallic impurities will still remain dissolved in the molten salt or perhaps weakly adhered onto the surfaces of the container. White (1981, 1983) provides excellent reviews of electrochemical applications to remove metallic and, to some extent, anionic impurities from molten halide systems. Basically, electroactive impurity species are transported between two electrodes and deposited by applying a potential. Choices of electrode potential, current density, cell parameters (e.g., electrode geometry and material), and other parameters such as mixing, will vary for the particular application to obtain suitable efficiency. Low levels of impurities (e.g., 10^{-2} to 10^{-3} M) and their low diffusivities (10^{-5} cm^2/s) often limit current density to 10^{-3} to 10^{-2} A/cm^2. Deposition or removal of impurities within a reasonable time frame may thus be promoted by mixing or stirring the melt and using a deposition electrode with a large surface area. The electrodes can be a choice of several different types of inert materials, e.g., carbonaceous (vitreous or glassy carbon) or a metal such as Pt, W, Ta, or Mo. White (1981, 1983) mentions that lithium from the salts can sometimes be intercalated or absorbed into carbonaceous materials. In such cases, tungsten was a suitable alternative. Examples of parameters given by White for the electrolytic purification in a FliNaK mixture at 750°C were a tungsten cathode, a vitreous carbon anode, and voltage control at about 3 V. This resulted in current densities of about 5×10^{-3} A/cm^2. White states that metallic impurities can be reduced below 2 mM by such electrochemical purification. Removal of water or hydroxide ions are more difficult but may be accomplished using a carbon anode. The oxygen reacts to form either CO or CO_2. These gases must be swept away by either vigorous purging or a reduced pressure or vacuum over the bath to keep the electrode from becoming polarized.

5.2   Electrochemical Analytical Methods

To control molten salt composition and impurities concentration it is necessary to develop accurate and reliable diagnostics, and electrochemical analysis is the most promising method. Several potential electrochemical analytical methods are reviewed in the section below. This review identifies which methods might be mostly readily applied and which might have the most sensitive detection limits. All the methods need not be developed as part of this project; however, diagnostic development must be part of the R&D test plan for any molten salt test facility.

5.2.1   Electrical Conductivity

Applications of measuring the resistance and obtaining specific conductance in molten salts, viz., FLiBe, have been thoroughly explored by ORNL during the MSRE Program (1968-1970). The major difference between electrical resistivity measurements in molten salts and aqueous solutions is the much higher conductivity of the salts compared to aqueous solutions. The resistance, or capacitance, encountered at electrodes become significant compared to that of the bulk solution for molten salt. Electrode contributions are manifested with frequency dependencies. The use of electrodes with a capillary design that provided a long path length and small area increased the resistance through the molten solutions. Influences from electrode capacitance can also be distinguished and identified by using a variable capacitance bank within the balancing circuit. As an example, Bamberger and Baes (1968) provided well characterized plots of specific conductance versus temperatures for molten LiF-BeF_2 mixtures. This type of measurement provides a relatively quick benchmark as to the purity levels, but it would not provide information on the specific type of impurities present. The established database, a rigid retractable probe with no need for a reference electrode, would be reasons to consider this method for characterizing the molten FLiBe.

5.2.2   Potentiometry-EMF Measurement

Measurements of cell potentials of a molten salt may be obtained between an inert electrode and a reference electrode. Such measurements may be used to show concentrations differences of a solely existing known ionic species in both the reference cell and the test solution. With several different types of ionic species present, the cell potential can represent the overall oxidizing/reducing power of the melt. For dilute solutions with assumed equilibrium, cell potentials may theoretically be expressed by the Nernst equation shown by

$$E_{cell} = E_{O/R}^{o} + RT/nF \ln C_O^i / C_R^i - E_{ref.electrode} + E_{junction} \tag{5-3}$$

where C^i_O and C^i_R represent the concentrations of each component that has a redox reaction expressed as: O + n e- → R. The terms $E^o_{O/R}$, $E_{ref\,electrode}$, and $E_{junction}$, represent the standard potential for the redox reaction, the potential of the reference electrode, and potentials at electrode and boundary interfaces.

Effects from chemical interactions at electrodes, transition of electrodes to nonstandard state, isothermal conditions, and electrode polarization imbedded in the latter term may cause deviations from theoretical expectations. However, EMF measurements can be used as rough estimates of the oxidizing power of molten FLiBe. Tables of EMF series, from both experimental and theoretical studies for single and mixed halide salts, are also available as a gauge for EMF measurements (Hamer et al. 1965, Palmbeck 1967). Applications of this method could involve determinations of changes to cell EMF as minor controlled amounts of additives are charged to a purified bath. The biggest challenge for this technique is obtaining a reference electrode that provides long-term stability and resistance to the aggressive molten salt environments. This issue of an appropriate reference electrode is discussed in detail in Section 5.2.5.

5.2.3   Various Methods of Voltammetry

There are various methods of voltammetry that may be applied to identify the presence and quantity of different electroactive species. Included are methods of linear sweep, cyclic, stripping, and square wave voltammetry, and chronopotentiometry. These methods and their capabilities and detection limits will be discussed in turn. All methods use a three electrode setup with a working electrode, a counter electrode, and a reference electrode. Similar problems of a stable reference electrode exist as discussed above. However, the rapid nature and short exposures associated with some of these tests make them more amenable to using certain refractory metals as quasi-reference electrodes.

5.2.3.1   Linear Sweep Voltammetry

This method linearly ramps up potential relative to the reference electrode while the current between the working and counter electrode is measured. As the reduction potential of a given electroactive species is reached, the species contributes to the current carrying capacity of the solution at the working electrode. A step-up in current occurs as the potential progresses through the range for the electroactive species. An ideal case for the detection of several impurities in 0.05 M aqueous solution of KCl is shown in Figure°5-1. The distinction and height of the peaks depend upon such variables as impurity concentration, sweep rate (mV/s), electrode size and type, and the proximity of reduction potentials of different species. Faster sweep rates results in higher step heights. The onset (of potential) at each step with available EMF series is used to provide information as to which impurities are present. Quantitative measurement requires calibrations performed by spiking known quantities of a given impurity into a purified salt.
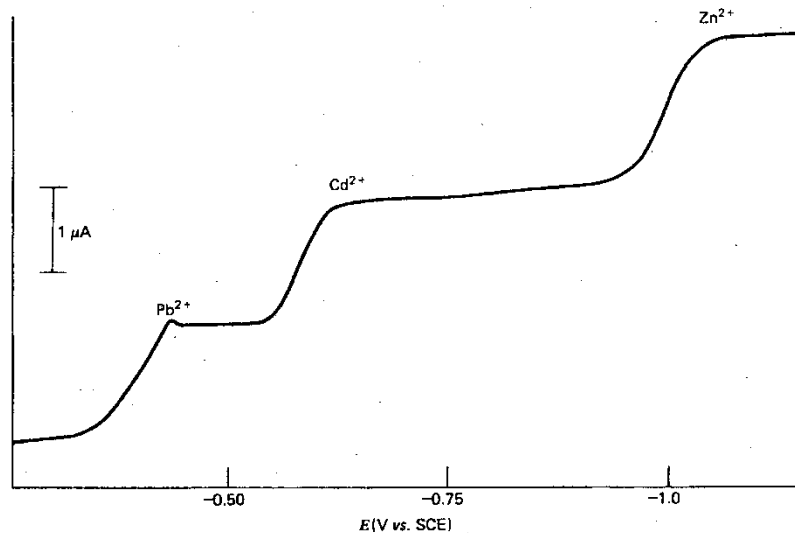
Figure 5-1. Plateaus shown for 0.2 nM Pb^{2+}, Cd^{2+}, and Zn^{2+} in 0.05 M KCl solution.

Another analytical approach develops a series of voltagrams run at different (faster) scan rates than portrayed above. Several studies provide illustrations of this approach (Mamantov and Manning 1966, Manning 1964, Manning and Mamantov 1964, Martinez et al. 2000). The scans in Figure 5-2(a) show voltagrams from FLiNaKak. Peaks in the current versus potential curve form when the electrode reaction process involves a simple reversible charge transfer. This process is quite rapid and the current then becomes limited by a mass transfer diffusion process in the solution after peak currents are achieved. The peaks in the current increase in proportion to the square root of the voltage scan rate and can be expressed by the Randles-Sevick equation

$$i_p = 1.67 x 10^5 \, n^{3/2} \, A D^{1/2} v^{1/2} \, C. \tag{5-4}$$

where i_p is the peak current (Amp), n is the electron charge involved in the redox reaction, C is the concentration, (moles/cm^3), A is the electrode area (cm^2), D is the diffusion coefficient (cm^2/s), and v is the scan rate (volts/s). Linear plots of i_p versus $v^{1/2}$, as shown in Figure 5-2(b), confirm that the process is diffusion controlled. The slope provides a means of obtaining the diffusion coefficient of a given ionic species in the molten salt. Please note the similarities in approach and the type of information that can be extracted from the rapid cyclic voltammetry tests and the chronopotentiometry (constant current) tests presented in Section 5.2.4.

Often a small or even microelectrode is used for the working electrode in cyclic voltammetry. This will limit the amount of the active species plated-out during a test and prevent significant changes to the bulk concentration during the course of an investigation. Manning and Mamantov (1964) and Mamantov and Manning (1966) used platinum wires and rods 0.5 to 3 mm in diameter and pyrolytic graphite for electrodes. One of the platinum electrodes was used as a quasi-reference electrode.

This is the preferred method to apply for initial electroanalytical analyses following the H_2/HF purification. The use of platinum as a "quasi-reference" electrode provides a much simpler system than other types of reference electrodes. The brief nature of the analysis negates problems from some potential drift at the Pt electrode. Reversed current could also be used to clean or refresh the surface before the tests. The above illustration shows results when only a single active species is present. Multiple impurities would result in several steps in cyclic voltagrams. This could cause some interference between different species and uncertainty in the application of Equation (5-4). Procedures whereby known impurities are added to a purified salt must be applied to provide a calibration for the current versus potential curves.
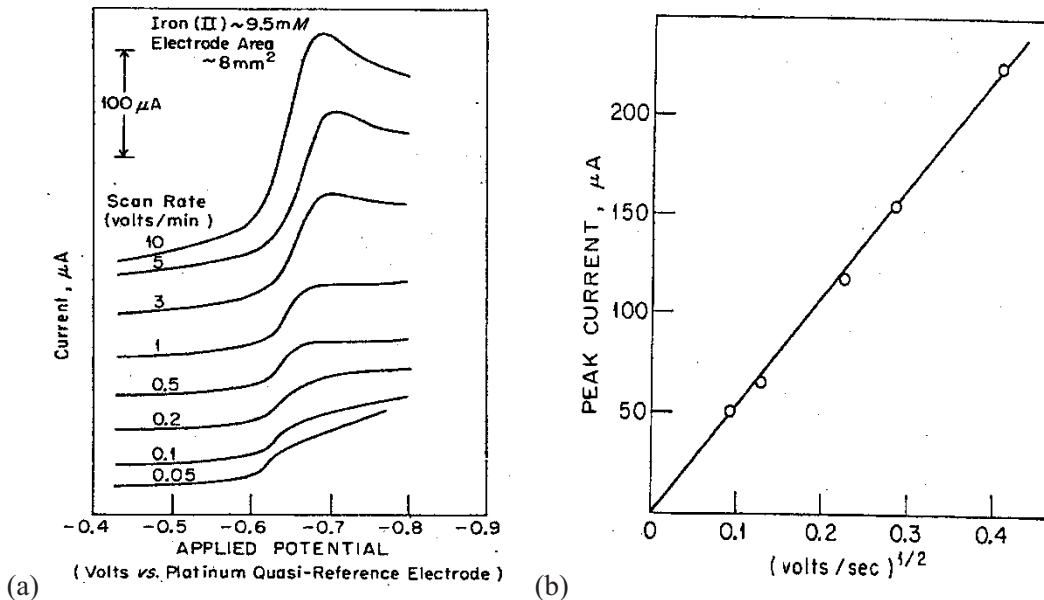
Figure 5-2. Current-potential curves from various scan rates and peak current versus square root scan rate plot for iron impurity in FLiNaK.

5.2.3.2   *Cyclic Voltammetry*

Cyclic voltammetry is an extension of the rapid linear sweep method. The potential scan is reversed over the same potential range while current is measured. Mamantov and Manning (1966) provide an example of such scans that provide the same information as described above. Such cyclic tests also checks for reversible conditions at the electrode and to the redox reactions. Bioanalytical Systems, Inc., provides information on detection limits for cyclic voltammetry. They point out that usually there is a potential difference of 60 to 70 mV observed between the oxidation peak and reduction peak for reversible reactions (the theoretical is about 58 to 59 mV). Charging currents are also often associated at the electrolyte working electrode interface. These contribute to the background current and render detection limit by cyclic voltammetry to about 10^{-5} M.

5.2.3.3   *Stripping Voltammetry*

Stripping voltammetry uses a combination of voltage control phases to provide more sensitive current versus potential plots from very dilute solutions. A constant voltage is applied for a given period, (e.g., 2°to 15 minutes) to concentrate or deposit metal ions at a cathode. According to Bard and Faulkner (2001), concentration factors of 100 to 1000 may be obtained. The potential is then reversed with a more rapid rate typical of those discussed for cyclic voltammetry above, e.g., a scan rate of 10 to 100 mV/sec. The anodic currents produced by stripping the impurity from the electrode will provide more distinct peaks for analyses than those obtained from linear voltammetry. Bard and Faulkner (2001) report that this technique can detect solutions as dilute as 10^{-10} to 10^{-11} M. BASi (formerly Bioanalytical Systems Inc.) also indicates that stripping techniques can provide quantitative measurements down to low (ppb) concentrations. Such sensitivities are likely those achievable for a cell that uses droplets such as Hg or a molten metal that have refreshed surfaces and can more closely represent ideal electrode conditions. Detection limits using solid metal or glassy carbon electrodes are likely not quite as low. However, an electrode such as Pt as a quasi-reference electrode, would probably work satisfactorily for this method. This would make this approach a very viable method for analysis of very dilute impurities in solution in the molten salts.

5.2.3.4   Square Wave Voltammetry

There are also some pulsed or square-wave, potential controlled methods, e.g., Osteryoung or Barker square wave voltammetry, that provide increased sensitivity. Descriptions and applications of these techniques are provided by Medlin et al. (1998). BASi reports that detection limits of 10^{-7} to 10^{-8} M may be obtained with such differential pulsed-voltammetry methods. This is a factor of 100 to 1000 more sensitive than the cyclic voltammetry discussed above. Clauβen and Rüssel (1997) report that they used pulses of 50 to 200 mV applied at frequencies between 5 to 500 Hz in their study in molten glass. They used 1-mm diameter platinum wire for the working electrode and a platinum plate for the counter electrode. A zirconia probe with an air purge was used for the reference electrode. Such a probe may be good for the oxygen-bearing glasses but not appropriate for molten fluorides, which needs to be maintained essentially oxygen-free. To apply this technique, an appropriate reference electrode would need to be developed as discussed in Section 5.2.5.

5.2.4   Chronopotentiometry

Other electrochemical methods involving various types of current controlled experiments (i.e.,°chronopotentiometry) have been used to obtain concentrations, saturation limits, and diffusion coefficients of impurities in molten salts. Van Norman et al. (1965, 1966) provide examples of methods that can be used to measure the solubility of metals in their chloride and bromide solutions. The concept behind this method of chronopotentiometry is quite simple. A constant current is applied across two electrodes in a homogeneous unstirred solution. The potential is recorded with time as conditions of the electroactive metal ion change at the working electrode to accommodate the current. Initially, the concentration of the ion M^{n+} is uniform throughout the solution and at the electrode. When a current is imposed, diffusion by a semi-infinite planar diffusion mode may be assumed to provide the mass transport from the solution to the electrode. The potential will change with time as polarization occurs at the electrode. The transition time has been identified as the time from the onset of the application of the current to the point where significant polarization occurs, which in turn causes a dramatic increase in the potential. A series of potential versus time plots for a set of different currents is obtained as shown in Figure 5-3. A more rapid onset of the transition time correlates with higher current densities.

5.2.5   Reference Electrodes for Electrochemical Analysis

The choice of an appropriate reference electrode is very important in electrochemical analysis. The electrode should provide a stable reference potential and also resist corrosive attack from the molten salt environments. Molten fluoride systems are particularly aggressive and place even additional requirements upon the containment material compared to molten chloride systems. Minh and Redey (1987) provide a comprehensive review of requirements and electrodes developed for various systems. They express the critical need of a stable electrode with known potential for studies into the thermodynamic properties of molten salt systems. The requirements for kinetic studies using voltammetric or chronopotentiometric methods are not as critical. They state that various metals (such as Pt, Ni, Mo, W, and Ta) and even graphite may be used as a quasi-reference electrode. They reference the report by Mamantov and Manning (1966) where potential variation of only 10 to 20 mV were observed over a weekly period from a Pt electrode.
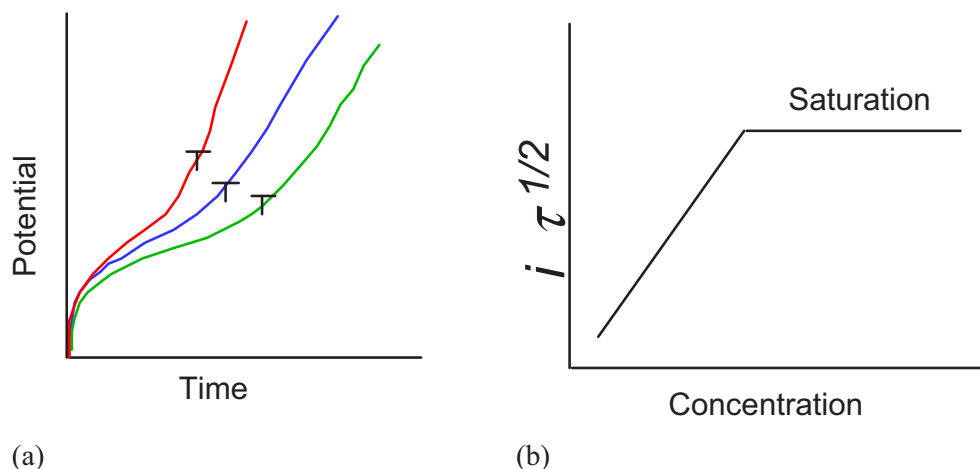
Figure 5-3. (a) Schematic illustration of anodic chronopotentiograms at different current densities and (b)°corresponding plot of $i\tau^{1/2}$ vs. concentration to determine solubility.

There are several common requirements for a suitable stable reference electrode. The media with the known redox potential must be isolated from the test solution; however, a bridge or membrane must exist allowing an electrolytic junction between the compartments. The bridge may allow limited diffusion through a porous media (such as a frit or graphite) or it can be a solid ionic conducting compound. The container material should also be resistant to the fluoride salt mixture to prevent contamination. There have been several reports showing the development of various reference electrodes during the MSRE project (Bronstein and Manning 1972, Bamberger 1975a). The development can be traced though the following basic designs:

- A design with boron nitride as the outer container (thinned to serve as the bridge at the bottom). The internal half-cell was a nickel electrode in a known molten fluoride. This electrode was reported to remain within ±3 mV over several days. This cell was reported as usable up to 800°C. However, other reports indicate susceptibility to chemical attack and thermal cycling.

- A design that used a silica or BeO tube to contain a mixture of FLiBe saturated with NiO or BeO. Nickel was again used as the internal electrode. This assembly was housed in a perforated nickel jacket.

- Advanced designs used single crystals of LaF_3 for the ionic conductor. A pool of molten fluoride (i.e.,°FLiBe saturated with NiF_2) with a Ni electrode was used for the internal component. This cell was contained in nickel and boron nitride components. A nickel frit was used for a porous junction. These were the types of cells that operated for several months in the flowing loops with EMF potential drifts of only a few mV.

A recent report presented an alternative to the types of reference cells described above (Kontoyannis 1995) in response to some of the problems with the reference cell in question. These include the availability of the LaF_3 used in the third type of cell and the susceptibility of boron nitride to thermal shock, which resulted in probes reported to survive only a few cycles. The alternative design used similar internal components; either a Ni or Ag wire electrode in FLiNaK saturated with either NiF_2 or AgF contained in a closed bottom graphite cell. However, pyrolytic boron nitride was coated onto the outer diameter of the graphite cell while the bottom was left uncoated to provide the porous membrane for the salt mixture. The probe showed good reversibility and response time was actually improved with additional thermal cycling.

5.3   Sampling and Chemical Analysis

It is essential that the experimenter is able to add/remove samples repeatedly during the course of long term operations of a heat transfer test facility. Bamberger (1975b) describes experimental hardware (flanges, bellows, seals, and valves) needed for such operations based on sample exchange chamber. Sampling is done with a rod through a gas tight fitting with gasket such as teflon, graphnol, or lavite that can withstand the temperature on the risers extending from the top lid of the test vessel. The rod is lowered to dip a sample and then raised into an inert gas chamber above the test cell. The chamber has a lower valve to isolate it from the bath, allowing sample removal and the attachment of a new sampling cup. The chamber is purged with helium to reestablish a high purity environment in the sampling chamber between operations. Such a system is also required in order to add material to the melt, either for composition control (eutectic title) or to provide known concentrations for the calibration of electrochemical analysis instruments.

Chemical analysis is performed on collected samples to determine their composition using inductively coupled plasma atomic emission spectroscopy (ICP-AES) or inductively coupled plasma mass spectroscopy (ICP-MS) for metallic elements and Leco analytical systems for oxygen, nitrogen, and carbon. ICP-MS has better detection limits for some elements but the system is not tolerant to strong acidic solutions. Detection limits reported for ICP-AES for impurities such as Fe, Cr, and Ni range from $2°$to 4 µg/L. This allows detection of these impurities at near ppm levels, depending upon the final procedures used for sample dissolution.

6. MATERIAL COMPATIBILITY ISSUES RELEVANT TO A TEST LOOP FACILITY

Material compatibility issues are likely not included within the scope of an experimental test plan aimed at the investigation of heat transfer properties of molten salts. However, any heat transfer test facility would likely involve a forced convection loop and its design and operation would inevitably have to consider material compatibility issues such as corrosion and the prevention or detection of components performance degradation.

The discussion on melt composition measurement in the previous chapter already addressed the issue of corrosion detection. The discussion that follows on structural materials compatibility has the main objective of providing guidance for the design of a heat transfer test facility aimed at minimizing the effect of corrosion on the system performance. It will also introduce limitations in the available properties database that may require the addition of specific R&D tasks related to material compatibility to the test plan.

Available options for active control of corrosion processes through the fluoride potential are also discussed. Although their development and characterization will not be part of the test plan, one or more methods may be employed in a heat transfer test facility, depending on the choice of materials adopted for system structures and components and other operation parameters, such as temperature.

6.1 Definition of Corrosion in Fluoride Molten Salts

In high-temperature nonaqueous systems, the redox state is a measure of the propensity for corrosion of the container metals (Olander 2002). Redox is a generalized term that is made specific according to the anion X exchanged between two valence states of a cation M. The redox condition is referred to as the *potential* of the anion species. Since the anion species is usually an elemental gas in its normal state, the potential is defined in terms of its partial pressure. The redox condition or potential fixes the ratio of the high and low valence states of a cation that is simultaneously present, or vice versa. The X-potential is defined in terms of the partial molar Gibbs free energy of the diatomic gas X_2, where $X = O, S, F, Cl$, etc

$$\Delta \overline{G}_{X_2} \equiv RT \ln p_{X_2}.$$ (6-1)

This particular definition follows from the equilibrium expression of the generalized oxidation reaction

$$MX_n + \tfrac{1}{2}X_2(g) = MX_{n+1} \text{ where } 0 \leq n \leq 4.$$ (6-2)

The most common redox potential is the oxygen potential, where $X = O$. This potential is an important thermodynamic property of oxide systems containing multivalent cations, such as U and Pu in nuclear fuels. The multivalent cation can be contained in a gas (e.g., $M = H_2$ or CO, $n = 0$), a metal (e.g., °M = Ca, $n = 0$), or an oxide (e.g., $M = Ti$, $n = 1$). It is not necessary that the gas X_2 be physically present in the system; a metal and its oxide can be enclosed in a gas-free container yet still exhibit the potential for generating an oxygen pressure. In the case where the cation is a gas, the equilibrium partial pressure of X_2 may be too small to include in material balances; many metal-metal oxide systems generate oxygen pressures of 10^{-25} atm or less.

In FLiBe and FLiNaK, it is clear that $X = F$, and the redox condition is properly termed the *fluorine potential*

$$\Delta \overline{G}_{F_2} \equiv RT \ln p_{F_2}.$$ (6-3)

The fluorine potential controls the equilibrium concentrations of structural metals dissolved in the fluoride-based salts. As such it provides a quantitative description of the corrosion process at the solid/liquid interface.

Various phenomena can alter the fluorine potential, either in the system as a whole or at a specific location, thus affecting the corrosion process. Those are sometimes identified as corrosion 'mechanism' and differentiate to what is then referred to as 'intrinsic' corrosion, which is the unaltered equilibrium condition defined above. All those 'mechanisms' can quantitatively be referred to as a variation in the fluorine potential as expressed by Equation (6-3). They include:

- *Corrosion by impurities*. The addition of oxidizing contaminants, such as HF or H_2O, residual oxides of metals and polyvalent metal ions can have a strong effect on the fluorine potential of the relative element.

- *Temperature gradients*. Steady or transient temperature gradients affect the fluorine potential of dissolved element. This mechanism is usually described in terms of solubility, a more familiar concept generally applied in the macroscopic description of aqueous solutions.

- *Galvanic effects*. The application of an external electromotive force (an applied electrical potential) between two interfaces in contact with the liquid results in the variation of the fluorine potential for elements present in the solid phases. Small electrical forces can locally arise from the presence of dissimilar materials, such as in welds. Large forces can be controlled by applying an external potential to two or more electrodes, which is the theoretical basis for electrochemical purification methods described in the previous section.

The effect of the mechanism described above on structural materials for FLiBe and FLiNaK systems has been summarized in the cited database evaluation report (Sohal et al. 2010). This qualitative evaluation, along with the quantitative measurement of the fluorine potential in thermodynamic equilibrium for relevant elements (expressed by the free energy of formation at a specific temperature), constitute the basis for the choice of structural materials in molten salt systems. An example of how such information can be employed for design studies is shown in Figure 6-1.
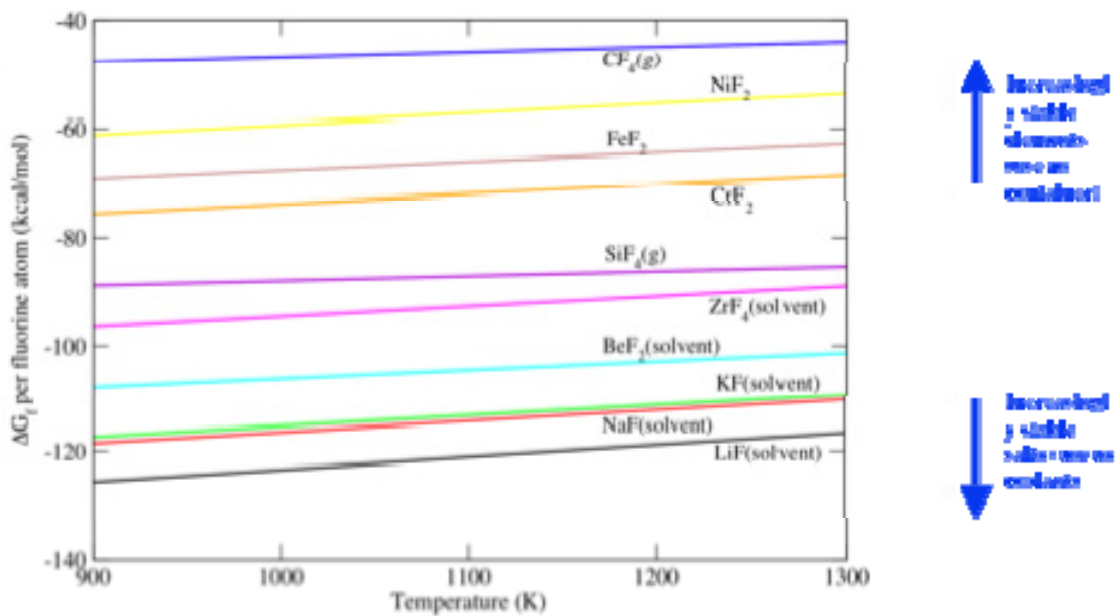

Figure 6-1. Comparison of the stability of structural alloy elements with respect to fluoride corrosion (Cassayre 2005).

6.2 Limitations in Available Database of Structural Materials Corrosion in Molten Salt

A few general observations can be drawn from the existing but limited data (Sohal et al. 2010). Nickel and alloys with dense Ni coatings are effectively inert to corrosion in fluoride salts. Of the chromium containing alloys, Hastelloy N appears to have the best corrosion resistance. In general, alloys with increasing carbon and chromium content are increasingly subject to corrosion by the fluoride salts FLiBe and FLiNaK, due to attack and dissolution of the intergranular chromium carbide.

In general, FLiNaK caused extensive intergranular corrosion in most of the alloys, producing substantial void structure at the grain boundaries that developed rapidly and extended deeply in susceptible alloys. In some cases, intergranular corrosion progressed to open, connected porosity with salt intrusion into the degraded alloy. On the other hand, FLiBe caused more moderate intergranular corrosion. Based on a single-test on reduced activation martensitic steel developed in Japan for fusion applications (JLF-1) (Kondo et al. 2009) and Incoloy 800H (Olson et al. 2009), FLiNaK appears to be much more corrosive than FLiBe.

Finally, thermal gradients and galvanic couples in the molten salts can enhance corrosion rates by one to two orders of magnitude relative to corrosion by residual contaminants in the molten salts. However, correlations of corrosion rate as a function of contaminant type, concentration, and temperature are not available for a quantitative comparison for many elements.

The existing data on material compatibility as a whole are insufficient to serve as a basis for reliable selection of containment materials. This stems from the fact that the large database available from MSRE operation was obtained for salts with dissolved fuel elements and not for pure salts envisioned for heat transfer applications. The corrosion data are limited, both in terms of coolant composition and the structural alloys tested. Comprehensive parametric investigation (for example, a range of impurities concentration at a specific temperature) is even more limited, and so are single effect test designed to focus on a single corrosion 'mechanism.' Finally, quantification of corrosion data rely mostly on mass loss measurements from exposed specimen, which might not represent a realistic measure of the effects of corrosion because intergranular corrosion could severely degrade the mechanical characteristics and cause premature failure in alloys even at low mass loss values.

All the above limitations need to be overcome by a new experimental R&D program on material compatibility focused on FLiBe and FLiNaK as heat transfer media. Such effort is likely to start in parallel with the evaluation of heat transfer performance, which is the subject of this report. The extent of material compatibility test necessary before the design of a heat transfer test facility will be determined by available funds, project schedule, and risk analysis, and as such, is beyond the scope of this report.

7.   ENHANCED MOLTEN SALT PURIFICATION BY ELECTROCHEMICAL METHODS: FEASIBILITY EXPERIMENTS WITH FLIBE

7.1   System Description

In the described electrochemistry experiments, the molten salt is contained within glassy carbon coated graphite, alumina coated metallic, or nickel crucible. The experiments are housed in a dry inert gas glove box that is purged with Argon (see Figure 7-1). Initially, the melt is prepared and tested using an induction heating system. The metallic (Nickel) crucibles are initially chosen to better couple with the magnetic field. Longer electrochemical experiments may utilize standard resistance furnaces, for which ceramic crucible may also be used. Electrochemical experiments will use metal or alloy wire for the working electrode (WE) and glassy carbon or platinum for the counter electrode (CE). The reference electrode (RE) will either be platinum wire for a pseudo-RE, gold alloy as a dynamic RE, or Ni/Ni(II) in pyrolytic boron nitride as a traditional RE. This system will be scalable for larger, more complex experiments.
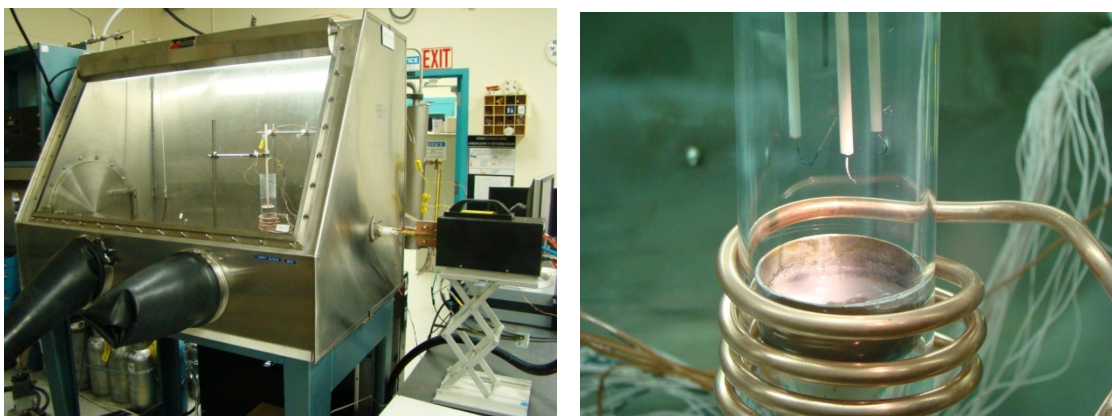

Figure 7-1. Glove box with induction heating system (left), molten FLiBe cell (right).

7.2   Instruments used in Electrochemistry Tests

Analysis of salt composition is based on electrochemical methods. An AMEL 2053 potentiostat-galvanostat with a National Instruments computer interface card (Card PCI-6259 with shielded SHC68-68-EPM cable) measures currents and potentials from a range of electrochemical experiments (Figure 7-2). The waveforms for these experiments are generated and data recorded from a Labview interface that was specifically designed at INL for the molten salt tests described here. The Labview graphical user interface (GUI) allows the users to design, test, and then execute simple to complex electrochemical experiments (such as cyclic voltammetry, anodic stripping voltammetry and bulk electrolysis). Utilizing the GUI's manual mode will allow plating of dynamic reference electrodes in order to test applicability within fluoride based molten salts. The current computer/PCI card configuration will allow scan rates from 1 to 80,000 mV/s and measure four data points per millivolt step. Validating functions of the AMEL involves use of the calibration side of a Gamry Universal Dummy Cell (Figure 7-2).

Figure 7-2. AMEL potentiostat with Labview interface (left) and dummy cell (right).

7.3   Validating Experiments with Reference Solution

User training and validation tests for the instrument and custom developed control interface involve use of a simple aqueous solution of 1.0M potassium nitrate with 0.010M potassium ferricyanide (see Figure 7-3). The ferricyanide provides a clear reversible one electron oxidation/reduction for cyclic voltammetry (CV) experiments. Multiple CV scans, as shown in Figure 7-3, can be used to determine concentration and diffusion coefficient of an analyte via the Randles-Sevick equation. In this equation. i_p is the peak current (Amp), n is the electron charge involved in the redox reaction, C is the concentration, (moles/cm^3), A is the electrode area (cm^2), D is the diffusion coefficient (cm^2/s), and v is the scan rate (volts/s):

$$ip = 1.67x105 \; n3/2 \; AD^{1/2} \; v^{1/2}C \tag{7-1}$$

Further experiments with the reference solution were done to validate approach in flow conditions for application in heat exchanger loop test. The flow conditions were simulated with a commercial magnetic stirrer commonly used for solution mixing. The tests also provided initial information on the electromagnetic (EM) noise induced in the data acquisition system by magnetic field fluctuations from the stirring unit, which will be applicable to minimize the effect of the induction heating system on instruments performance. A validating test with a reference solution also provided valuable experience and solutions to problems that may arise with the actual molten salt, such as comparison of performance of various electrodes materials (i.e., gold, nickel, stainless steel, and glassy carbon).

As an example of such scoping tests, Figure 7-4 shows a dramatic loss in current signal between the electrodes after the solution is stirred to simulate flow conditions. However, by increasing the sweep rate of the potential (millivolts/s), the disruption from the induced flow can be resolved. Another example is how a fluctuating magnetic field can affect the measurements (see Figure 7-5). The test reported used glassy carbon as a working electrode as it was the most affected by EM noise of the materials tested, which may ultimately limit its use with the induction heating system in the glove box.
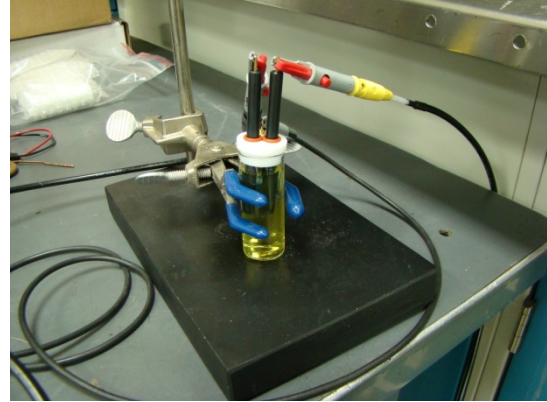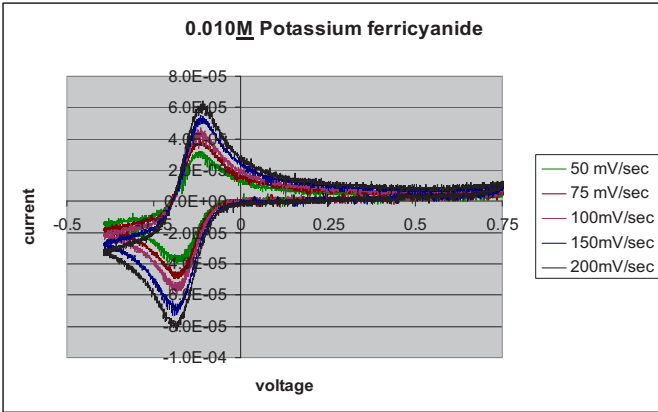
Figure 7-3. Multi-sweep scans (left) with gold WE, platinum quasi-RE, and platinum CE (right).
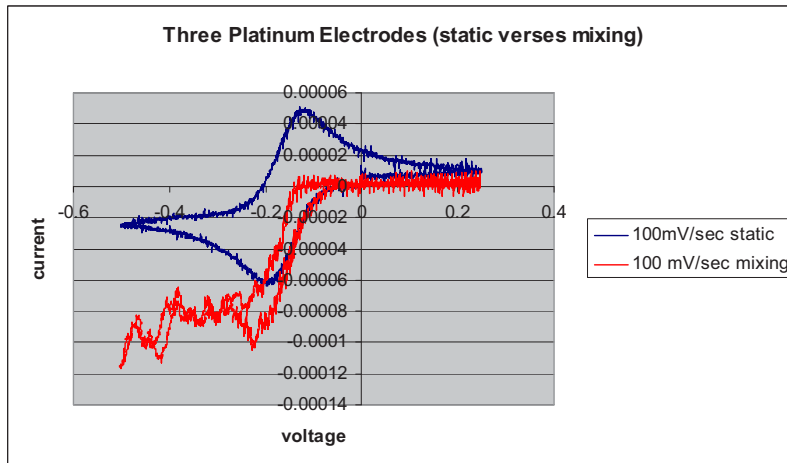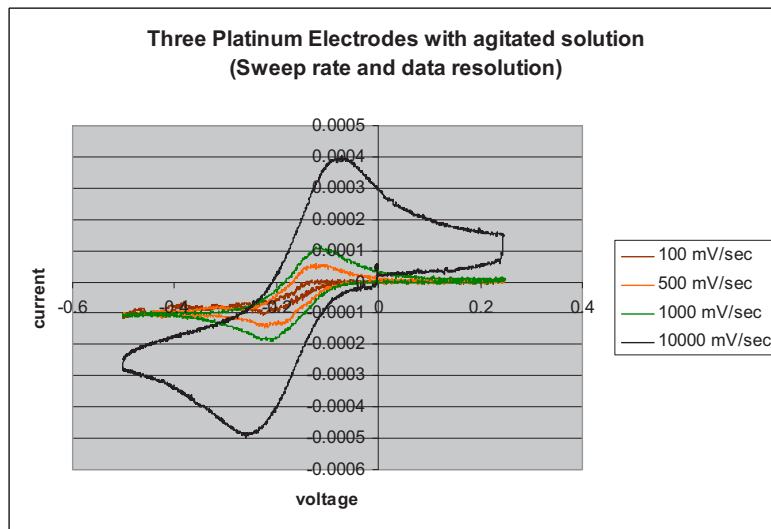

Figure 7-4. Differences in resolution from a static in blue and flowing solution loop in red (right) and increased resolution under flowing condition with faster sweep rates (left).
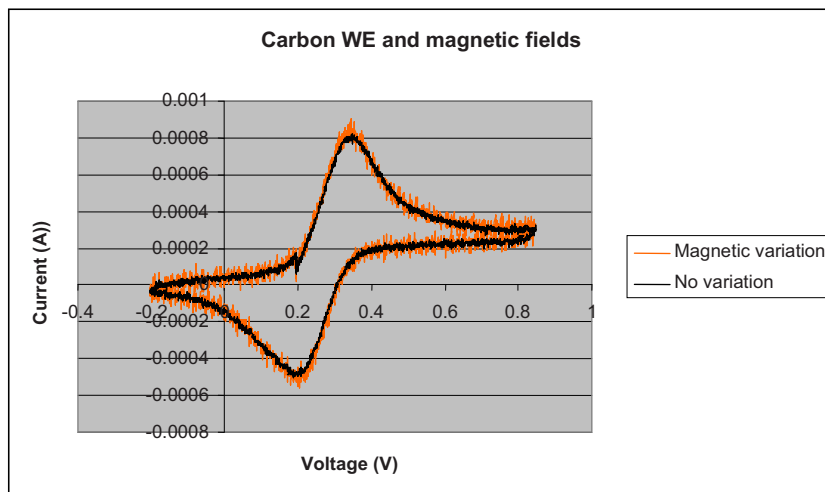
Carbon WE and magnetic fields

Current (A)) vs Voltage (V)

Legend: Magnetic variation, No variation

Figure 7-5. Noise experienced with magnetic variation and use of a glassy carbon WE.

7.4   ElectrochemistryTests in FLiBe

FLiBe was prepared from single salt components beryllium di-fluoride (Alfa Aesar, stock #35827, Lot # L15J29, 100g total of labeled 99.9% BeF_2 on metal basis) and lithium fluoride (Alfa Aesar, stock #36359, Lot # B09R001, 50g total of labeled 99.85% LiF on metal basis). The materials are mixed according to eutectic composition (33-66% on molar basis, 1.1036 mass ratio), with calculations shown in Table 7-1. The crucible used is a 48 mm diameter pure nickel crucible (see Figure 7-6) purchased from Metal Technology, Inc. The crucible is initially filled with 11.14 gm of BeF_2 crystals. The necessary amount of LiF (12.30 gm) powder is then added to reach the desired eutectic composition. Glove box condition during mixing operation is 430.7 ppm moisture, which is higher than desirable for large scale preparation. Improvement of dry conditions in the glove box will be necessary for further testing.

The materials are melted using the induction heater assembly visible in Figure 7-1. A quartz tube is situated between the coils and the crucible to prevent accidental contact and possible spills while allowing unobstructed view. Two type-K thermocouples are installed in the system. One is inserted within the mixed crystal and powder materials, and it measures the melting temperature of the eutectic. The second one is embedded in the boron nitrate rod holding the crucible and measured the crucible temperature. The induction heater was set in stable condition for a desired current in the coils of 88.2A, resulting in 101kW of power coupled with the crucible at a natural frequency of 328 kHz. In approximately 10 minutes of operation, the salt started to melt from visual observation for a measured temperature of 470ºC compared to the theoretical eutectic melting point of 459.1ºC. At the time of melting the glove box conditions had improved to 248 ppm moisture under argon gas flow. Figure 7-6 shows the salt at 700ºC in a subsequent melting operation prior to an electrochemical test run. The immersed thermocouple was retracted from the bath through the central alumina tube visible in the picture.

The three-electrode assembly used in the test (see Figure 7-6) was constructed from a boron nitride disc and all electrodes were made of a 0.5 mm diameter platinum wire. The working and reference electrodes are simple, straight wires. The immersed portion of the wire is not accurately defined during the tests since their objective is a qualitative validation of the proposed method. The estimated immersed length is 5 mm. Accurate measurement of the immersed surface is necessary for quantitative evaluation of ionic species concentrations and will be implemented in the second test phase. Both wires were 29 mm long, including the section going through the ceramic holder. In any electrochemical set-up, the counter electrode must have a substantially larger immersed surface area compared to the working electrode. This

ensures that the electrode surface area does not impact the conclusions derived from ionic current saturation. To allow a larger immersed area, the counter electrode is bent horizontally and folded twice as shown in Figure 7-7. The difference in immersed length between CE and WE is at least 33 mm.

During previous experiments on fluoride salts at the STAR facility batches of similar constituent materials (BeF_2 and LiF) have been analyzed to characterize 'as-received' metallic impurities with Inductively Couple Plasma (ICP) analysis. A representative sample of results is shown in Table 7-2. The results show that iron and nickel are the dominant impurities in the as-received material. Among the two impurities, initial scoping test was focused on nickel because of its anticipated reversible behavior at the platinum electrode surfaces due to the low solubility in the melt. The objective of the test was therefore to identify and analyze the nickel peak in the voltammetry (CV) scan obtained from the FLiBe prepared during the operation described above. This was done by repeating the CV scan with the same parameters and electrodes after the addition of 0.14 gm of nickel fluoride (NiF_2) to the melt. The comparison of the two CV scans is shown in Figure 7-8. The cathodic and anodic peaks grew at -1.7 and -1.0 volts, respectively. The reduction of nickel is relatively close to the cathodic limit of FLiBe, and the overall chemical window of FLiBe with this electrochemical cell is 4 volts.

A second qualitative test to validate the electrochemical method employed as a technique to characterize FLiBe composition was performed by adding a further 0.07 gm of silver fluoride (AgF) to the same melt. Figure 7-9 shows the result of the last addition alone, comparing CV scans and FLiBe after the addition of NiF_2 with that after the addition of NiF_2 and AgF. Figure 7-10 compares the initial CV scan of the 'as-melted' eutectic with the final melt after both additions. The analysis of the scans in Figures 7-9 and 7-10 is not straightforward because of the addition of different materials to the same melt. Furthermore, the thermodynamic and chemical properties of silver fluoride in FLiBe melts are not as well know as for nickel, so it is hard to anticipate the impact on the voltammetry scans.

Table 7-1. Stochiometric preparation of FLiBe eutectic composition.

|	Li	Be	F	LiF	BeF2	Flibe
1 mole of Flibe is 2/3 moles of LiF and 1/3 moles of BeF2						
Molecular weight [g/mol]	6.941	9.012	18.998	25.939	47.008	32.962
Molar ratio in flibe				0.66666667	0.33333333	1
Elements mass in 1 mole of flibe [g]	5.88018664	2.10640419	24.9754092	17.2926667	15.6693333	32.962
Weight fraction	0.1783929	0.06390402	0.75770309	0.52462431	0.47537569	1
Li / Be reference molar ratio	2					
Li / Be reference weight ratio	1.10359939					
			Theorical			
	Temp [C]	Temp [K]				
Flibe density [g/cm3]	500	773	2.035776			
Crucible #1 - Aug 10, 2010						
Crucible mass [g]	35.24					
BeF2 mass [g]	11.14					
LiF required mass [g]	12.2940972					
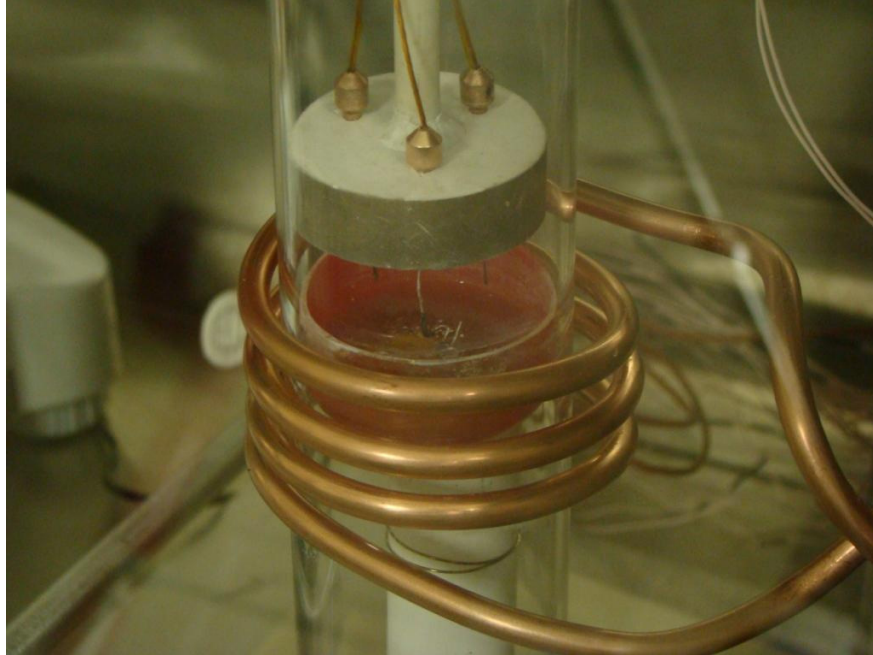
Figure 7-6. Induction heating of FLiBe (at 700ºC) in progress.

Figure 7-7. Platinum electrodes during operation: the counter electrode bent shape is visible.
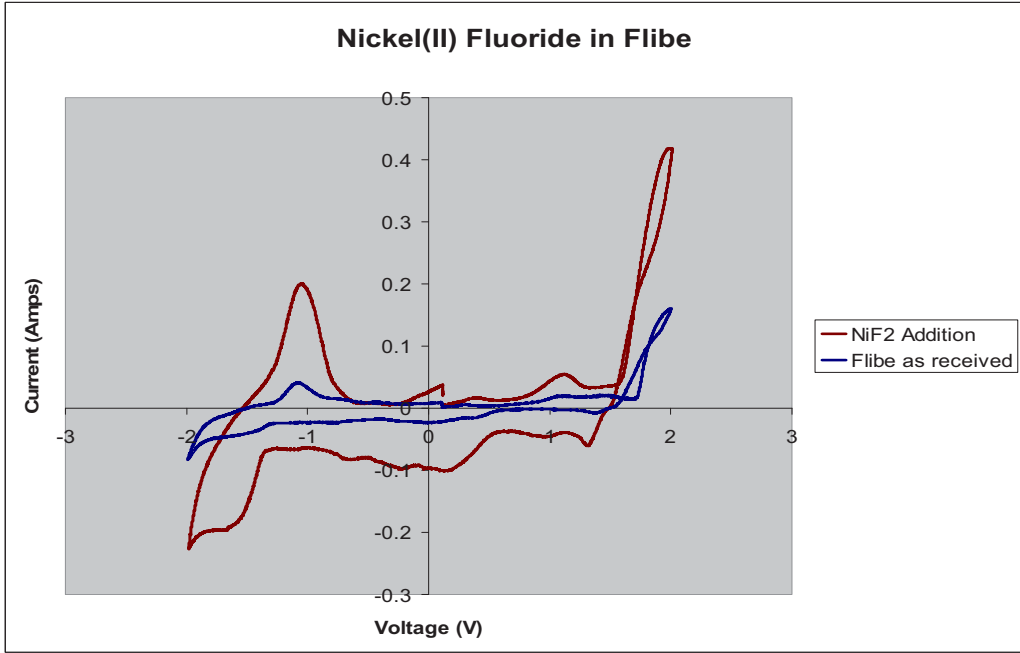
Figure 7-8. Flibe CV scans before and after Nickel(II) Fluoride addition.

Table 7-2. A representative sample of Inductively Couple Plasma (ICP) analysis.

| Salt	Lot No.	Analyses		Be	Li	Cr	Mn	Fe	Ni	Cu	Zn	Mo	Ag	Ba	Pb
								Concentration of Various Elements (ppm)							
BeF$_2$	A13K03	ICP-AES	1	155390	10	38	11	249	42	3		<16			
		ICP-AES	2	139720	3	16	6	201	28	2		<11			
BeF$_2$	A13K03	ICP-MS	1			9	6	403	11	4	10	1	4	9	2
		ICP-MS	2			9	6	322	10	4	8	1	4	6	2
BeF$_2$	L15J29	ICP-AES	1	140770	<4	8	6	180	116	<2		<13			
		ICP-AES	2	130350	2	4	6	162	47	<2		<9			
		ICP-AES	3	127160	3	3	6	174	36	2		<9			
BeF$_2$	L15J29	ICP-MS	1			10	7	317	11	4	9	1	<0.01	5	10
		ICP-MS	2			8	6	296	10	4	10	1	<0.01	6	3
		ICP-MS	3			10	7	265	11	4	9	1	<0.01	15	4
			2												
LiF	09809AO	ICP-AES	1	<3	14130	2	2	110	88	<1		<4			
LiF	09809AO	ICP-MS	1			5	4	141	11	3	15	2	<0.01	15	10
			2			5	4	104	5	3	13	2	<0.01	4	3
			3			2	2	43	4	2	6	1	<0.01	5	4
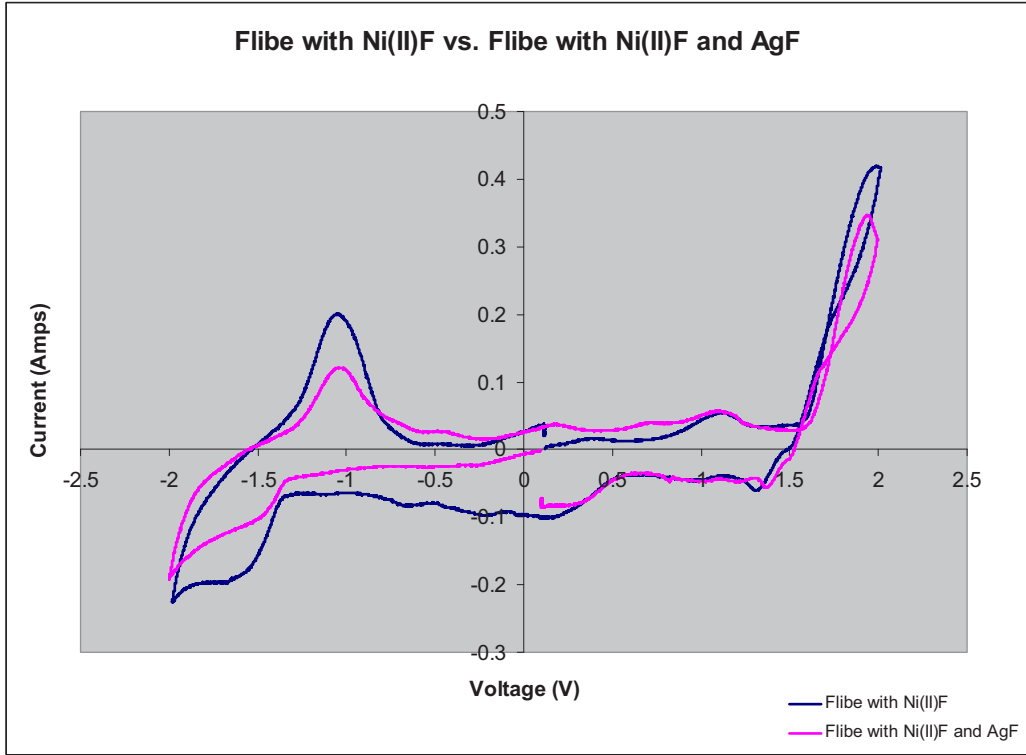
Figure 7-9. FLiBe CV scans before and after the addition of AgF, additional NiF2 already present.
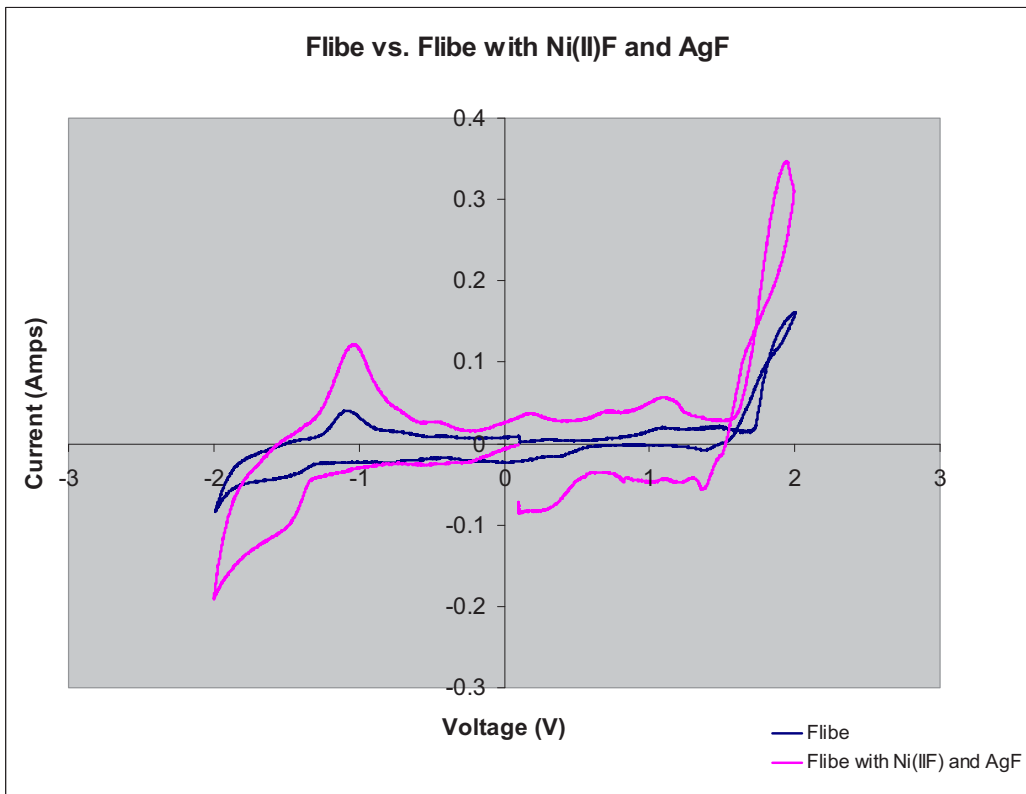

Figure 7-10. As received FLiBe CV scan compared to after $Ni(II)F_2$ and AgF addition.

8.   FREEZING OF MOLTEN SALT AND RELATED ISSUES

In FCL, the loss of circulation pump power could cause freezing. It°may not be economical and also may be physically difficult to melt all the salt in the pipes or the test section or heat exchanger. Also, if heating were possible, thermal expansion of the salt may cause problems (leaks, pipe rupture). So, to avoid the freezing issue, the FCL circulation pump should have an alternate power source and the loop should either have heat tracing wire around the pipe or a mechanism to input warm/hot gas into the loop in order to melt the salt. A feasibility of the proposed solution should be carried out. Following the example of freezing of reactor fluid provides some general guidelines.

Sohal and Werner (2008) analyzed freezing of NaK in a reactor piping when exposed to lunar atmosphere. This work gives guidelines about safety precautions one has to take when exposed to severe cold environment. Lunar surface temperature fluctuates between 400 K (during lunar day) to 100 K (during lunar night). When exposed to such a harsh environment and even with a 4 in. thick best available insulation, freezing of NaK cannot be avoided forever. Figure 8-1 compares the NaK temperature with and without insulation. The insulation (plastic insulation material) has thermal conductivity of 0.03 W/(m K), density of 50 kg/m^3, heat capacity of 2,000 J/(kg K), and thermal diffusion of 3×10^{-7} m^2/s. A thickness of 2 in. was selected. Because of the thermal diffusivity effects (time rate for heat to flow in or out of the pipe) with the insulation, NaK or pipe outer surface temperatures reach the same temperature as without the insulation. In other words, the problem of NaK freezing cannot be eliminated with insulation, but just gets delayed by a few hours.
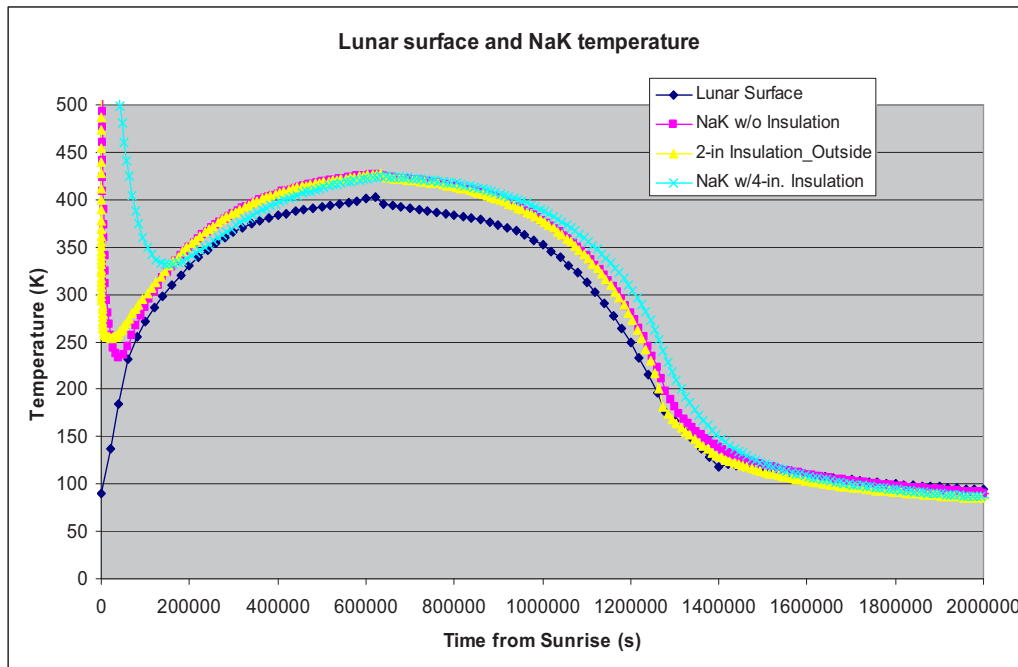
Figure 8-1. Lunar surface and NaK temperatures in K (nearly same as the pipe surface temperature in case without insulation), with and without insulation, for a lunar day (time in seconds) with solar radiation during the day time. Initial NaK temperature = 840 K (Sohal and Werner 2008).

From these curves, it is obvious that the thickness of insulation is not a determining factor. Within 15–20 hours of the sunset or sunrise, the NaK will approach the temperature of the ambient (lunar surface or the assumed ambient sink temperature in the example shown here). If the ambient temperature is below a freezing temperature, the NaK temperature will also very quickly approach that temperature.

Therefore, the one solution to avoiding freezing is to have a small amount of molten salt flowing at all times, a solution sometimes used by homeowners to avoid freezing of the water pipes. Another costly, but effective solution, is to utilize heating of the molten salt whenever the ambient temperature dips below a set value.

9. CONCLUSIONS AND RECOMMENDATIONS FOR FUTURE WORK

Higher energy inefficiencies are associated with helium for use in transporting thermal energy, it is commonly accepted that molten salts should be used for transporting heat from a nuclear reactor to a processing plant. The salt proposed by Task et al. (2005) is 50%LiF-50%BeF2 mainly because of its low melting point and high specific heat capacity. However, the presence of beryllium makes the salt toxic. Therefore, other salts (possibly zirconium-based salts with similar characteristics) need to be investigated. Several possible choices are listed in Table 1.1.

Earlier work by the present authors (Sohal et al. 2010) has clearly shown that the existing knowledge on thermodynamic, thermophysical, thermochemical, and thermal-hydraulic properties of molten salts is incomplete. This conclusion is reinforced in Section 1.3 of this report. That and the present report recommend what development work needs to be done to enable deployment of molten salt to transport heat from a nuclear reactor to other applications. Although some knowledge and experience can be gained from the past MSBR and other molten salt programs, most of the knowledge gap can be only bridged by a combination of extensive experimental investigation and/or empirical correlations for all essential properties and characteristics. Only after obtaining reliable and verifiable properties of the molten salts, a reliable design of heat transport systems and intermediate heat exchanger can be developed.

High temperature molten salt systems introduce some unique requirements not generally considered for other common fluids. These include the use of unconventional materials for molten salt transport, heat exchanger construction, joining of dissimilar materials, unique corrosion considerations probability of freezing and thawing, and the high temperatures (>700°C) expected in designs that use these salts.

Therefore to answer many such questions, a large-scale testing capability is needed to mitigate technical and performance risks, and to ensure the performance and reliability of liquid salts as process heat transfer coolant. Testing is critical to acquiring confidence that the system will function as intended. Testing in the proposed forced convection testing loop will be needed to verify the thermal, fluid, and structural performance of heat transfer components. This testing should be carried out in an environment where these components will be exposed to the temperatures and pressures of a real prototype system. Testing at scaled heat loads and prototypic temperatures can be used in the FCL to characterize heat transfer performance. If unconventional heat exchanger designs (any design apart from shell and tube) are chosen, additional emphasis should be used to obtain high confidence in the feasibility of the design.

It is proposed to design and construct a forced convection test loop. A detailed test plan will then be conducted to obtain data on heat transfer, thermodynamic, and corrosion characteristics of the molten salts and fluid-solid interaction. In particular, the report outlines an experimental research and development test plan that would include following steps:

- **Molten Salts:** Select the candidate molten salts for investigation. This activity cannot be completed unilaterally by experimentalists, but should be finalized with input from many stakeholders in government, research institutions, and private industry.
- **Materials of Construction:** Select materials of construction for the test loop, heat exchangers, and fluid-solid corrosion tests in the test loop. In this activity also, opinion of many stakeholders will be needed.
- **Scaling Analysis:** Perform scaling analysis to design the test loop. This task is discussed in Section 2 of this report. However, many steps of the scaling analysis have to be revisited considering the physical constraints of the proposed test loop, objectives of the thermal-hydraulics phenomena, and correct governing equations.
- **Test Plan:** Develop a comprehensive test plan to include all the tests that are being planned in the short and long term time frame. Long term tests may not be conducted immediately, but these will be

useful in designing the test loop so that maximum benefit can be derived from the loop in the long run.

- **Design the Test Loop:** Design the forced convection test loop. This task would require extensive mechanical design, instrument selection, data acquisition system, safety requirements, and related precautionary measures. The details of many activities under this task are listed in Section 3.

- **Fabricate the Test Loop:** This activity is not covered in this report. However, all the present tasks are geared towards this objective.

- **Perform the Tests:** This activity is also slated for future.

- **Uncertainty Analysis:** As a part of the data collection, one must perform the uncertainty analysis to develop probability of confidence in what is measured in the test loop. This activity is an integral part of data collection system. Details of this task are given in Section 4.

Overall, the testing loop will allow development of needed heat transfer related thermophysical parameters for all the salts, validate existing correlations, validate measuring instruments under harsh environment, and have extensive corrosion testing of materials of construction.

Some experimental activities have started at the INL Safety and Tritium Applied Research facility in support of the development of electrochemistry-based instrumentation and purification methods for molten salt heat transfer systems within the VHTR program. The experiments have been focused on the LiF-BeF$_2$ eutectic (67 and 33 mol%, respectively), also known as FLiBe. A batch of FLiBe has been prepared from the constituent materials using an innovative induction-heating set-up with nickel crucibles housed inside an inert gas glove box. A diagnostic system based on a commercial potentiostat and a custom developed software interface for control and real-time data acquisition has been developed and its behavior validated with reference solutions and electrodes. The instrument has then been successfully applied to the generated high-temperature FLiBe melt.

Regarding chemistry control of the molten salt and their thermochemical behavior following task will be performed

- **Molten Salt Chemistry and Corrosion:** At first, prepare and purify the materials with focus on the development of suitable diagnostics to detect material composition and impurities concentration. Consider issues specific to each molten salt and its application with a focus on its compatibility with structural materials and the extension of the existing properties database. Specific impurities in the melt with intensity proportional to their concentration will be detected.

The main material considerations are: (1) Is it compatible with its environments; (2) Is it capable of being fabricated with reasonable ease, and (3) Does it have acceptable mechanical properties? The thermo-fluids and heat exchanger problems, other than its material composition, can be resolved with analysis, development, and through INL and ORNL collaborations.

Experience gained in FCL should facilitate development of algorithms that might be applied to the next generation reactors. Operating a complex test loop throughout the entire range of parameters—from ambient to maximum value of temperature, flow rate, and pressure—will be a challenging endeavor. However, it should provide much needed information, data, and insight in designing optimized systems for process heat transfer.

10. REFERENCES

Abernethy, R. B., Benedict, R. P., and Dowdell, R. B. (1985). "ASME Measurement Uncertainty," *Trans. ASME, J. Fluids Engineering*, **107,** 161-164**.**

Ambrosek, J., Anderson, M., Sridharan, K., and Allen, T. (2009). "Current Status of Knowledge of the Fluoride Salt (FLiNaK) Heat Transfer," *Nuclear Technology*, **165,** 1–8.

Ambrosek, J. (2010). "Molten Chloride Salts for Heat Transfer in Nuclear Systems," Preliminary Proposal for Ph.D. Dissertation, University of Wisconsin, Madison, WI.

Anderson, M., et al. (2010). "University of Wisconsin-Madison Molten Salt Program- Experiments and Lessons Learned," Unpublished University of Wisconsin Report March 2010.

Badar, M. A., Zubair, S. M., and Sheikh, A. K. (1993). "Uncertainty Analysis of Heat-Exchanger Thermal Designs using the Monte Carlo Simulation Technique," *Energy*, **18** (8), 859-866.

Baes, C. F. Jr., (1974). "The Chemistry and Thermodynamics of Molten Salt Reactor Fuels," *Journal of Nuclear Materials,* **51** (1), 149-162.

Bamberger, C. E. and Baes, Jr., C. F. (1968). "The Chemistry of Silica in Molten $LiF-BeF_2$", in Oak Ridge National Laboratory Report ORNL-4254, 146-149.

Bamberger, C. E. (1975a). "Electrochemistry of Molten Fluoride Solutions", in Advances in Molten Salt Chemistry Volume 3, Plenum Press, 220-231.

Bamberger, C. E. (1975b). "Electrochemistry of Molten Fluoride Solutions", in Advances in Molten Salt Chemistry Volume 3, Plenum Press, 190-204.

Bard, A. J. and Faulkner, L. R. (2001). "Electrochemical Methods – Fundamentals and Applications," 2nd Edition, J. Wiley, New York, NY.

Barth, D., (2009). "High Temperature Molten Salt Pumps," Presentation - A. R. Wilfley Centrifugal Pumps.

Bronstein, H. R. and Manning, D. L. (1972). "Lanthanum Trifluoride as a Membrane in a Reference Electrode for use in Certain Molten Fluorides," *J. Electrochem. Soc.*, **119**, (2), 125-128.

Cassayre, L. (2005) Ph.D. Thesis, Université Paul Sabatier de Toulouse.

Cho, S. M. (1987). "Uncertainty Analysis of Heat Exchanger Thermal-Hydraulic Designs," *Heat Transfer Engineering*, **8** (2), 63-74.

Clarke, D.D., Vasquez, V. R., Whiting, W. B., and Greiner, M. (2001). "Sensitivity and Uncertainty Analysis of Heat Exchanger Design to Physical Properties Estimation," *Applied Thermal Engineering*, **21**, 993-1017.

Clauβen, O. and Rüssel, C. (1997). "Thermodynamics of Various Polyvalent Main Group Elements in a Borosilicate Glass Melt," *J. NonCrystalline Solids*, **209**, 292-298.

Coblentz, L. C. (2002). "Uncertainty Analysis of Heat Exchangers," Master's (M. Ing.) Thesis, University of Johannesburg (formerly Rand Afrikaans University), Johannesburg, South Africa.

Coleman, H. W. and Steele, W. G. (1995). "Engineering Application of Experimental Uncertainty Analysis,"*AIAA Journal*, **33** (10), 1888-1896.

Coleman, H. W. and Steele, W. G. (2009). "Experimentation, Validation, and Uncertainty Analysis for Engineers, 3rd Edition", John Wiley & Sons, Inc., Hoboken, NJ.

Forsberg, C. W., Peterson, P. F., Pickard, P. S. (2003). "Molten-salt-cooled Advanced High-temperature Reactor for Production of Hydrogen and Electricity," *Nuclear Technology*, **144** (2003) 289-302.

Grimes, W. R., Bohlmann, E. G., Meyer, A. S., and Dale, J. M. (1972). "Fuel can Coolant Chemistry," Chapter 5 in M. W. Rosenthal, P. N. Haubenreich, and R. B. Briggs, The Development Status of Molten-Salt Breeder Reactors, Oak Ridge National Laboratory Report ORNL-4812.

Hamer, W. J., Malmberg, M. S., and B. Rubin, B. (1965). "Theoretical Electromotive Forces for Cells Containing a Single Solid or Molten Fluoride, Bromide, or Iodide," *J. Elect. Soc*., **112** (7), 750-755.

Harrison, S. J. (2000). "Measurement Errors and Accuracy" Chapter 13 in *The Engineering Handbook*.

Edited by R. C. Dorf, CRC Press LLC, Boca Raton, FL.

Holcomb, D. E., Cetiner, S. M., Flanagan, G. F., Peretz, F. J. and Yoder, G. L., Jr. (2009). "An Analysis of Testing Requirements for Fluoride Salt-Cooled High Temperature Reactor Components," Oak Ridge National Laboratory Report, ORNL/TM-2009/297.

Ingersoll, D. T., Forsberg, C. W., and MacDonald, P. E. (2007). "Trade Studies on the Liquid-Salt-Cooled Very High-Temperature Reactor: Fiscal Year 2006 Progress Report," Oak Ridge National Laboratory Report ORNL/TM-2006/140.

Ishii, M. and Kataoka, I. (1984). "Scaling Laws for thermal-Hydraulic System under Single Phase and Two-Phase natural Circulation," *Nuclear Engineering and Design*, **81**, 411-425.

Ishii, M. et al. (1998). "The Three-level Scaling Approach with Application to the Purdue University Multi-Dimensional Integral Test Assembly (PUMA)," *Nuclear Engineering and Design*, **186,** 177-211.

James, C. A., Taylor, R. P., and Hodge, B. K. (1995), "The Application of Uncertainty Analysis to Cross-Flow Heat Exchanger Performance Predictions," *Heat Transfer Engineering*, **16** (4), 50 – 62.

Janz, G. J., Gardner, G. L., Krebs, U., and Tomkins, R. P. T. (1974). "Molten Salts: Properties of Fluorides and Mixtures, Vol. 4, Part 2, Edited by D. R. Lide, *Journal of Physical and Chemical Reference Data*, **3** (1), 1-151.

Janz, G. J. and Tomkins, R. P. T. (1981). "Physical Properties Data Compilations Relevant to Energy Storage: IV Molten Salts: Data on Additional Single and Multi-Component Salt Systems," National Standard Reference Data System, National Bureau of Standards Report NSRDS-NBS 61 Part IV.

Janz, G. J. (1988). "Thermodynamic and Transport Properties for Molten Salts: Correlation Equations for Critically Evaluated Density, Surface Tension, Electrical Conductance, and Viscosity Data," *J. Physical and Chemical Reference Data*, **17** (2), 1.

Kline, S. J. and McClintock, F. A. (1953). "Describing Uncertainities in Single Sample Experiments, *Mechanical Engineering*, January, 3-8.

Kocamustafaogullari, G. and Ishii, M. (1983). "Scaling Criteria for Modeling Natural- and Forced-Convection Loops," DOE Report CONF-831047-15.

Kondo, M., et al. (2009). "Corrosion Characteristics of Reduced Activation Ferritic Steel, JLF-1 (8.92Cr-2W) in Molten Salts FLiNaK and FLiNaK," *Fusion Engineering and Design*, **84,** 1081-1085.

Kontoyannis, C. (1995). "Pyrolytic Boron Nitride Coated Graphite as a Container of Reference Electrodes for Molten Fluorides,"*Electrochimica Acta*, **40** (15), 2547-2551.

LeBlanc, D. (2010a). "Molten Salt Reactors: A New Beginning for an Old Idea," *Nuclear Engineering and Design*, **240**, 1644-1656.

LeBlanc, D. (2010b). "Too Good to Leave on the Shelf," available at
http://memagazine.asme.org/Articles/2010/May/Too_Good_Leave_Shelf.cfm Accessed on
27th August 2010

Liu, B., Wu, Y.-T., Ma, C.-F., Ye, M., and Guo, H. (2009). "Turbulent Convective Heat Transfer with
Molten Salt in Circular Pipe," *Int. Commun. Heat Mass Transfer*, **36**, 912-916.

Lovering, D. G. and Gale, R. J. (1983). "Molten Salt Techniques - Volume 1," Plenum Press, New York,
Chapter 1.

Mamantov, G. and Manning, D. L. (1966). "Voltammetry and Related Studies of Uranium in Molten
Lithium Fluoride-Beryllium Fluoride-Zirconium Fluoride," *Analytical Chemistry*, **38**, (11),
1494-1498.

Manning, D. L. (1964). "Voltammetry of Nickel in Molten Lithium Fluoride-Sodium Fluoride-Potassium
Fluoride," *J. Electroanalytical. Chem.*, **7**, 302-306.

Manning, D. L. and Mamantov, G. (1964). "Rapid Scan Voltammetry and Chronopenttiometric Studies of
Iron in Molten Fluorides," *J. Electroanalytical. Chem.*, **7,** 102-108.

Martinez, A. M. et al., (2000). "Chemical and Electrochemical Behavior of Chromium in Molten
Chlorides", *J. Electroanalytical. Chem.*, **493**, 1-14.

Medlin, M. W., Sienerth, K. D., and Schreiber, H. D. (1998). "Electrochemical Determination of
Reduction Potentials in Glass-Forming Melts", *J. NonCrystalline Solids*, **240**, 193-201.

Minh, N. Q. and Redey, L. (1987). "Reference Electrodes for Molten Electrlytes", in Molten Salt
Techniques Volume 3, edited by D. G. Lovering and R. J. Gale, Plenum Press, 105-287.

Moffat, R. J. (1982), "Contributions to the Theory of Single Sample Uncertainty Analysis," *Trans. ASME,
J. Fluids Engineering*, **104,** 250-258.

Moffat, R. J. (1985). "Using uncertainty analysis in the planning of an experiment," *Trans. ASME, J.
Fluids Engineering*, **107,** 173-178.

Moffar, R. J. (1988). "Describing the Uncertainties in Experimental Results," *Experimental Thermal and
Fluid Science*, **1**, 3-17.

Olander, D. (2002). "Redox condition in molten fluoride salts: Definition and control," *Journal of
Nuclear Materials*, **300,** 270-272.

Olson, L. C. (2009). "Material Corrosion in Molten LiF-NaF-KF Eutectic Salt," Ph.D. dissertation,
University of Wisconsin, Madison, WI.

Olson, L. C., Ambrosek, J. W., Sridharan, K., Anderson, M. H., and Allen, T. R. (2009). "Materials
Corrosion in Molten LiF-NaF-KF Salt," *Journal of Fluorine Chemistry*, **130,** 67-73.

ORNL (1968-1970). "Molten Salt Reactor Program Semiannual Reports" Oak Ridge National Reports
ORNL-4254; 168-149; ORNL-4344; 163-167; ORNL-4449, 141-142; ORNL-4548, 156-159.

Palmbeck, J. A. (1967). "Electromotive Series in Molten Salts", *J. of Chem. and Eng. Data*, **12**, (1),
77-82.

Phoenix, W.C. (2010). "Instrumentation Strategy for Test Loops and Facilities for the Heat Transport of
the NGNP," PLN-3501.

Ransom, V. H., Wang, W., and Ishii, M. (1998). "Use of an Ideal Scale Model for Scaling Evaluation,"
Nuclear Engineering and Design, **186,** 135-148.

Renault, C., Hron, M., Konings, R., and Holcomb, D.E., (2009). "The Molten Salt Reactor (MSR) in
Generation IV: Overview and Perspectives", GIF Symposium, Paris.

Reyes, Jr., J. N. and Hochreiter, L. (1998). "Scaling Analysis for the OSU AP600 Test Facility (APEX)," *Nuclear Engineering and Design*, **186,** 53-109.

Reyes, Jr., J. N. (2001). "Integral System Experiment Scaling Methodology," Annex 11, IAEA, Vienna, Austria.

Reyes, Jr., J. N. (2007). "Integral System Experiment Scaling Methodology," IAEA-ICTP Natural Circulation Training Course, Lecture T14, International Centre for Theoretical Physics, Trieste, Italy, June 25–29.

Rosenthal, M. W., Haubenreich, P. N., and Briggs, R. B. (1972). "The Development Status of Molten-Salt Breeder Reactors," Oak Ridge National Laboratory Report ORNL-4812.

Sabharwall, P., Utgikar, V., and Gunnerson, F. (2008). "Effect of Mass Flow Rate on the Convective Heat Transfer Coefficient: Analysis for Constant Velocity and Constant Area Case," *Nuclear Technology*, **166**, 197-200.

Sabharwall, P. (2009). "Engineering Design Elements of a Two-Phase Thermosyphon to Transfer NGNP Thermal Energy to a Hydrogen Plant," Idaho National Laboratory Report INL/EXT-09-15383.

Sabharwall, P. and Gunnerson, F., (2009). "Engineering Design Elements of a Two-Phase Thermosyphon to Transfer NGNP Thermal Energy to a Hydrogen Plant," *Nuclear Engineering and Design*, **239 (**11), 2293-2301.

Sabharwall, P., Ebner, M., Sohal, M. S., Sharpe, P., Anderson, M., Sridharan, K., Ambrosek, J., Olson, L., and Brooks, P. (2010a). "Molten Salts for High Temperature Reactors: University of Wisconsin Molten Salt Corrosion and Flow Loop Experiments – Issues Identified and Path Forward," Idaho National Laboratory Report INL/EXT-10-18090.

Sabharwall, P., Patterson, M., Utgikar, V., and Gunnerson, F. (2010b). "Phase Change Heat Transfer Device for Process Heat Applications," *Nuclear Engineering and Design*, In Press.

Shaffer, J. H. (1964). "Preparation of MSRE Fuel, Coolant, and Flush Salts", Oak Ridge National Laboratory Molten-Salt Reactor Program Semiannual Progress Report for Period Ending July 31, 1964, ORNL-3708, 288-303.

Shaffer, J. H. (1971). "Preparation and Handling of Salt Mixtures for the Molten Reactor Experiment," Oak Ridge National Laboratory Report ORNL-4616.

Smirnov, M. V., Khoklov, V. A., and Filatov, E. S. (1987). "Thermal Conductivity of Molten Alkali Halides and their Mixtures," *Electrochimica Acta*, **32** (7) 1019-1026.

Smith, D. C., Rush, E. E., Mathews, C. W., Chavez, J. M., and Bator, P. A. (1992). "Report on the Test of Molten-Salt Pump and Valve Loops," Sandia National Laboratory Report SAND-91-1747.

Sohal, M. S., Ebner, M. A., Sabharwall P., and Sharpe, P. (2010). "Engineering Database of Liquid Salt Thermophysical and Thermochemical Properties," Idaho National Laboratory Report INL/EXT-10-18297.

Sridharan, K., et al. (2008). "Molten Salt Heat Transport Loop: Materials Corrosion and Heat Transfer Phenomena," University of Wisconsin, Madison, Nuclear Energy Research Initiative (NERI) Final Report.

Task, K. D., Lahoda, E. J., and Paoletti, L. (2005). "Molten Salt /Helium Comparison for Intermediate Heat Exchange Loop," 39th Annual Loss Prevention Symposium, Atlanta, GA.

Taylor, B. N. and Kuyatt, C. E. (1994). "Guidelines for Evaluating and Expressing the Uncertainty of NIST Measurement Results," National Institute of Standards and Technology, NIST Technical Note 1297, U.S. Government Printing Office, Washington, DC.

Van Norman, J. D. (1965). "A Chronopotentiometric Study of the Silver-Silver Chloride and Silver-Silver Bromide Systems," *J. Electrochemical Soc.*, **112**, 1126-1129.

Van Norman, J. D., Booless, J. D., and Egan, J. J. (1966). "A Spectrophotometric and Chronopotentiometric Study of the Lead-Lead Chloride and the Zinc-Zinc-Chloride Systems", *J. Phys. Chem.*, **70** (4), 1276-1281.

Vijayan, P. K. and Austregesilo, H. (1994). "Scaling Laws for Single-Phase Natural Circulation Loops," *Nuclear Engineering and Design*, **186**, 53-109.

White, S. H. (1981). "Water in Molten Salts: Industrial and Electrochemical Consequences" in Ionic Liquids, edited by D. Inman and D. G. Lovering, Plenum Press, 165-247.

White, S. H. (1983). "Halides," in Molten Salt Techniques, Volume 1, edited by D. G. Lovering and R. J. Gale, Plenum Press, 19-52.

Wilkins, S.C. and Evans, R.P. (2005). "Assessment of High-Temperature Measurements for Use in the Gas Test Loop," Idaho National Laboratory Report INL/EXT-05-00298.

Williams, D. F. and Toth, L. M. (2005). "Chemical Considerations for the Selection of the Coolant for the Advanced High-Temperature Reactor," Oak Ridge National Laboratory Report ORNL/GEN4/LTR-05-011.

Williams, D. F. (2006). "Assessment of Candidate Molten Salt Coolants for the NGNP/NHI Heat-Transfer Loop," Oak Ridge National Laboratory Report ORNL/TM-2006/69.

Williams, D. F., Toth, L. M., and Clarno, K. T. (2006). "Assessment of Candidate Molten Salt Coolants for the Advanced High-Temperature Reactor (AHTR)," Oak Ridge National Laboratory Report ORNL/TM-2006/12.

Wu, Y-T., Liu, B., Ma, C.-F., and Guo, H. (2009). "Convective Heat Transfer in Laminar-turbulent Transition Region with Molten Salt," *Experimental Thermal and Fluid Science*, **33**, 1128-1132.

Wulff, W. (1996). "Scaling of Thermohydraulics System," *Nuclear Engineering and Design*, **163,** 359-395.

Yadigaroglu, G. and Zeller, M. (1994). "Fluid-to-Fluid Scaling for a Gravity- and Flashing-Driven Natural Circulation Loop," *Nuclear Engineering and Design*, **151**, 49-64.

Zuber, N. (1991). "Appendix D: Hierarchical, Two-Tiered Scaling Analysis - An Integrated Structure and Scaling Methodology for Severe Accident Technical Issue Resolution," U.S Nuclear Regulatory Commission Report NUREG/CR-5809, Washington, D.C.

Zuber, N. (2001). "The Effects of Complexity, of Simplicity and of Scaling in Thermal-Hydraulics," *Nuclear Engineering and Design*, **204**, 1-27.